# Coulomb drag

B. N. Narozhny

*Institut für Theorie der Kondensierten Materie, Karlsruhe Institute of Technology, 76128 Karlsruhe, Germany and National Research Nuclear University MEPhI (Moscow Engineering Physics Institute), Kashirskoe shosse 31, 115409 Moscow, Russia*

A. Levchenko

*Department of Physics, University of Wisconsin–Madison, Madison, Wisconsin 53706, USA and Institut fur Nanotechnologie, Karlsruhe Institute of Technology, 76021 Karlsruhe, Germany*

(published 10 May 2016)

Coulomb drag is a transport phenomenon whereby long-range Coulomb interaction between charge carriers in two closely spaced but electrically isolated conductors induces a voltage (or, in a closed circuit, a current) in one of the conductors when an electrical current is passed through the other. The magnitude of the effect depends on the exact nature of the charge carriers and the microscopic, many-body structure of the electronic systems in the two conductors. Drag measurements have become part of the standard toolbox in condensed matter physics that can be used to study fundamental properties of diverse physical systems including semiconductor heterostructures, graphene, quantum wires, quantum dots, and optical cavities.

DOI: 10.1103/RevModPhys.88.025003

## CONTENTS



## I. FRICTIONAL DRAG

Inner workings of solids are often studied with the help of transport measurements. Within the linear response, the outcome of such measurements is determined by the properties of the unperturbed system, which are often the object of study. In a typical experiment a current is driven through a conductor and the voltage drop along the conductor is measured. In conventional conductors at low temperatures the resulting Ohmic resistance is mostly determined by disorder (which is always present in any sample) (Ziman, 1965; Lifshitz and Pitaevskii, 1981), while interactions between charge carriers

 

lead to corrections that affect the temperature dependence of transport coefficients (Altshuler and Aronov, 1985).

In his pioneering work, Pogrebinskii (1977) suggested an alternative measurement that involves two closely spaced, but electrically isolated conductors (hereafter referred to as "layers"). In such a system, an electric current $I_1$ flowing through one of the layers, known as the "active" layer, induces a current (or, in an open circuit, a voltage $V_2$, see Fig. 1) in the other, "passive" layer by means of "mutual friction." By this one typically understands scattering between charge carriers belonging to different layers due to long-range interactions. These scattering events are accompanied by energy and momentum transfer from the carriers in the active layer to the carriers in the passive layer, effectively "dragging" them along. At the simplest level, such friction effects can be described by introducing a phenomenological relaxation rate. In the case of frictional drag, the corresponding rate $\tau_D^{-1}$ generally depends on the exact nature of the charge carriers, interlayer interaction, and microscopic structure of the electronic system. Thus, measurements of this relaxation rate provide additional insight into microscopic properties of interacting many-body systems.

A related phenomenon, where a quasiparticle flow instigates a partial transfer of energy and momentum between separate, but interacting subsystems of quasiparticles, is known as "phonon drag" (Gurevich, 1946a, 1946b; Herring, 1954) and manifests itself in a rising thermoelectric power in semiconductors at low temperatures (Frederikse, 1953; Geballe and Hull, 1954). In the presence of a temperature gradient, lattice vibrations become anisotropic since the phonons travel preferentially from hot to cold (providing a mechanism for thermal conduction). Interacting with electrons, the phonons effectively drag them toward the cold end of the sample, creating an excess charge density (this process continues until the electrostatic field created by the accumulated charge counterbalances the drag effect). In a nonequilibrium system of electrons and phonons, their mutual drag is intertwined with heating effects and affects charge transport (Gurevich and Mashkevich, 1989). The resulting correction to the standard transport theory is important in thermoelectric measurements.

In contrast, frictional drag in double-layer systems is *not a correction*: in the absence of the interlayer interaction, charge carriers in two disjoined conductors are insensitive to each other (therefore, any drag effect should necessarily vanish in the limit of infinitely remote layers). In other words, *the drag phenomenon simply does not exist in noninteracting systems*. Consequently, initial experimental work on mutual drag was devoted to quantitative measurement of the strength of interactions between quasiparticle subsystems in various semiconductor devices including $p$-modulation-doped GaAs quantum wells (Höpfel *et al.*, 1986; Höpfel and Shah, 1988), capacitively coupled two- and three-dimensional (2D-3D) electron systems in AlGaAs/GaAs heterostructures (Solomon *et al.*, 1989; Solomon and Laikhtman, 1991), 2D electron systems in AlGaAs/GaAs double quantum wells (Gramila *et al.*, 1991, 1992, 1994; Solomon and Laikhtman, 1991; Eisenstein, 1992), and electron-hole bilayers (Sivan, Solomon, and Shtrikman, 1992). Numerical simulations of the drag effect between 3D systems were performed by Jacoboni and Price (1988) and between 2D systems by Moško, Cambel, and Mošková (1992), Cambel and Moško (1993), and Mosko, Pelouard, and Pardo (1994). At low temperatures and for closely spaced layers, the interlayer scattering rate $\tau_D^{-1}$ appeared to be dominated by the Coulomb interaction (Price, 1983, 1988).

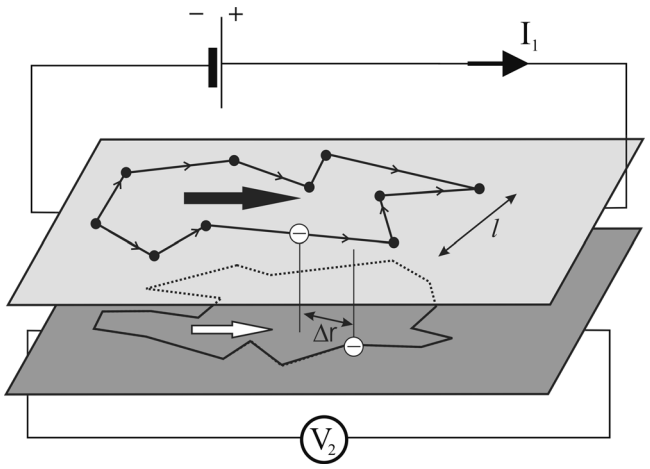


FIG. 1. The drag signal $V_2$ induced by the current $I_1$. From Price *et al.*, 2007.

Coulomb drag between spatially separated electron systems is ultimately caused by fluctuations (or inhomogeneities) of the charge density in the two layers (Zheng and MacDonald, 1993). Indeed, an infinite layer with uniformly distributed electric charge creates a uniform electric field in the normal direction that does not exert any lateral force upon the carriers in another layer. If both layers are in the Fermi-liquid state, then the usual phase-space argument (Gramila *et al.*, 1991) yields the quadratic temperature dependence $\tau_D^{-1} \propto T^2$ in qualitative agreement with the observed behavior at low enough temperatures. A more detailed analysis of the experimental data revealed the presence of additional mechanisms leading to frictional drag, such as the indirect interlayer interaction mediated by phonons (Gramila *et al.*, 1993; Rubel *et al.*, 1995, 1996; Noh *et al.*, 1999), plasmon effects (Hill *et al.*, 1997; Noh *et al.*, 1998), and thermoelectric phenomena (Solomon and Laikhtman, 1991).

Theoretically, it was realized early on that mutual Coulomb scattering between electrons in the two layers results in the *exchange of both energy and momentum* (Price, 1983; Boiko and Sirenko, 1988; Maslov, 1992). Initial calculations aimed at energy and momentum relaxation in a nondegenerate 2D electron gas (2DEG) due to proximity to a 3D conductor (Boiko and Sirenko, 1988, 1990) were followed by the investigation of transport properties in coupled 2D and 3D systems (Laikhtman and Solomon, 1990; Boiko, Vasilopoulos, and Sirenko, 1992), 1D systems coupled to conductors of arbitrary dimensionality (Sirenko and Vasilopoulos, 1992), coupled 1D wires (Tso and Vasilopoulos, 1992; Tanatar, 1996, 1998; Gurevich, Pevzner, and Fenton, 1998), and quantum Hall (QH) edge states (Orgad and Levit, 1996). Following the groundbreaking experiments in AlGaAs/GaAs double quantum wells (Gramila *et al.*, 1991; Eisenstein, 1992), a lot of work was devoted to drag between two degenerate 2DEGs. While the purely Coulomb mechanism (Jauho and Smith, 1993; Zheng and MacDonald, 1993; Flensberg *et al.*, 1995; Kamenev and Oreg, 1995) captures the most qualitative features of the effect, other mechanisms of momentum transfer may also contribute to the observed

behavior. In samples with larger interlayer spacing ($d \sim 50 - 500$ nm) as much as 30% of the measured signal was attributed to phonon-mediated interactions (Gramila *et al.*, 1993). These measurements appeared to be consistent with the virtual-phonon exchange mechanism (Tso, Vasilopoulos, and Peeters, 1992, 1994). Other suggested scattering mechanisms involved acoustic (Bønsager *et al.*, 1998a) and optical (Hu, 1998) phonons, plasmon effects (Flensberg and Hu, 1994), and coupled plasmon-phonon modes (Güven and Tanatar, 1997a). Bilayers subject to strong magnetic fields were shown to form interlayer correlated states (Varma, Larkin, and Abrahams, 1994; Girvin and MacDonald, 1997). For superconducting (SC) layers, interlayer magnetic interaction due to spontaneously created vortices was also suggested (Shimshoni, 1995).

Mutual Coulomb scattering was studied also in a hybrid device (Huang, Bazan, and Bernstein, 1995) comprising normal (Au/Ti) and superconducting ($AlO_x$) 2D films separated by an insulating ($Al_2O_3$) layer. In that case, as well as in "cross-talk" measurements in superconductor–insulator–normal-metal trilayers (Giordano and Monnier, 1994), the phenomenological Drude-like description of drag in terms of $\tau_D^{-1}$ does not apply. The Drude description also fails when the system is subjected to a strong magnetic field: in contrast to the naive description, numerous experiments (Hill *et al.*, 1996, 1998; Patel *et al.*, 1997; Rubel *et al.*, 1997; Rubel, Fischer, Dietsche, von Klitzing, and Eberl, 1997; Feng *et al.*, 1998; Jörger, Dietsche *et al.*, 2000; Lok, Kraus, Pohlt, Dietsche *et al.*, 2001; Lok, Kraus, Pohlt, Güven *et al.*, 2001) showed significant dependence of the measured drag resistivity $\rho_D$ on the applied field, especially in the extreme quantum regime (Lilly *et al.*, 1998). More sophisticated theoretical calculations on Coulomb drag in quantum Hall states (Shimshoni and Sondhi, 1994), superfluid condensates in paired electron-hole layers (Vignale and MacDonald, 1996), drag of composite fermions (Ussishkin and Stern, 1997, 1998; Kim and Millis, 1999; Zhou and Kim, 1999), vortex drag (Vitkalov, 1998), nondissipative drag (Rojo and Mahan, 1992), supercurrent drag (Duan and Yip, 1993), as well as drag between charged Bose gases (Tanatar and Das, 1996) and mesoscopic rings (Shahbazyan and Ulloa, 1997a, 1997b; Baker, Vignale, and Rojo, 1999) confirmed the expectation that *the drag resistivity reflects not only the exact character of interlayer interaction, but also the nature of elementary excitations in each layer and their fundamental properties*.

After the turn of the century, drag measurements became part of the standard toolbox in condensed matter physics. They have been used to investigate properties of electron-electron scattering in low-density 2D electron systems (Kellogg, Eisenstein *et al.*, 2002; An *et al.*, 2006); signatures of metal-insulator transition in dilute 2D hole systems (Jörger, Cheng, Dietsche *et al.*, 2000; Jörger, Cheng, Rubel *et al.*, 2000; Pillarisetty *et al.*, 2002; Pillarisetty, Noh, Tsui *et al.*, 2005; Pillarisetty, Noh, Tutuc *et al.*, 2005); quantum coherence of electrons (Price *et al.*, 2007, 2008; Kim *et al.*, 2011) and composite fermions (Price, Savchenko, and Ritchie, 2010); exciton effects in electron-hole bilayers (Keogh *et al.*, 2005; Croxall *et al.*, 2008; Morath *et al.*, 2009; Seamons *et al.*, 2009); exotic bilayer collective states (Eisenstein, 2014), especially the quantum Hall effect (QHE) at the total filling factor $\nu_T = 1$ (Kellogg, Spielman *et al.*, 2002; Kellogg *et al.*, 2003; Spielman *et al.*, 2004; Tutuc, Pillarisetty, and Shayegan, 2009; Finck *et al.*, 2010; Schmult *et al.*, 2010); compressible QH states at half-integer filling factor (Zelakiewicz *et al.*, 2000; Muraki *et al.*, 2004); integer QH regime (Lok *et al.*, 2002); Luttinger liquid effects (Debray *et al.*, 2001; Laroche *et al.*, 2008, 2014); Wigner crystallization in quantum wires (Yamamoto *et al.*, 2002, 2006, 2012); and one-dimensional (1D) subbands in quasi-1D wires (Debray *et al.*, 2000; Laroche *et al.*, 2011). More generally, interlayer interaction and corresponding transport properties have been studied in hybrid devices comprising a quantum wire and a quantum dot (Krishnaswamy, Goodnick, and Bird, 1999), a SC film and a 2D electron gas (Farina *et al.*, 2004), Si metal-oxide-semiconductor systems (Laikhtman and Solomon, 2005), quantum point contacts (Khrapai *et al.*, 2007), insulating *a*-SiNb films (Elsayad, Carini, and Baxter, 2008), ferromagnetic-antiferromagnetic-SC trilayers (Cuoco *et al.*, 2009), nanosize CdSe-CdS semiconductor tetrapods (Mauser *et al.*, 2010), electron-hole scattering in quantum wells (Prunnila *et al.*, 2008; Takashina *et al.*, 2009; Yang *et al.*, 2011), graphene monolayers (Kim *et al.*, 2011; Gorbachev *et al.*, 2012; Kim and Tutuc, 2012; Titov *et al.*, 2013), and hybrid graphene-semiconductor systems (Gamucci *et al.*, 2014).

On the theory side, the variety of suggested extensions and generalizations of the original drag problem is even richer. The theory of Coulomb drag between two 2DEGs was extended to dilute 2D hole systems (Hwang *et al.*, 2003) and to the cases where one allows for certain tunneling processes between the layers (Oreg and Kamenev, 1998; Oreg and Halperin, 1999), interlayer disorder correlations (Gornyi, Yashenkin, and Khveshchenko, 1999; Hu, 2000a), in-plane potential modulation (Alkauskas *et al.*, 2002), and disorder inhomogeneities (Apalkov and Raikh, 2005; Spivak and Kivelson, 2005; Zou, Refael, and Yoon, 2009, 2010). Theory of Coulomb drag between composite fermions was generalized to include phonon-mediated coupling (Bønsager, Kim, and MacDonald, 2000; Khveshchenko, 2000). Mutual friction was also suggested to occur between non-Fermi-liquid phases including Luttinger liquids (Flensberg, 1998; Nazarov and Averin, 1998; Klesse and Stern, 2000), Wigner crystals (Baker and Rojo, 2001; Braude and Stern, 2001), and strongly localized electrons (Raikh and von Oppen, 2002). Drag or similar measurements of interlayer interactions were also considered for composite (or hybrid) systems comprising ballistic quantum wires (Gurevich and Muradov, 2000, 2005; Raichev and Vasilopoulos, 2000a; Wang, Mishchenko, and Demler, 2005), coupled 2D-1D systems (Lyo, 2003), nonequilibrium charged gases (Wang and da Cunha Lima, 2001), multiwall nanotubes (Lunde and Jauho, 2004; Lunde, Flensberg, and Jauho, 2005), quantum point contacts (Levchenko and Kamenev, 2008a), few level quantum dots (Moldoveanu and Tanatar, 2009), optical cavities (Berman, Kezerashvili, and Lozovik, 2010a; Berman, Kezerashvili, and Kolmakov, 2014), coupled mesoscopic rings (Yang and MacDonald, 2001), superconductors (Levchenko and Norman, 2011), and normal-metal–ferromagnet–normal-metal structures (Zhang and Zhang, 2012). Other developments include mesoscopic fluctuations of Coulomb drag (Narozhny and Aleiner, 2000; Narozhny, Aleiner, and Stern, 2001), frictional drag mediated by virtual photons (Donarini *et al.*,

2003) and plasmons (Badalyan *et al.*, 2007), exciton effects in semiconductors (Laikhtman and Solomon, 2006) and topological insulators (Mink *et al.*, 2012), interlayer Seebeck effects (Lung and Marinescu, 2011) and spin drag (D'Amico and Vignale, 2000; Flensberg, Stibius Jensen, and Asger Mortensen, 2001; Vignale, 2005; Pustilnik, Mishchenko, and Starykh, 2006; Tse and Das Sarma, 2007; Badalyan and Vignale, 2009; Duine and Stoof, 2009; Duine *et al.*, 2010, 2011; Glazov *et al.*, 2011). Recently, the focus of the theoretical work was shifted toward the drag effect in graphene-based devices (Narozhny, 2007; Tse, Hu, and Sarma, 2007; Song, Abanin, and Levitov, 2013; Narozhny *et al.*, 2015) and strongly interacting high-mobility double layers with low-density carrier concentration (Apostolov, Levchenko, and Andreev, 2014; Chen, Andreev, and Levchenko, 2015).

Given the rather large amount of literature devoted to frictional drag, it seems unreasonable to cover all possible angles in a single paper. Early work on frictional drag was reviewed by Rojo (1999). Various experimental aspects were discussed in reviews on exciton condensates (Snoke, 2002; Eisenstein, 2014), electron-hole bilayers (Das Gupta *et al.*, 2011), strongly correlated 2D electron fluids (Spivak *et al.*, 2010), and 1D ballistic electron systems (Debray *et al.*, 2002). A discussion of drag in strong magnetic fields was included in a review of magnetotransport in 2D electron systems (Dmitriev *et al.*, 2008). In this review, we limit ourselves to the discussion of standard ("electrical") Coulomb drag. Spin-related phenomena and thermoelectric effects are beyond the scope of this review.

## II. COULOMB DRAG IN SEMICONDUCTOR HETEROSTRUCTURES

In an idealized experiment, a constant (dc) current $I_1$ is passed through the active layer, keeping the passive layer isolated at the same time (such that no current is allowed to flow in it); see Fig. 1. The voltage $V_2$ induced in the passive layer is proportional to $I_1$ and the coefficient[1]

$$R_D = -V_2/I_1 \tag{1}$$

is a direct measure of interlayer interactions.

In his original paper, Pogrebinskii (1977) derived the Drude-like description of transport in double-layer systems comprising two coupled equations of motion

$$\frac{d\boldsymbol{v}_1}{dt} = \frac{e}{m_1}\boldsymbol{E}_1 + \frac{e}{m_1 c}[\boldsymbol{v}_1 \times \boldsymbol{B}] - \frac{\boldsymbol{v}_1}{\tau_1} - \frac{\boldsymbol{v}_1 - \boldsymbol{v}_2}{\tau_D}, \tag{2a}$$

$$\frac{d\boldsymbol{v}_2}{dt} = \frac{e}{m_2}\boldsymbol{E}_2 + \frac{e}{m_2 c}[\boldsymbol{v}_2 \times \boldsymbol{B}] - \frac{\boldsymbol{v}_2}{\tau_2} - \frac{\boldsymbol{v}_2 - \boldsymbol{v}_1}{\tau_D}, \tag{2b}$$

where $e$ is the electric charge, $\boldsymbol{v}_i$, $m_i$, and $\boldsymbol{E}_i$ are the drift velocities, effective masses, and electric fields in the two layers, and the nonquantizing magnetic field $\boldsymbol{B}$ is assumed to be uniform. Intralayer impurity-scattering processes yielding the Drude resistivity in the two layers are described by the mean-free times $\tau_i$. The last term in each of Eqs. (2) describes the mutual friction between the charge carriers in the two layers that tends to equalize drift velocities. If treated phenomenologically, the model (2) describes two distinct types of carriers coupled by the friction term, but does not explicitly require them to be spatially separated (Hänsch and Mahan, 1983; Cui, Lei, and Horing, 1988; Söderström, Buyanov, and Sernelius, 1996).

Solving the equations (2), one finds the resistivity matrix $\rho_{\alpha\beta}^{(ij)}$ [hereafter the indices $i, j = 1, 2$ denote the two layers and $\alpha, \beta = x, y$—spatial coordinates orthogonal to $\boldsymbol{B} = B\boldsymbol{e}_z$; the layers described by Eqs. (2) can represent 2D or 3D conductors, see Sec. VI for the 1D case]. The "drag resistivity" (also called the transresistivity or the drag coefficient) is given by the Drude-like formula

$$\rho_D = -\rho_{xx}^{(12)} = m_2/(e^2 n_1 \tau_D). \tag{3a}$$

The expression (3a) is *independent of the magnetic field*. This statement has the same status as the absence of the classical magnetoresistance.[2] Indeed, the single-layer longitudinal resistivity derived from Eqs. (2) is given by

$$\rho_{xx}^{(11)} = \frac{m_1}{e^2 n_1}\left(\frac{1}{\tau} + \frac{1}{\tau_D}\right). \tag{3b}$$

In most cases, drag is rather weak ($\tau_D \gg \tau$) and the usual Drude formula remains a good approximation for $\rho_{xx}^{(11)}$ (Eisenstein, 1992; Rojo, 1999). The single-layer Hall coefficient is unaffected by the presence of the second layer and is determined solely by the carrier density

$$\rho_{yx}^{(11)} = B/(n_1 e c). \tag{3c}$$

Within the applicability of the Drude model, frictional drag is purely longitudinal: "Hall drag" does not occur[3]

$$\rho_D^H = \rho_{yx}^{(12)} = 0. \tag{3d}$$

At the phenomenological level, the drag resistivity (3a) is independent of the disorder strength. Moreover, in the "clean" limit $\tau \to \infty$ the interlayer and intralayer resistivities tend to the same value and the resistivity matrix becomes degenerate (the corresponding conductivities diverge):

$$\rho_{xx}^{(11)}(\tau \to \infty) = \rho_D(\tau \to \infty). \tag{4}$$

Thus a system comprising two capacitively coupled, ideal conductors is characterized by nonzero resistivity and exhibits *perfect drag!*

[1] The minus sign in Eq. (1) is motivated by Eq. (3a). An alternative definition without the explicit minus sign is also widely used in literature.

[2] In this section we are discussing the simplest situation, where both $\tau_D$ and $\tau$ are unaffected by weak enough magnetic fields.

[3] Under the assumptions of this section, magnetic field has no effect on drag. Hence, up until Sec. II.G we focus on the zero-field, longitudinal transport. Drag in magnetic field is discussed in Secs. II.G, IV.E, and VII.A.

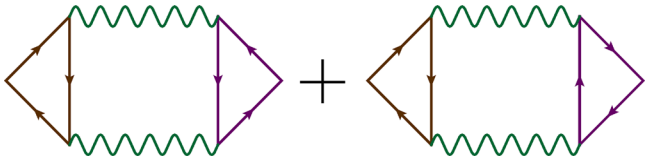

FIG. 2. Aslamazov-Larkin diagrams describing the lowest-order contribution to drag. The solid lines refer to quasiparticle Green's functions and the wavy lines describe the interlayer interaction. The left and right triangles correspond to nonlinear susceptibilities of the two layers.

### A. Interlayer Coulomb interaction

The "Drude formula" (3a) for the drag resistivity becomes falsifiable provided that something is known about the properties of the "drag rate" $\tau_D^{-1}$ (e.g., its dependence on temperature, carrier density, interlayer separation, and other experimentally relevant parameters). To leading order, the contribution of the interlayer Coulomb interaction to $\tau_D^{-1}$ can be calculated within the Born approximation (or, equivalently, using Fermi's golden rule) (Laikhtman and Solomon, 1990; Jauho and Smith, 1993). In the language of Feynman diagrams, the corresponding process (Zheng and MacDonald, 1993; Flensberg *et al.*, 1995; Kamenev and Oreg, 1995) is described by the Aslamazov-Larkin diagrams (Aslamazov and Larkin, 1968) shown in Fig. 2.

The effective interlayer interaction can be found as a solution to the Poisson equation for the potential of a point source belonging to one of the layers. In principle, this can be done for any system of coupled conductors. Coupling between a 2DEG and a 3DEG was considered by Laikhtman and Solomon (1990). A double-quantum-well system was discussed by Jauho and Smith (1993), where the finite width of the wells was taken into account by assuming a specific form of the electron wave function in the direction perpendicular to the layers. However, the obtained results are qualitatively the same as in the simplest case of purely two-dimensional layers.

If electrons in each layer are confined to move in a 2D plane, the "bare" Coulomb potential[4] has the form[5]

$$V_{11} = V_{22} = 2\pi e^2/q, \qquad V_{12}(q) = (2\pi e^2/q)e^{-qd}. \quad (5)$$

Here $e$ is the electron charge and $d$ is the interlayer separation that determines the maximum value (or, rather, the order of magnitude thereof) of the momentum $q$ that can be transferred between the layers (see footnote 5):

$$q \ll 1/d. \quad (6)$$

Taking into account dynamical screening within the usual random phase approximation (RPA) modifies the interlayer interaction (Das Sarma and Madhukar, 1981; Santoro and Giuliani, 1988; Halperin, Lee, and Read, 1993; Stern and Halperin, 1995), but does not change the exponential decay at large $q$. The resulting retarded interaction propagator can be written as

$$\mathcal{D}_{12}^R = -\frac{1}{\Pi_1^R\Pi_2^R(4\pi e^2/q)\sinh qd + [q/(2\pi e^2) + \Pi_1^R + \Pi_2^R]e^{qd}}. \quad (7)$$

Here $\Pi_i^R$ is the single-layer retarded polarization operator. It is quite common [see, e.g., Laikhtman and Solomon (1990) and Jauho and Smith (1993)] to include the dielectric constant $\epsilon$ of the insulating spacer into the bare potential. Since the same $\epsilon$ should enter the expression for the inverse Thomas-Fermi screening length

$$\varkappa = 2\pi e^2\nu = 2\pi e^2\Pi^R(q < 2k_F, \omega = T = 0), \quad (8)$$

the dielectric environment can be taken into account by expressing the results in terms of $\varkappa$ ($\nu$ denotes the thermodynamic density of states of the 2DEG). For high carrier densities (Gramila *et al.*, 1991), Eq. (7) can be simplified (Kamenev and Oreg, 1995) by assuming the small screening length $\varkappa d \gg 1$ [see Eqs. (20) and (33b)].

The condition (6) allows one to distinguish the following two regimes (Kamenev and Oreg, 1995):

(i) If the interlayer separation is large compared to the mean-free path $d \gg \ell$, then it follows from Eq. (6) that $q \ll 1/\ell$; in this case the motion of charge carriers is *diffusive*.

(ii) In the opposite case, $d \ll \ell$, transport is dominated by *ballistic* propagation of charge carriers with $1/d \gg q \gg 1/\ell$; see Eq. (36). Most measurements (Gramila *et al.*, 1991; Gorbachev *et al.*, 2012) are performed on ballistic samples.

The majority of analytic (Rojo, 1999) and numerical (Moško, Cambel, and Mošková, 1992) work on Coulomb drag in semiconductor heterostructures was performed treating the interaction (7) in the lowest order of perturbation theory. For generalizations see Secs. II.D and II.F.

### B. Kinetic theory of ballistic drag

Ballistic motion of charge carriers in semiconductors can be described by using the kinetic equation approach, where impurity scattering is taken into account within the simplest $\tau$ approximation (Pogrebinskii, 1977; Laikhtman and Solomon, 1990; Jauho and Smith, 1993). One starts with the generic Boltzmann equation

$$\frac{\partial f_i}{\partial t} + \boldsymbol{v}_i\boldsymbol{\nabla} f_i + \left(e\boldsymbol{E}_i + \frac{e}{c}[\boldsymbol{v}_i \times \boldsymbol{B}]\right)\frac{\partial f_i}{\partial \boldsymbol{p}} = -\frac{\delta f_i}{\tau} + \mathcal{I}_{ij}, \quad (9)$$

where $f_i$ is the distribution function (in layer $i = 1, 2$), $\mathcal{I}_{ij}$ is the collision integral due to interlayer Coulomb interaction, $\tau$ is the transport impurity-scattering time, and $\delta f_i$ is the nonequilibrium correction to the distribution function. Here we consider only *degenerate* electron systems [as realized in semiconductor heterostructures (Gramila *et al.*, 1991)]. Weak deviations from the equilibrium Fermi-Dirac distribution

[4]Although electrons are confined to move in two dimensions, they interact by means of "real, 3D" Coulomb interaction.

[5]While discussing the theory, we use the natural units where temperature and relaxation rates are measured in energy units ($\hbar = k_B = 1$). We attempt to restore the Planck's constant in final expressions for the drag resistivity and while discussing experimental findings.

function $f_i^{(0)}$ (as appropriate within the linear response) are described by (Lifshitz and Pitaevskii, 1981)

$$\delta f_i \equiv f_i - f_i^{(0)} \equiv f_i^{(0)}[1 - f_i^{(0)}]h_i = -T[\partial f_i^{(0)}/\partial\epsilon]h_i. \quad (10)$$

Here we consider only the steady state and uniform fields

$$\partial f_i/\partial t = 0, \qquad \boldsymbol{\nabla} f_i = 0. \quad (11)$$

The latter condition physically means that the sample size is large compared to the length scale of typical relaxation processes in the system; see also Sec. IV.D.

In the absence of interlayer interaction, the task of finding linear-response transport coefficients from Eq. (9) is a textbook problem (Ziman, 1965; Smith and Jensen, 1989; Seeger, 2002). Under the above assumptions, the theory is qualitatively equivalent to the Drude theory (2) yielding the standard results (3b) and (3c). Not surprisingly, taking into account the collision integral $\mathcal{I}_{ij}$ leads to the Drude-like description of the drag resistivity (3a) and (3d). The advantage of the present "microscopic" calculation is that now we can determine the phenomenological relaxation time $\tau_D$ in terms of the model parameters.

The standard perturbative calculation (Lifshitz and Pitaevskii, 1981; Laikhtman and Solomon, 1990; Boiko, Vasilopoulos, and Sirenko, 1992; Jauho and Smith, 1993) amounts to finding the nonequilibrium distribution functions $h_i$ in the two layers to the leading order in the interlayer interaction and the electric field $\boldsymbol{E}_1$ applied to the active layer. Then one uses the definition of the electric current (here the sum runs over all of the single-particle states)

$$\boldsymbol{j}_i = e\sum \boldsymbol{v}\delta f_i, \quad (12)$$

and finds the current $\boldsymbol{j}_2$ in the passive layer. The coefficient of proportionality between $j_{2x}$ and $E_{1x}$ defines the drag conductivity $\sigma_D$. The drag coefficient $\rho_D$ can then be obtained by inverting the $2\times 2$ conductivity matrix (see footnote 3)

$$\rho_D = \frac{\sigma_D}{\sigma_1\sigma_2 - \sigma_D^2} \approx \frac{\sigma_D}{\sigma_1\sigma_2}, \quad (13)$$

where $\sigma_i$ is the longitudinal conductivity in layer $i$; the latter relation follows from the smallness of the effect

$$\sigma_D \ll \sigma_i, \quad (14)$$

as observed in experiment (Eisenstein, 1992; Rojo, 1999). This way, one finds for the phenomenological drag rate

$$\tau_D^{-1} = \frac{m_1}{16\pi e^2\tau^2 n_2 T}\int_{-\infty}^{\infty}\frac{d\omega}{\sinh^2[\omega/(2T)]} \times \int\frac{d^2q}{(2\pi)^2}|\mathcal{D}_{12}(\omega,\boldsymbol{q})|^2\Gamma_1^x(\omega,\boldsymbol{q})\Gamma_2^x(\omega,\boldsymbol{q}). \quad (15)$$

A similar expression[6] can be derived for $\rho_D$ and $\sigma_D$. The nonlinear susceptibility (also known as the rectification function) $\Gamma_i(\omega,\boldsymbol{q})$ (in layer $i$) is a response function relating a voltage $V(r_i)e^{i\omega t}$ to a dc current it induces by the quadratic response:

$$\boldsymbol{J} = \int d\mathbf{r}_1\int d\mathbf{r}_2\Gamma(\omega;\mathbf{r}_1,\mathbf{r}_2)V(\mathbf{r}_1)V(\mathbf{r}_2), \quad (16)$$

with $\boldsymbol{J}$ being the induced dc current. From gauge invariance $\int d\mathbf{r}_1\Gamma(\omega) = \int d\mathbf{r}_2\Gamma(\omega) = 0$.

The same result follows from the standard Kubo formula approach within the diagrammatic perturbation theory (Flensberg *et al.*, 1995; Kamenev and Oreg, 1995), memory function formalism (Zheng and MacDonald, 1993), and the more general Boltzmann-Langevin theory of the stochastic kinetic equation (Chen, Andreev, and Levchenko, 2015).

### 1. Electron-hole asymmetry and rectification

The rectification function $\boldsymbol{\Gamma}(\omega,\boldsymbol{q})$ is the central object in the perturbative theory of Coulomb drag. Equation (15) of the interlayer relaxation rate in terms of $\boldsymbol{\Gamma}(\omega,\boldsymbol{q})$ explicitly demonstrates the key role of electron-hole asymmetry in the leading-order drag effect.[7]

Indeed, in order to induce a voltage (or generate a current) in the passive layer, one needs to somehow move the charge carriers. This is achieved by transferring momentum from the active layer. The macroscopic state of the electronic system in the active layer is characterized by the finite electric current driven by an external source. In a typical electron gas, there are two kinds of excitations—"electronlike," with energies $\epsilon > E_F$ above the Fermi energy (i.e., the occupied states outside the Fermi surface), and "holelike," with $\epsilon < E_F$. These quasiparticles are oppositely charged. As the current is driven through the active layer they move in opposite directions; see Fig. 3. Then the active layer can be characterized by a nonzero total momentum only if there is some asymmetry between electronlike and holelike quasiparticles. Likewise, in the passive layer the momentum is transferred equally to electrons and holes, such that the resulting state can carry the current only in the case of electron-hole asymmetry. In conventional semiconductors (Kamenev and Oreg, 1995), the electron-hole asymmetry appears due to curvature of the conduction band spectrum [leading to the energy dependence of the density of states (DOS) and/or diffusion coefficient]. Consequently, in the Fermi-liquid theory the electron-hole asymmetry can be expressed (Narozhny, Aleiner, and Stern, 2001) as a derivative of the single-layer conductivity $\sigma_{1(2)}$ with respect to the chemical potential (assuming either a constant impurity-scattering time or diffusive transport). The simple estimate $\partial\sigma_{1(2)}/\partial\mu \sim \sigma_{1(2)}/\mu$ then explains the typical smallness of the effect (Solomon *et al.*, 1989; Gramila *et al.*, 1991; Sivan, Solomon, and Shtrikman, 1992); see Eq. (14).

The same arguments can be applied to any system containing carriers with opposite signs of the electric charge. For instance, one can consider semimetals (or even band insulators at high enough temperature), where the electric current can be carried by electrons from the conduction band and holes from

[6]The three quantities $\rho_D$, $\sigma_D$, and $\tau_D^{-1}$ are proportional to each other and differ only by trivial prefactors; see Eqs. (3a) and (13). All three are used in the literature on equal footing.

[7]Another known effect of the electron-hole asymmetry in electronic systems is the thermopower described by the Mott formula (Mott and Jones, 1936; Lunde, Flensberg, and Glazman, 2006, 2007).

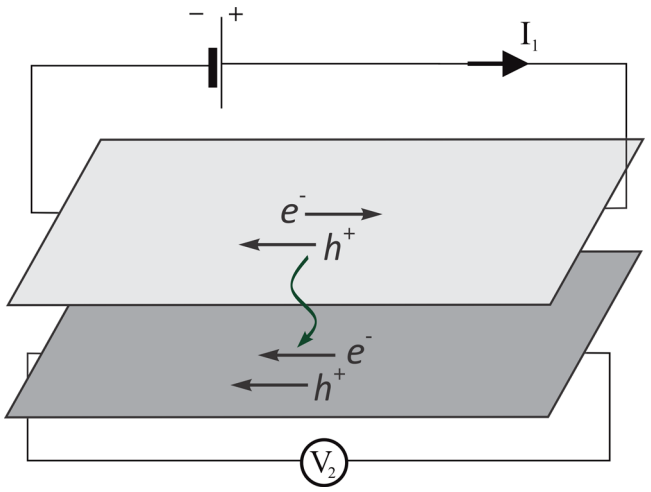


FIG. 3. The momentum transfer due to interlayer interaction. As the current $I_1$ is driven through the active layer, electrons and holes are moving in the opposite directions since they carry the opposite charge. Such a state has nonzero total momentum only due to electron-hole asymmetry. Once the momentum is transferred to the passive layer, the electrons and holes there are pushed in the same direction. This process can induce a voltage again only due to electron-hole asymmetry.

the valence band. A particularly interesting example is graphene (see Sec. IV), which exhibits exact particle-hole symmetry at the charge neutrality point (Katsnelson, 2012). At that point, the nonlinear susceptibility of graphene [Eq. (73)] vanishes (Narozhny, 2007; Tse, Hu, and Sarma, 2007) implying the absence of the drag effect. In contrast, experiment (Gorbachev *et al.*, 2012) shows nonzero drag resistivity at charge neutrality, which in addition is greatly enhanced by the external magnetic field (Titov *et al.*, 2013).

Indeed, the outlined physical picture is not universal. In fact, it describes only a particular (although often dominant) scattering process, where momentum is transferred from an electron-hole pair in the active layer to another electron-hole pair in the passive layer. Technically, this process is described by the leading-order perturbation theory, see Fig. 2, yielding Eq. (15). Higher-order processes [including the so-called "third-order" drag (Levchenko and Kamenev, 2008b; Schütt *et al.*, 2013), see Sec. II.D, and the effect of the correlated disorder (Gornyi, Yashenkin, and Khveshchenko, 1999, 2000; Schütt *et al.*, 2013; Song, Abanin, and Levitov, 2013), see Sec. IV.F] may result in additional contributions which are less sensitive to electron-hole symmetry.

In conventional heterostructures, higher-order processes remain subleading at least within the temperature range where most of the experiments are performed; see Sec. II.D. Specifically in the ballistic regime, the dominant contribution to drag is indeed given by Eq. (15) [with the corresponding drag resistivity Eq. (3a)] and is determined by the nonlinear susceptibility, which in the simplest case of energy-independent impurity-scattering time $\tau$ is given by (Kamenev and Oreg, 1995)

$$\Gamma(\boldsymbol{q},\omega)=\frac{2}{\pi}e\tau\boldsymbol{q}\frac{\omega}{v_F q}\theta(v_F q-\omega). \tag{17}$$

As shown in Kamenev and Oreg (1995), the resulting Eq. (17) for the nonlinear susceptibility is proportional to the imaginary part of the single-layer polarization operator

$$\boldsymbol{\Gamma}(\boldsymbol{q},\omega)=\frac{2e\tau\boldsymbol{q}}{m}\mathrm{Im}\Pi^R(\boldsymbol{q},\omega), \tag{18}$$

where (for two-dimensional, noninteracting electron gas in the ballistic regime)

$$\mathrm{Im}\Pi^R(\boldsymbol{q},\omega)=\nu\frac{\omega}{v_F q}\theta(v_F q-\omega). \tag{19}$$

Within the kinetic theory, one can observe Eq. (18) already at the level of the collision integral (Giuliani and Quinn, 1982); hence many [see, e.g. Jauho and Smith (1993), Zheng and MacDonald (1993), Shimshoni and Sondhi (1994), and Ussishkin and Stern (1997)] proceed to express Eq. (15) in terms of $\mathrm{Im}\Pi^R(\boldsymbol{q},\omega)$ instead of the nonlinear susceptibility. Under the assumption of energy-independent impurity-scattering time $\tau$ and neglecting intralayer correlations (Flensberg *et al.*, 1995; Kamenev and Oreg, 1995), such calculations lead to the correct result [see Eq. (21)]. At the same time, within such an approach the physics of electron-hole asymmetry remains hidden. Generalization to more general settings is also nontrivial: Eq. (18) is by no means a general theorem (Flensberg *et al.*, 1995; Kamenev and Oreg, 1995; Narozhny and Aleiner, 2000; Narozhny *et al.*, 2012); for explicit examples of the two quantities being inequivalent see Secs. III and IV.

### 2. Drag resistivity in ballistic samples

In the limit of strong screening $\varkappa d\gg 1$, one can approximate (Kamenev and Oreg, 1995) the interlayer interaction propagator (7) by

$$\mathcal{D}_{12}^R=-\frac{\pi e^2}{\varkappa_1\varkappa_2}\frac{q}{\sinh qd}. \tag{20}$$

Combining Eq. (20) and the nonlinear susceptibility (18) with the interlayer relaxation rate (15) and Eq. (3a), one finds the following expression for the drag resistivity (Jauho and Smith, 1993; Zheng and MacDonald, 1993; Flensberg and Hu, 1994; Kamenev and Oreg, 1995):

$$\rho_D=\frac{\hbar}{e^2}\frac{\pi^2\zeta(3)}{16}\frac{T^2}{E_{F1}E_{F2}}\frac{1}{\varkappa_1\varkappa_2 k_{F1}k_{F2}d^4}. \tag{21a}$$

The same result can also be expressed[8] in terms of the interlayer relaxation rate (15) [e.g., using Eq. (3a)]

[8]Most expressions for $\rho_D$ (Jauho and Smith, 1993; Zheng and MacDonald, 1993; Flensberg and Hu, 1994; Flensberg *et al.*, 1995; Rojo, 1999) can be reduced to Eqs. (21) using the following simple relations, valid under the assumptions of this section: $E_F=\pi n/m$, $n=E_F\nu$, and $\nu D=E_F\tau/\pi$, where $D=v_F^2\tau/2$ is the diffusion constant and $\nu=m/\pi$ is the density of states.

$$\tau_D^{-1} = \frac{\pi^2\zeta(3)}{16}\frac{n_1}{m_2}\frac{T^2}{E_{F1}E_{F2}}\frac{1}{\varkappa_1\varkappa_2 k_{F1}k_{F2}d^4}. \tag{21b}$$

Physically, these expressions (see footnote 8) can be understood based on the Fermi golden rule [which was explicitly used in the solution of the kinetic equation (Laikhtman and Solomon, 1990; Jauho and Smith, 1993)]. Indeed, there are three basic elements that combine into the result (21): (i) the phase space available for electron-hole pairs in the two layers, which is limited by temperature, hence $\tau_D^{-1} \propto T^2$; (ii) the electron-hole asymmetry, which results in the overall smallness of the effect, $\tau_D^{-1} \propto (E_{F1}E_{F2})^{-1}$; and (iii) the matrix element of the interlayer interaction, determining the dependence on the interlayer separation; in the ballistic case the matrix element is dominated by small-angle scattering (Gramila *et al.*, 1991).

The drag resistivity (21), and especially the quadratic temperature dependence, is often quoted as the "Fermi-liquid" result. However, Eq. (21) was obtained under a number of assumptions: (i) $\varkappa d \gg 1$, (ii) $d \gg \ell$, and (iii) $T \ll T_d \sim v_F/d \sim E_F/(k_F d)$. The latter assumption appears only implicitly and is often overlooked.

Indeed, substituting the interaction propagator (20) and the nonlinear susceptibility (17) into Eq. (15), one finds that except for the $\theta$ function in Eq. (17) the frequency and momentum integrals factorize. The exponential decay of the corresponding integrands allows one to estimate the typical values of transferred energy $\omega \sim T$ and momentum $q \sim 1/d$. Assuming $T \ll T_d$, this yields $\omega < v_F q$, which automatically satisfies the $\theta$ function. Based on this observation, one may omit the $\theta$ function and subsequently extend the integration limits in both integrals in Eq. (15) to infinity. The remaining integration is straightforward and yields Eq. (21).

At higher temperatures $T \gg T_d$, the $\theta$ function in Eq. (17) is not satisfied automatically. Physically, it represents kinematic restrictions on the phase space available to electron-hole pairs associated with predominantly small-angle scattering (Gramila *et al.*, 1991). The frequency integration is now cut off at $v_F q$ (or $T_d$), rather than $T$, which leads to the *linear* temperature dependence [first reported by Gramila *et al.* (1991) and Solomon and Laikhtman (1991), see also Jauho and Smith (1993), and recently rediscovered by Chen, Andreev, and Levchenko (2015)],

$$\rho_D(T \gg T_d) = \frac{\hbar}{e^2}\frac{\pi^3}{360}\frac{1}{(k_F d)^3(\varkappa d)^2}\frac{T}{E_F}. \tag{22}$$

This behavior may be observable in samples with either nondegenerate 2DEGs or large interlayer separation. In the latter case $T_d \ll T \ll E_F$, both layers are perfectly described by the Fermi-liquid theory which is not synonymous with quadratic temperature dependence of transport coefficients.

### 3. Plasmon contribution

The approximate form of the interlayer Coulomb interaction (20) appears justified in the "ballistic" regime where the dominant interlayer relaxation processes are characterized by relatively large momentum transfers $\omega < v_F q$. The imaginary part of the single-particle polarization operator (19) vanishes at smaller momenta (or larger frequencies) making these calculations consistent. At the same time, approximating the interlayer interaction propagator (7) by Eq. (20) one completely neglects a possible contribution of plasmon modes that (within the simplest RPA approach) can be found by setting the denominator of Eq. (7) to zero. At zero temperature and for $\omega \gg v_F q$ (where $\mathrm{Im}\Pi^R = 0$), the polarization operator is known to be given by (Stern, 1967)

$$\Pi(\boldsymbol{q}, \omega) \simeq -nq^2/(m\omega^2).$$

Using this expression and expanding the bare Coulomb potential in small momenta yields the acoustic ("−") and optical ("+") plasmon modes with dispersions

$$\omega_- = eq\sqrt{2\pi nd/m}, \qquad \omega_+ = e\sqrt{4\pi nq/m}.$$

Both of these modes lie outside of the particle-hole continuum and in the parameter region, where the nonlinear susceptibility (17) vanishes. Hence, one may conclude that the plasmons cannot contribute to frictional drag.

However, at finite temperatures thermally excited quasiparticles and plasmons may coexist in the same parameter region, which may result in an additional contribution to drag (Flensberg and Hu, 1994). In order to accurately describe the plasmon contribution to $\rho_D$, one has to consider intralayer equilibration due to electron-electron collisions (Chen, Andreev, and Levchenko, 2015) which gives rise to two important features: (i) the polarization operator acquires nonvanishing spectral weight within the high-frequency part of the spectrum at $\omega > v_F q$ (Flensberg and Hu, 1994), and (ii) the plasmons acquire a finite lifetime (Hruska and Spivak, 2002; Mishchenko, Reizer, and Glazman, 2004) that regularizes the pole in the interaction propagator.

The theory discussed in Secs. II.A, II.B.1, and II.B.2 is based on the implicit assumption that the intralayer equilibration is the fastest process in the system. Characterizing inelastic electron-electron scattering by the quasiparticle lifetime $\tau_{ee}$, one finds that the standard theory [and hence Eq. (22)] is valid as long as the time $\tau_{ee}$ is much smaller than the interlayer scattering time $\tau_{ee} \ll \tau_D$ and at temperatures below the corresponding threshold $T \ll T_c \sim E_F\sqrt{k_F/(\varkappa^2 d)}$.

At higher temperatures $T > T_c$, the system enters the collision-dominated regime, where Coulomb drag is dominated by plasmons. In this regime, Chen, Andreev, and Levchenko (2015) found a stronger temperature dependence

$$\rho_D(T_c < T < T_h) \simeq \frac{\hbar}{e^2}\frac{1}{(k_F d)^4}\frac{T^3}{E_F^3}. \tag{23}$$

The rise of the plasmon contribution to drag persists so long as the quasiparticle decay rate remains small compared to the plasma frequency (at the wave vector $1/d$), i.e., up to the third crossover temperature $T_h \sim E_F\sqrt{k_F/\varkappa}\sqrt[4]{1/(\varkappa d)}$. At temperatures above the crossover $T > T_h$, the electronic system enters the hydrodynamic regime that can be understood on the basis of the classical Navier-Stokes hydrodynamics (Apostolov, Levchenko, and Andreev, 2014). In this limit the drag resistivity decays as

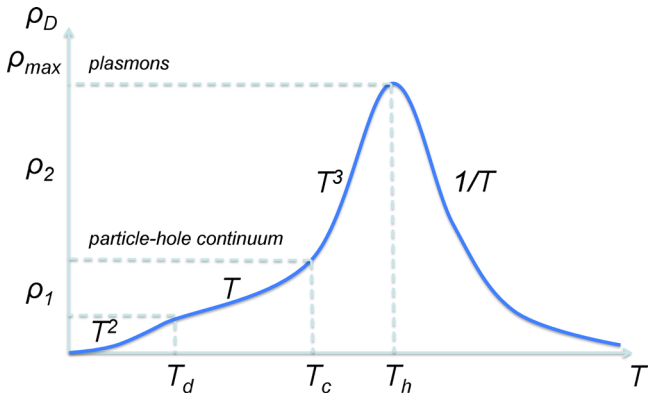


FIG. 4. Schematic illustration for the drag resistivity at high temperatures showing the plasmon peak at $T \sim T_h$. The asymptotic dependences are exaggerated for clarity. Definitions of the three crossover scales are given in the main text. From Chen, Andreev, and Levchenko, 2015.

$$\rho_D(T > T_h) \simeq \frac{\hbar}{e^2} \frac{1}{(k_F d)^2 (\varkappa d)^3} \frac{E_F}{T}. \tag{24}$$

The resulting temperature dependence of the drag coefficient is summarized in Fig. 4. The nonmonotonicity of $\rho_D$ originates from the delicate interplay of various scattering channels in the electronic system. Perhaps the most striking feature of the theory of Chen, Andreev, and Levchenko (2015) is that intralayer collisions promote stronger drag. Indeed, should one naively continue Eq. (22) up to the temperatures of the order $T_h$ one would underestimate the actual maximum value of $\rho_D$ by $\sqrt{k_F d} \gg 1$.

### C. Effects of potential disorder

In ballistic samples, potential disorder played a limited role. In fact, the resulting drag resistivity (21) is independent of the impurity-scattering time $\tau$. In diffusive samples with $d \gg \ell$ only small momenta $q \ll 1/\ell$ can be transferred between the layers. Typically this results in a small contribution to the drag resistivity, which in ballistic samples can be neglected. This is not always the case—at low enough temperatures drag is dominated by mesoscopic fluctuations which are mostly due to processes with small momentum transfers; see Sec. III.

Coulomb drag in diffusive systems was considered by Zheng and MacDonald (1993) using the memory function formalism and by Kamenev and Oreg (1995) using the diagrammatic technique. To the lowest order in interlayer interaction, one can use the Kubo formula analysis (Kamenev and Oreg, 1995; Narozhny and Aleiner, 2000) to derive the expression for the drag conductivity ($S$ is the area of the sample)

$$\sigma_D = \frac{1}{16\pi T S} \int \frac{d\omega}{\sinh^2(\omega/2T)} D^R_{12} \Gamma^x_{23} D^A_{34} \Gamma^{x*}_{41}, \tag{25}$$

where numerical subscripts indicate spatial coordinates and are implied to be integrated over. Averaging over disorder restores translational invariance. In the absence of interlayer disorder correlations [this special case was considered by Gornyi, Yashenkin, and Khveshchenko (1999)], the nonlinear susceptibilities in each layer have to be averaged independently of each other. Then one recovers the drag relaxation rate (15), where each quantity should be understood as disorder averaged, i.e., $\langle \Gamma^x_{23} \rangle \to \Gamma^x(\boldsymbol{q})$.

#### 1. Drag resistivity in diffusive regime

In the diffusive regime, the nonlinear susceptibility $\boldsymbol{\Gamma}$ can be found from Ohm's law (Landau, Lifshitz, and Pitaevskii, 1984),

$$\boldsymbol{j} = \hat{\sigma} \boldsymbol{E} - eD \boldsymbol{\nabla} n, \tag{26}$$

where $\hat{\sigma}$ is the conductivity matrix and $D$ is the diffusion coefficient (in two dimensions $D = v_F^2 \tau/2$). Combining Eq. (26) with the continuity equation, one finds the linear response of the carrier density $n$ to the electric field $\boldsymbol{E}$:

$$\langle n(\boldsymbol{q}, \omega) \rangle = \frac{1}{e} \frac{i q^\alpha \sigma^{\alpha\beta} E^\beta(\boldsymbol{q}, \omega)}{-i\omega + Dq^2}, \tag{27}$$

where $\langle \cdots \rangle$ indicates averaging over disorder. Nonlinear response follows from the density dependence of the conductivity $j_{dc} = \mathrm{Re}(\partial\sigma/\partial n) n(\boldsymbol{q}, \omega) E(-\boldsymbol{q}, -\omega)$ and yields

$$\langle \Gamma^\gamma \rangle = \frac{2\nu}{e} \frac{\partial \langle \sigma^{\gamma\delta} \rangle}{\partial n} q^\delta \frac{\omega D q^2}{\omega^2 + D^2 q^4}. \tag{28}$$

In the absence of a magnetic field $\langle \sigma^{\alpha\beta} \rangle = \sigma \delta^{\alpha\beta}$, and the nonlinear susceptibility (28) is parallel to $\boldsymbol{q}$. The disorder-averaged conductivity is linear in the carrier density $\partial\sigma^{\alpha\beta}/\partial n \approx \sigma^{\alpha\beta}/n$. As a result,

$$\langle \boldsymbol{\Gamma} \rangle = 2\boldsymbol{q} \frac{e\nu D}{E_F} \frac{\omega D q^2}{\omega^2 + D^2 q^4}. \tag{29}$$

This expression can be recast into two equivalent forms. Noting the similarity between Eq. (29) and the standard diffusive form of the polarization operator (Altshuler and Aronov, 1985; Smith and Jensen, 1989)

$$\Pi^R(\boldsymbol{q}, \omega) = \nu \frac{Dq^2}{-i\omega + Dq^2}, \tag{30}$$

one finds (Kamenev and Oreg, 1995)

$$\langle \boldsymbol{\Gamma} \rangle = 2\boldsymbol{q} \frac{eD}{E_F} \mathrm{Im}\Pi^R(\boldsymbol{q}, \omega). \tag{31}$$

Furthermore, one can emphasize the fact that the density dependence of the conductivity $\sigma$ is a manifestation of electron-hole asymmetry by rewriting the fraction in Eq. (31) as (Narozhny and Aleiner, 2000)

$$\langle \boldsymbol{\Gamma} \rangle = 2e\boldsymbol{q} D \frac{\partial \ln(\nu D)}{\partial \mu} \mathrm{Im}\Pi^R(\boldsymbol{q}, \omega). \tag{32}$$

In the simplest case (see footnote 8), this expression can be obtained directly from Eq. (28) by noticing that

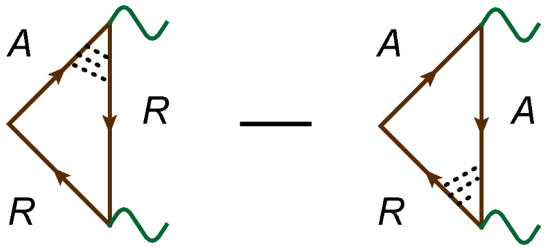


FIG. 5. Disorder averaging of the nonlinear susceptibility (Kamenev and Oreg, 1995). The dotted lines represent the diffuson ladder (Altshuler and Aronov, 1985).

$\partial\sigma^{\alpha\beta}/\partial n = (\partial\sigma^{\alpha\beta}/\partial\mu)(\partial\mu/\partial n) = (\partial\sigma^{\alpha\beta}/\partial\mu)(1/\nu)$ and using the Einstein relation. The same result can be found evaluating diagrams shown in Fig. 5.

The diffusive approximation for the interlayer interaction follows from Eqs. (7) and (30). Focusing on small momenta $q \ll 1/d$, one can obtain alternative expressions for the interaction propagator by either expanding the bare matrix element (5) in small $qd$ (and subsequently limiting the momentum integration from above) or keeping the exponential in Eq. (5) intact, leaving the momentum integral converging in the ultraviolet. The former approach was taken by Narozhny and Aleiner (2000). Generalizing to inequivalent layers one finds

$$\mathcal{D}_{12}^{R} = -\frac{1}{q^2}\frac{(-i\omega + D_1 q^2)(-i\omega + D_2 q^2)}{(\nu_1 D_1 + \nu_2 D_2)[-i\omega + (1+\varkappa^* d)D^* q^2]}, \tag{33a}$$

where

$$\varkappa^* = 4\pi e^2 \frac{\nu_1\nu_2}{\nu_1+\nu_2}, \qquad D^* = \frac{(\nu_1+\nu_2)D_1 D_2}{\nu_1 D_1 + \nu_2 D_2}.$$

The latter alternative was taken by Kamenev and Oreg (1995), where in addition (just as in the ballistic case) the limit $\varkappa d \gg 1$ was used. As a result, the interaction propagator takes the form

$$\mathcal{D}_{12}^{R} = -\frac{\pi e^2 q}{\varkappa_1\varkappa_2 \sinh qd}\frac{-i\omega + D_1 q^2}{D_1 q^2}\frac{-i\omega + D_2 q^2}{D_2 q^2}. \tag{33b}$$

With logarithmic accuracy, the resulting drag coefficient is independent of the distinction between the two and can be written as (Kamenev and Oreg, 1995)

$$\langle\rho_D\rangle = \frac{\hbar}{e^2}\frac{\pi^2 T^2}{12 E_{F1}E_{F2}}\frac{1}{\varkappa_1\varkappa_2 k_{F1}k_{F2}\ell_1\ell_2 d^2}\ln\frac{T_0}{2T}. \tag{34a}$$

The only difference between using the two expressions for the interaction propagator in Eq. (33) is the exact value of $T_0$. Using Eq. (33a) in the limit $\varkappa^* d \gg 1$, one finds

$$T_0 = \frac{4\pi e^2 \nu_1 D_1 \nu_2 D_2}{(\nu_1 D_1 + \nu_2 D_2)d},$$

while Eq. (33b) leads to (Kamenev and Oreg, 1995)

$$T_0 = \min\{\varkappa_1 D_1, \varkappa_2 D_2\}/d.$$

Both expressions are of the same order of magnitude and coincide for the case of identical layers.

The result can be expressed also in terms of the interlayer relaxation rate (Zheng and MacDonald, 1993)

$$\frac{1}{\tau_D} = \frac{\pi^2}{12}\frac{n_1}{m_2}\frac{T^2}{E_{F1}E_{F2}}\ln\frac{T_0}{2T}\frac{1}{\varkappa_1\varkappa_2 k_{F1}k_{F2}\ell_1\ell_2 d^2}. \tag{34b}$$

Equivalently, one can use Eq. (32) and express the drag conductivity (Narozhny and Aleiner, 2000) as (here the layers are assumed to be identical for simplicity)

$$\sigma_D = \frac{e^2}{\hbar}\frac{\pi^2}{3}\frac{(\hbar T)^2}{g^2(\varkappa d)^2}\left(\frac{\partial}{\partial\mu}(\nu D)\right)^2 \ln\frac{T_0}{2T}, \tag{35}$$

where the derivative highlights the crucial role of the electron-hole asymmetry in the leading-order drag effect.

The diffusive result for the drag resistivity (34) appears to be rather similar to its ballistic counterpart Eq. (21). Indeed, disregarding the numerical prefactors and the logarithm in Eq. (34), one finds

$$\rho_D^{\rm diff}/\rho_D^{\rm bal} \sim d^2/(\ell_1\ell_2). \tag{36}$$

This relation may serve as an *a posteriori* justification for the statement that the drag effect in samples with $d \ll \ell$ is dominated by ballistic propagation of carriers with momenta $\ell^{-1} \ll q \ll d^{-1}$. Carriers with small momenta $q \ll \ell^{-1}$ also participate in drag, but their contribution is small [according to Eq. (36)] and is typically neglected.

### 2. Weak localization corrections

The nonlinear susceptibility (29) and drag coefficient (34) were obtained as the leading approximation in the standard perturbation theory of disordered metals (Altshuler and Aronov, 1985), controlled by the large parameter $g = 25.8\ \mathrm{k\Omega}/R_\square$ representing the dimensionless conductance of the layers [with $R_\square$ being the layer (sheet) resistance]. Within the assumptions adopted in this section (see footnote 8) $g \sim \nu D \sim k_F\ell \sim E_F\tau \gg 1$.

The next-order terms in the perturbation theory are known as quantum corrections to transport coefficients (Altshuler and Aronov, 1985; Aleiner, Altshuler, and Gershenson, 1999). Physically, they describe leading interference processes that arise in the course of subsequent scattering events. Although the resulting contribution to transport is proportional to a small factor $1/g$, quantum corrections dominate the temperature and magnetic field dependence of transport coefficients at low temperatures.

To the leading order in $1/g$, one may distinguish three types of corrections: (i) interference between self-intersecting, time-reversed scattering paths leads to a positive correction to resistivity, known as the weak localization correction (Abrahams *et al.*, 1979; Gorkov, Larkin, and Khmel'nitzkii, 1979; Altshuler *et al.*, 1980); (ii) coherent scattering off Friedel oscillations yields the Altshuler-Aronov correction (Altshuler and Aronov, 1979; Finkelstein, 1983, 1984; Zala,

Narozhny, and Aleiner, 2001); and (iii) in small, mesoscopic samples interference between scattering paths gives rise to universal conductance fluctuations (Altshuler, 1985; Lee and Stone, 1985). The latter effect has a direct counterpart in double-layer systems, namely, mesoscopic fluctuations of Coulomb drag discussed in Sec. III. At the time of writing, no qualitative interference effect due to electron-electron interaction has been identified for drag measurements. At the technical level, the third-order drag effect (see Sec. II.D) bears certain resemblance to the Altshuler-Aronov diagrams (Gornyi and Narozhny, 2014). Here we discuss the weak localization correction to Coulomb drag (Flensberg *et al.*, 1995; Kamenev and Oreg, 1995).

In the absence of interlayer disorder correlations [such effects were discussed by Gornyi, Yashenkin, and Khveshchenko (1999)], impurity scattering is confined to each individual layer. It should come as no surprise that the same mechanism behind the weak localization correction to single-layer conductivity (i.e., interference between time-reversed, self-intersecting paths) yields a correction to the nonlinear susceptibility. Technically, this interference mechanism is described by a "maximally crossed" element of the diagram technique known as the Cooperon (Gorkov, Larkin, and Khmel'nitzkii, 1979). Diagrams for the corresponding corrections to the nonlinear susceptibility are shown in Fig. 6 [further corrections, e.g., two-Cooperon diagrams, considered by Flensberg *et al.* (1995) and Kamenev and Oreg (1995) were found to be subleading]. The resulting nonlinear susceptibility is given by

$$\langle \mathbf{\Gamma} \rangle = 2\boldsymbol{q} \frac{e\nu D(\tau_\varphi^{-1},0)}{E_F} \frac{\omega D(\omega,\boldsymbol{q}) q^2}{\omega^2 + D^2(\omega,\boldsymbol{q}) q^4}, \tag{37}$$

where the renormalized diffusion coefficient in two dimensions is (Gorkov, Larkin, and Khmel'nitzkii, 1979)

$$D(\omega,\boldsymbol{q}) = D\left(1 - \frac{1}{\pi k_F \ell} \ln \frac{1}{\omega\tau}\right), \tag{38}$$

and $\tau_\varphi$ is the dephasing time (Altshuler *et al.*, 1980). The result (37) is valid in the first order in $\delta D = D(\omega,\boldsymbol{q}) - D$.

The resulting leading-order weak localization correction to Coulomb drag is (Kamenev and Oreg, 1995)

$$\frac{\delta\rho_D}{\rho_D} = -\frac{1}{\pi k_{F1}\ell_1} \ln \frac{1}{2T\tau_1} - \frac{1}{\pi k_{F2}\ell_2} \ln \frac{1}{2T\tau_2}, \tag{39}$$

where $\rho_D$ is given by Eq. (34). The result (39) is similar to the weak localization corrections in 2D (Gorkov, Larkin, and Khmel'nitzkii, 1979; Altshuler *et al.*, 1980), except that in Eq. (39) the logarithmic singularity is cut by temperature rather than by the dephasing time.

In conventional 2DEG, weak localization effects result in a dependence on a weak magnetic field (Altshuler *et al.*, 1980). Here the characteristic scale of the magnetic field is $H_c \sim T/eD$. A similar scale describes intralayer interaction corrections to magnetoresistance (Altshuler and Aronov, 1985), making the weak localization corrections to the drag coefficient hard to observe experimentally (Kamenev and Oreg, 1995).

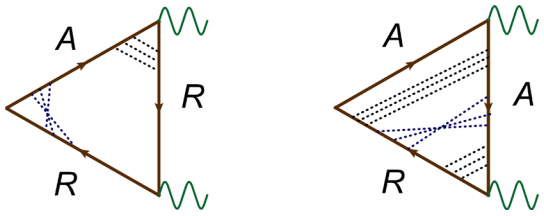


FIG. 6. Leading weak localization corrections to the nonlinear susceptibility (Kamenev and Oreg, 1995). The black, parallel dotted lines represent the diffuson ladder (Altshuler and Aronov, 1985; Aleiner, Altshuler, and Gershenson, 1999). The dotted (blue), crossing lines represent the Cooperon (Gorkov, Larkin, and Khmel'nitzkii, 1979).

### D. Third-order drag effect

The leading contribution to Coulomb drag, Eqs. (15) and (25), describes the effect to the lowest order in the interlayer Coulomb interaction; see Fig. 2. Since the particles belonging to different layers interact through a layer of an insulating material, a certain weakness of the effective interaction is intuitively expected. In many-body electron systems the Coulomb interaction is usually screened and the perturbative analysis gives a reasonable account of most basic observable quantities (Ziman, 1965; Altshuler and Aronov, 1985). Consequently, the vast majority of theoretical studies of Coulomb drag are devoted to the investigation of the lowest-order effect. Notable exceptions are given by the studies of the interlayer correlated states, in the context of either quantum Hall devices (Girvin and MacDonald, 1997; Yang, 1998; Stern *et al.*, 2000; Kim *et al.*, 2001; Yang and MacDonald, 2001; Stern and Halperin, 2002) or quantum wires (Nazarov and Averin, 1998; Klesse and Stern, 2000), as well as strongly correlated intralayer states, such as Wigner crystals (Baker and Rojo, 2001; Braude and Stern, 2001) or Anderson insulators (Raikh and von Oppen, 2002).

The "single-particle" drag resistivity, Eqs. (21) and (34), is determined (besides the interlayer interaction) by the quasiparticle phase space, electron-hole asymmetry (see Sec. II.B), and disorder effects (see Secs. II.C and III). At $T = 0$ or at a point of exact electron-hole symmetry (e.g., in neutral graphene, see Sec. IV), these factors may conspire to nullify the effect. Then $\rho_D$ may be determined by higher orders of the perturbation theory, implying that saturation of drag resistivity at low temperatures should not necessarily point toward a strongly correlated state.

To the third order in interlayer interaction (see Fig. 7 for the "skeleton" diagram), Coulomb drag was first discussed by Levchenko and Kamenev (2008b) in the diffusive regime $T\tau \ll 1$. It was shown that the third-order drag contribution remains finite at zero temperature[9]:

[9]More precisely, the result is valid down to lowest temperatures $T \sim \tau^{-1} e^{-\pi g}$. Below this scale the diffusive approximation breaks down.

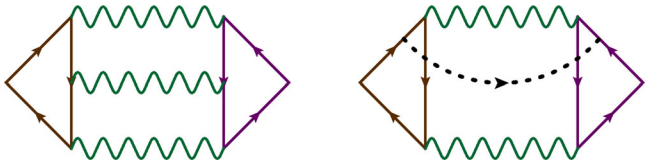

FIG. 7. Typical diagrams describing higher-order drag effects. Left: Third-order drag (Levchenko and Kamenev, 2008b). Right: The effect of interlayer disorder correlations (Gornyi, Yashenkin, and Khveshchenko, 1999; Hu, 2000a).

$$\rho_D^{(3)}(T < h/\tau) = 0.27(h/e^2)g^{-3}(\varkappa d)^{-2}. \tag{40}$$

This surprising result was attributed (Levchenko and Kamenev, 2008b) to the singular behavior of matrix elements in the diffusive regime. In single-layer systems, a similar enhancement of the matrix elements leads to singular interaction effects (Altshuler and Aronov, 1985). Here the divergence of the matrix elements is compensated by the smallness of the phase space yielding the $T$-independent contribution to the drag resistivity.

The third-order effect (40) does not rely on electron-hole asymmetry (technically, the third-order diagram in Fig. 7 contains four-point vertices instead of the triangular vertices in Fig. 2). Hence, $\rho_D^{(3)}$ is independent of $E_F$. This provides an additional explanation of the $T$-independent result (40): in the diffusive regime there is no other scale for a temperature dependence.

Another contribution to drag that is insensitive to electron-hole symmetry is due to interlayer disorder correlations (Gornyi, Yashenkin, and Khveshchenko, 1999; Hu, 2000a). For temperatures higher than the inverse interlayer coherence time, but still in the diffusive regime $\tau_g^{-1} \ll T \ll \tau$, one finds

$$\rho_D(\tau_g^{-1} \ll T \ll \tau_{tr}^{-1}) \sim (h/e^2)(k_F^2 d^2 \varkappa \ell)^{-2} \ln(T\tau_g), \tag{41}$$

which might dominate over Eq. (34).

While these higher-order effects have not been observed in semiconductor samples, they may provide an explanation of the observed nonzero drag resistivity in neutral graphene (Gorbachev *et al.*, 2012); see Sec. IV.

### E. Transconductance due to tunneling bridges

A qualitatively different mechanism of transconductance takes place in the double-layer systems with pointlike shortages (bridges) or when the insulating layer is sufficiently thin such that electrons may tunnel between the two layers (Raichev, 1997; Oreg and Kamenev, 1998; Oreg and Halperin, 1999). Such bridges can be present in metallic double-layer systems due to device fabrication imperfections, or they can be introduced on purpose (Giordano and Monnier, 1994).

One should distinguish two mechanisms of transresistivity due to tunneling. The first one is essentially classical and originates from a voltage drop in the passive layer due to the current leaking directly from the active layer. This mechanism can be simply visualized and understood using a resistive network model where the two layers are connected in parallel by a set of resistors (Raichev, 1997). Applying Kirchhoff's laws to such a circuit, one finds that for sufficiently long samples $L > \sqrt{D\tau_{12}}$ (here $\tau_{12}$ is the mean intralayer scattering time associated with the interlayer tunneling conductance per unit area $\sigma_\perp = e^2\nu/\tau_{12}$), half of the current supplied to the active layer leaks into the passive one. In this case, the *sign* of the drag effect is *reversed* compared to the standard result of Eq. (3a) and $\rho_D$ is given by the resistance of a single layer of a doubled width. This classical effect is practically insensitive to temperature. Furthermore, the tunneling rate $\tau_{12}$ is strongly dependent on a Fermi-surface mismatch between the layers and thus may be affected by a gate voltage or an in-plane magnetic field (Boebinger *et al.*, 1991; Berk *et al.*, 1995), which gives an experimental knob to control the magnitude of the classical tunnel drag resistivity.

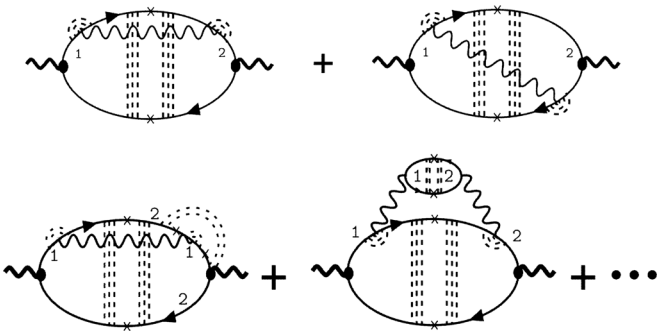

FIG. 8. Top: Two diagrams contributing to the transconductance that are second order in the tunneling matrix element denoted by a cross. The solid lines with arrows are electron Green's functions, the dashed lines represent diffusons, and the wavy lines screened interactions. Two additional diagrams with arrows in the opposite direction should be included. The numbers indicate the layer index. Bottom: Examples of diagrams contributing to the transconductance that are fourth order in tunneling. Diagrams with interaction lines connecting "upper" and "lower" Green's functions, as well as diagrams with an opposite direction of electron lines are also implicit. From Oreg and Kamenev, 1998.

The second, purely quantum effect was suggested by Oreg and Kamenev (1998) and Oreg and Halperin (1999). Here drag originates from the intralayer exchange correlations due to wave-function overlap of carriers in different layers (that may exist in the presence of interlayer tunneling). The sign of the quantum effect is *negative* for the carriers of the same charge, i.e., the same as in the above classical effect. This mechanism yields a strongly temperature-dependent drag resistivity, which saturates to a constant value at zero temperature. The latter feature is an indication that the exchange contribution to drag resistivity does not require electron-hole asymmetry. Hence, even for a small tunneling rate, this mechanism may become stronger than the standard effect of Eq. (3a) at low enough temperatures.

The interplay among tunneling, Coulomb interaction, and intralayer disorder scattering yields the three energy scales $\tau_{12}^{-1}$, $\varkappa d\tau_{12}^{-1}$, and $\tau^{-1}$. Here the factor of $\varkappa d$ stems from the screening effects. At high temperatures $T > \tau^{-1}$, the quantum drag resistivity can be computed to the lowest order in tunneling (the corresponding diagrams are shown in Fig. 8, top panel). Furthermore, since for $T\tau \gg 1$ the motion of electrons is ballistic, one can omit disorder ladders (diffusons)

in these diagrams. Then the transconductance is given by the temperature-independent expression (Oreg and Kamenev, 1998)

$$\sigma_D = -\frac{e^2}{\hbar}\frac{\pi}{32}\frac{1}{\varkappa d}\frac{v_F\tau^2}{d\tau_{12}}. \tag{42}$$

At lower temperatures $T < \tau^{-1}$, the diffusive character of the electron motion should be taken into account. The drag resistivity can still be computed to the leading order in tunneling using the same set of diagrams in Fig. 8 (top panel), but with the insertion of disorder renormalizations. As a result, one finds the following temperature-dependent contribution to the transconductance (Oreg and Kamenev, 1998):

$$\sigma_D = -\frac{e^2}{\hbar}\frac{1}{24\pi}\frac{\ln(\varkappa d)}{\varkappa d}\frac{1}{T\tau_{12}}. \tag{43}$$

In the diffusive limit, such singular temperature dependence is not entirely unexpected. Indeed, the diagrams in Fig. 8 (top) are analogous to the Altshuler-Aronov corrections to the conductivity of 2D systems, which are known to be logarithmically singular (Altshuler and Aronov, 1985; Zala, Narozhny, and Aleiner, 2001). In the present context, the interplay of tunneling and Coulomb interaction makes this singularity stronger.

Quantum physics becomes even more pronounced at lower yet temperatures $T < \varkappa d\tau_{12}^{-1}$, where the quantum drag mechanism is dominated by coherent tunneling of electrons to the passive layer and back to the active one accompanied by intralayer Coulomb interactions; see Fig. 8 (bottom). In this regime, the temperature dependence is even stronger (Oreg and Kamenev, 1998)

$$\sigma_D = -\frac{e^2}{\hbar}\frac{3\zeta(3)}{8\pi^4}\frac{\ln(T\tau_{12})}{(T\tau_{12})^2}. \tag{44}$$

The low-temperature divergence in the transconductance of Eqs. (43) and (44) should be cut off by the finite-size effects at the Thouless energy $E_T = D/L^2$. Interestingly enough, for large systems $L \gg \sqrt{D\tau_{12}}$, there is an additional temperature range $E_T < T < \tau_{12}^{-1}$, where the exchange contribution to $\sigma_D$ is due to multiple tunneling processes. In that case, the transconductance becomes logarithmic in temperature (Oreg and Kamenev, 1998)

$$\sigma_D = -\frac{e^2}{\hbar}\frac{1}{8\pi^2}\ln\frac{1}{T\tau_{12}}. \tag{45}$$

Up to the factor of $1/4$, this result coincides with the standard Altshuler-Aronov correction to the 2D conductivity (Altshuler and Aronov, 1985; Zala, Narozhny, and Aleiner, 2001). This extra numerical factor is not accidental and reflects the essence of the drag measurement setup, where the current is allowed to flow in one part of the system only while the induced potential is measured in another part.

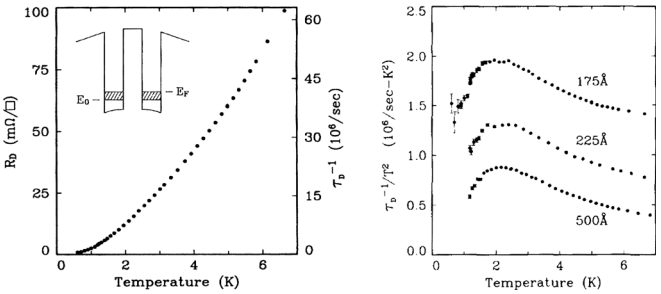


FIG. 9. Left panel: Temperature dependence of the drag resistivity GaAs double-quantum wells. The additional scale on the right provides the corresponding values of the momentum-transfer rate (see main text for more details). Inset: An idealized energy diagram for a double-quantum-well structure indicating the ground subband energy $E_0$ and the Fermi energy $E_F$. From Gramila *et al.*, 1991. Right panel: Temperature dependence of the interlayer momentum transfer rate divided by $T^2$. The three sets of data were measured in samples with interwell barrier widths of 175, 225, and 500 Å. From Gramila *et al.*, 1992.

### F. Comparison to experiment

The theory outlined in the preceding sections describes an idealized phenomenon of mutual friction between two two-dimensional electron systems. The electrons were assumed to belong to a parabolic band, with energy-independent impurity-scattering time and negligible intralayer correlations. Clearly, such assumptions can be realized in any experimental sample only approximately.

Coulomb drag between two two-dimensional electron gases was first observed by the group of J. Eisenstein (Gramila *et al.*, 1991; Eisenstein, 1992) in GaAs double-quantum wells; see Fig. 9. A detailed comparison of the experimental data to the quantitative predictions of the Coulomb drag theory showed that the latter accounts for about 50% of the measured values.[10] This was judged as sufficient evidence of the relevance of the Coulomb mechanism of frictional drag. Also, the overall reduction of the drag resistance with the increase of the interwell barrier width (see Fig. 9) was in rough agreement with Eq. (21b). At the same time, the data (see the right panel in Fig. 9) show noticeable deviations from the $T^2$ behavior predicted by Eqs. (21) and (34), indicating that other scattering mechanisms might also be important.

One additional mechanism (Gramila *et al.*, 1991) is due to electron-phonon interaction. This suggestion was developed theoretically by Tso, Vasilopoulos, and Peeters (1992), Bønsager *et al.* (1998a, 1998b), and Badalyan and Rössler (1999) and experimentally by Rubel *et al.* (1995), Noh *et al.* (1999), and Jörger, Cheng, Dietsche *et al.* (2000); see Fig. 10.

[10]The momentum relaxation time reported by Gramila *et al.* (1991) is twice smaller than Eq. (21b). In addition, the paper cited unpublished calculations of MacDonald, Gramila, and Eisenstein involving a more realistic modeling of finite-width quantum wells. In particular, these calculations were reported to include vertex corrections to the RPA interaction propagator Eq. (7). Hence, it is difficult to judge whether that factor of 2 has played any role in the actual analysis of Gramila *et al.* (1991).

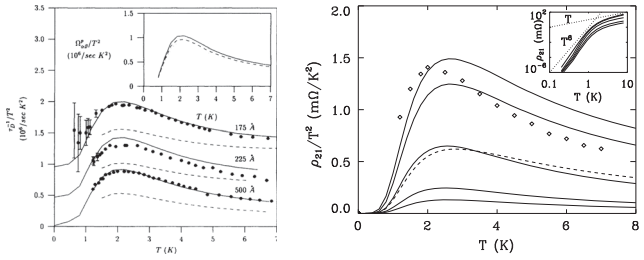


FIG. 10. Left panel: Calculated $\tau_D^{-1}/T^2$ (solid curves) compared to the data of Gramila *et al.* (1991). A less optimal choice of a fitting parameter yields results shown by the dashed curves. Inset: Calculated contribution of virtual-phonon exchange processes to $\tau_D^{-1}/T^2$). From Tso, Vasilopoulos, and Peeters, 1992. Right panel: Calculated $\rho_D/T^2$ for various values of the phonon mean-free path and $d = 500$ Å (solid curves). The dots show the data of Gramila *et al.* (1992). The dotted line represents the contribution of the modified plasmon pole. Inset: The crossover of the $T^6$ to $T$ temperature dependence. From Bønsager *et al.*, 1998a.

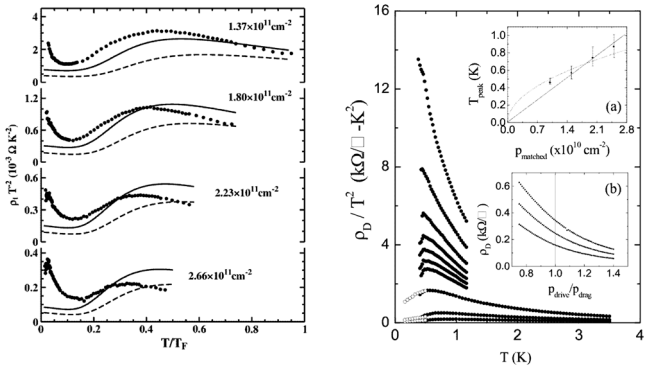


FIG. 11. Left panel: Measured $\rho_D/T^2$ for various values of the carrier density $n_1 = n_2$. Dashed lines represent the results of Flensberg and Hu (1994) adjusted for the sample parameters of the experiment. Solid lines show the results of additional calculations taking into account intralayer many-body correlations within the Hubbard approximation. From Hill *et al.*, 1997. Right panel: Measured $\rho_D/T^2$ for different carrier densities. Inset: (a) Peak position temperature vs matched layer density; (b) $\rho_D$ vs density ratio for $T = 860$, 730, and 600 mK. From Pillarisetty *et al.*, 2002.

Both the Coulomb and phonon drag mechanisms assume smallness of the transferred momentum $q$ [see, e.g., Eq. (6)], which is fully justified for samples with the small screening length $\varkappa d \gg 1$. In addition, for low-density samples with closely spaced layers (i.e., for $k_F d \sim 1$) backward scattering processes with $q \sim 2k_F$ may become important (Kellogg, Eisenstein *et al.*, 2002). The contribution of such processes to drag shows the $T^2 \ln T$ temperature dependence [in contrast to Eq. (21)]. While such logarithmic correction is difficult to ascertain, the experiment (Kellogg, Eisenstein *et al.*, 2002) shows sizable deviations from Eq. (21) with the observed unusual density dependence of $\rho_D$ suggesting the importance of the $2k_F$ scattering processes. A quantitative theoretical description of these results was later achieved by Yurtsever, Moldoveanu, and Tanatar (2003) and Asgari, Tanatar, and Davoudi (2008) using a numerical approach based on the effective interaction scheme developed by Kukkonen and Overhauser (1979) and Vignale and Singwi (1985).

Further corrections to the single-particle Coulomb mechanism are associated with the plasmon contribution. As shown by Flensberg and Hu (1994), plasmons are expected to be most important at intermediate temperatures $T \sim 0.5T_F$. This prediction was tested experimentally by Hill *et al.* (1997); see the left panel in Fig. 11 and in Noh *et al.* (1998). While the theoretical results show qualitative agreement with the data, discrepancies persist. Taking into account many-body correlations [see, e.g., Swierkowski, Szymanski, and Gortel (1995)] improves the agreement, but further advances in many-body theory are necessary before a more precise quantitative description of the correlation effects in double-layer structures is achieved.

The discrepancies between the simple single-particle description and laboratory experiments are by no means universal, especially since many measurements were performed in very different systems. One of the first drag experiments (Solomon *et al.*, 1989) was performed on a hybrid 2D-3D system. This device showed considerable thermoelectric effects masking the purely Coulomb contribution to drag. Experiments on electron-hole systems (Sivan, Solomon, and Shtrikman, 1992) showed behavior that could not be accounted for by either the phonon or plasmon corrections. Instead, generalized RPA (taking into account exchange processes to all orders) (Tso, Vasilopoulos, and Peeters, 1993) appears to yield satisfactory agreement with observations of Sivan, Solomon, and Shtrikman (1992) at low temperatures. Apparently, the traditional RPA overestimates screening which results in the underestimated drag resistivity.

Experiments on dilute 2D hole systems (Pillarisetty *et al.*, 2002, 2004) show marked enhancement of the drag resistivity, along with the stronger temperature dependence (empirically, $\rho_D \propto T^{2.5}$ at low temperatures, followed by a crossover toward a sublinear temperature dependence at $T \simeq E_F$). These systems are characterized by rather high values of the dimensionless Wigner-Seitz radius[11] (Ando, Fowler, and Stern, 1982; Giuliani and Vignale, 2005) $r_s \simeq 20$–40 and also exhibit signs of a metal-insulator transition in single-layer measurements (Pillarisetty, Noh, Tutuc *et al.*, 2005). The data obtained by Pillarisetty *et al.* (2002) are not explained by taking into account corrections due to phonons (Bønsager *et al.*, 1998a), plasmons (Flensberg and Hu, 1994), or many-body effects (Swierkowski, Szymanski, and Gortel, 1995), as follows from the density dependence of the measured drag illustrated in the right panel of Fig. 11. The lack of adequate theoretical description of these experiments is not surprising, given that the regime of relatively high $r_s$ remains an unsolved problem in single-layer (bulk) systems as well.

Croxall *et al.* (2008) and Das Gupta *et al.* (2008) reported anomalous drag in electron-hole bilayers. Below $T = 1$ K, the measured drag resistivity exhibits an upturn that may be

[11]Physically, the dimensionless Wigner-Seitz radius can be understood as the ratio of the average potential energy to the average kinetic energy of the electronic system. In 2D systems it can be estimated as $r_s = e^2 m^*/(\hbar^2 \epsilon \sqrt{\pi n}) = (\sqrt{2}/\epsilon)[e^2/(\hbar v_F)]$, where $m^*$ is the band mass and $\epsilon$ is the dielectric constant.

followed by a downturn, although $\rho_D$ does not seem to vanish for $T \to 0$. The observed upturn may indicate exciton formation (Vignale and MacDonald, 1996; Hu, 2000b); however, neither the observed violation of Onsager reciprocity nor the apparent downturn at lower temperatures is anticipated by the theory. The effect of density imbalance on the drag upturn was studied by Morath *et al.* (2009). The data were interpreted in terms of a pairing-fluctuations mechanism based on the theory of Hwang and Das Sarma (2008b). The theory accounts for most qualitative features of the effect; however the predicted peak in $\rho_D$ at equal layer densities was not observed in experiment (Morath *et al.*, 2009).

Further experiments demonstrate interesting correlation effects such as Wigner crystallization in quantum wires (Yamamoto *et al.*, 2006, 2012), exciton formation in electron-hole bilayers (Seamons *et al.*, 2009), or quantum Hall effect (Girvin and MacDonald, 1997; Lilly *et al.*, 1998); see Sec. VII.A. Clearly these phenomena cannot be described by the simple theory presented in this section. At the same time, single-particle effects are still important at relatively low temperatures ($T \lesssim 0.2T_F$) in traditional semiconductor heterostructures hosting two-dimensional electron systems and even more so in graphene (see Sec. IV), where interlayer separation can be as small as several interatomic distances (Gorbachev *et al.*, 2012).

### 1. Phonon effects

Electrical resistivity due to electron-phonon scattering is a standard topic in condensed matter physics (Ziman, 1965). At temperatures higher than the Debye frequency $T \gg \omega_D$, it exhibits linear behavior $\rho \propto T$ that is observed in a wide class of materials including high-mobility 2DEG (Stormer *et al.*, 1990) and graphene (Efetov and Kim, 2010). At low temperatures $T \ll \omega_D$ [in low-density electron systems the crossover occurs at a lower scale, the so-called Bloch-Grüneisen temperature $T \ll T_{\rm BG} < \omega_D$ (Stormer *et al.*, 1990)], the phonon contribution is rapidly decreasing as $\rho \propto T^5$ in metals (Bloch, 1930; Grüneisen, 1933) and heterostructures (Price, 1984; Stormer *et al.*, 1990) and as $\rho \propto T^4$ in graphene (Hwang and Das Sarma, 2008a; Efetov and Kim, 2010).

Qualitative physics of the electron-phonon interaction in semiconductor double-quantum-well heterostructures is captured by the following interaction Hamiltonian:

$$\mathcal{H}_{\rm ep} = \frac{1}{\sqrt{V}} \sum_{\lambda,\lambda';\boldsymbol{k}} \sum_{\boldsymbol{Q};\eta} M^{\eta}_{\lambda,\lambda'}(\boldsymbol{Q}) F_{\lambda,\lambda'}(q_z) \times [\hat{b}^{\dagger}_{\eta}(-\boldsymbol{Q}) + \hat{b}_{\eta}(\boldsymbol{Q})] \hat{c}^{\dagger}_{\lambda}(\boldsymbol{k}) \hat{c}_{\lambda'}(\boldsymbol{k}+\boldsymbol{q}). \quad (46)$$

Here $\boldsymbol{Q} = (\boldsymbol{q}, q_z)$ is the 3D wave vector of a phonon with polarization $\eta$, $\boldsymbol{k}$ is the 2D electron wave vector, and $M^{\nu}_{\lambda,\lambda'}$ is the bulk electron-phonon matrix element corrected by the subband form factor

$$F_{\lambda,\lambda'}(q_z) = \int_{-\infty}^{\infty} dz \xi_{\lambda}(z) \xi^{*}_{\lambda'} e^{iq_z z}, \quad (47)$$

where $\xi_{\lambda}(z)$ is the bound state wave function associated with the quantized motion in the subband $\lambda$. This Hamiltonian was used to study the effects of interaction between electrons and longitudinal optical phonons in Das Sarma and Mason (1985) and to calculate quasiparticle properties in weakly polar 2DEG in Jalabert and Das Sarma (1989). In double-layer systems, the Hamiltonian (46) was used to describe interlayer interaction mediated by acoustic phonons in Zhang and Takahashi (1993) and Bønsager *et al.* (1998a) and by optical phonons in Hu (1998).

Electrons experience the phonon-mediated interaction (46) alongside the Coulomb interaction. The propagator of the effective interlayer interaction can be obtained within the RPA (Jalabert and Das Sarma, 1989; Zhang and Takahashi, 1993; Bønsager *et al.*, 1998a) similarly to Eq. (7). The result can be represented in the form $\mathcal{D}_{12} = (V_{12} + D_{12})/\epsilon(\boldsymbol{q}, \omega)$, where $D_{12}$ is the propagator of the phonon-mediated interaction and $\epsilon(\boldsymbol{q}, \omega)$ is the effective dielectric function for interlayer interactions that is also determined by the sum of the Coulomb interaction (5) and the phonon propagator. Thus the phonon and Coulomb mechanisms are generally not independent of each other. However, the Coulomb interaction contributes only to small momentum transfers (6), while the phonon contribution peaks at $q \sim 2k_F$ (Bønsager *et al.*, 1998a). Neglecting interference between the two, one can estimate the effect of phonon-mediated interaction by considering only the phonon part $\mathcal{D}_{12} \to D_{12}/\epsilon(\boldsymbol{q}, \omega)$.

A simple analytical estimate for the strength of the phonon-mediated interaction in GaAs/AlGaAs systems was suggested by Bønsager *et al.* (1998a). In this material, electron-phonon interaction is due to the deformation potential and piezoelectric effect. It turns out that the deformation mechanism dominates (except for very low electron densities). Assuming an infinite phonon mean-free path, the corresponding (unscreened) effective interaction has the form

$$\mathcal{D}_{12} = -\frac{C_{DP}\omega^2 e^{-d\sqrt{q^2-\omega^2 c_l^{-2}}}}{\nu k_F c_l \sqrt{c_l^2 q^2 - \omega^2}}, \quad (48)$$

where $c_l$ is the velocity of longitudinal acoustic phonons and $C_{DP} \approx 2.7 \times 10^{-3} k_F/(10^6\ {\rm cm}^{-1})$. The smallness of electron-phonon coupling constants implies weakness of the phonon-mediated interlayer interaction as compared to the Coulomb interaction. However, the effective interaction (48) diverges near $\omega \approx c_l q$ leading to a logarithmic divergence in the drag resistivity. Although this divergence is removed by either dynamic screening or phonon relaxation, this argument illustrates the reason behind the relative strength of the phonon-mediated interlayer interaction.

Detailed calculations of the phonon-mediated drag resistivity have been performed numerically by several authors. Tso, Vasilopoulos, and Peeters (1992) showed that combining the phonon and Coulomb mechanisms of mutual friction accounts for the nonparabolic temperature dependence observed in GaAs/AlGaAs devices (Gramila *et al.*, 1991); see the left panel of Fig. 10. A refined discussion of the phonon mechanism was given by Bønsager *et al.* (1998a); see the right panel of Fig. 10. It was shown that the temperature dependence of the phonon contribution to drag exhibits a crossover from linear to $T^6$ behavior around the

Bloch-Grüneisen temperature (see the inset in Fig. 10), explaining the peak in the drag resistivity, Fig. 9. In addition, it was shown that there exists a collective mode that can be found setting $\epsilon(\boldsymbol{q},\omega)=0$. This mode is similar to the usual plasmon and results from coupling of the electrons from both layers to the phonons with $\omega\sim c_l q$. A similar mode resulting from interaction between electrons and optical phonons was discussed by Güven and Tanatar (1997a, 1997b). A detailed analysis of the mutual friction due to optical phonons was given by Hu (1998).

#### 2. Interlayer interaction beyond RPA

Equation (7) for the dynamically screened interlayer Coulomb interaction has been obtained within the RPA. While capturing the qualitative physics of the effect, this representation is by no means exact. In particular, RPA-based calculations seem to underestimate the value of $\rho_D$ as compared to experimental data (Sivan, Solomon, and Shtrikman, 1992). A pedagogical discussion of the RPA and possible approaches to interacting many-body systems that go "beyond" the RPA can be found in Giuliani and Vignale (2005). Most of these approaches are not parametrically justified. The results of the calculations are typically compared to either experimental data or computer simulations.

Coulomb drag between electron and hole layers within the generalized RPA approach was considered by Tso, Vasilopoulos, and Peeters (1993). The resulting $\rho_D$ is about twice larger than that calculated within the RPA, but still about twice smaller than the experimental data. Furthermore, Swierkowski, Szymanski, and Gortel (1995) understood that the true temperature dependence of $\rho_D$ should exhibit a crossover from the $T^2$ dependence at low temperatures to a power law at higher temperatures. However, the local field approach [or the Singwi-Tosi-Land-Sjölander method (Singwi *et al.*, 1968)] used in this work still fails to reproduce $\rho_D(T)$ measured by Sivan, Solomon, and Shtrikman (1992), although it yields roughly the same magnitude of the effect (in contrast to the RPA and generalized RPA calculations). This approach was further extended to drag between two 2DEG by Swierkowski, Szymanski, and Gortel (1996, 1997). The results of that work suggested that many-body correlations enhance interlayer interaction and improve agreement with experiments. Nevertheless, experiments [see, e.g., Hill *et al.* (1997) and Fig. 11] show that existing theoretical methods are still incapable of providing a precise quantitative description of real systems.

A detailed consideration of Coulomb drag resistivity based on an extrapolation of Fermi-liquid-based formulas to the region where intralayer correlations are strong was carried out by Hwang *et al.* (2003) in an attempt to address the striking data of Pillarisetty *et al.* (2002) in low-density and high-mobility hole bilayers. The observed drag was 2 to 3 orders of magnitude larger than previously reported values. The calculations of Hwang *et al.* (2003) were different from that leading to Eq. (21a) in several points, all of them leading to an increase of the drag resistivity: (i) a Hubbard approximation was employed to obtain the polarization operator, which accounts for the exchange-driven local field corrections; (ii) an experimentally measured dependence of conductivity on density was used to extract the electron-hole asymmetry factor; (iii) a large momentum transfer component was included to calculate drag; (iv) a finite thickness of quantum wells was included to calculate form factors of Coulomb matrix elements; and (v) last, phonon contribution was added. Combining all these factors, Hwang *et al.* (2003) were able to account for most of the results of the measurements within a Fermi-liquid approach.

### G. Single-particle drag in magnetic field

The semiclassical Drude model described by Eqs. (2) predicts that the drag resistivity is independent of the magnetic field. Moreover, there is no Hall drag: the direction of the induced motion of charge carriers in the passive layer is expected to coincide with that of the driving current. These predictions contradict numerous experiments [see, e.g., Rubel, Fischer, Dietsche, von Klitzing, and Eberl (1997), Lilly *et al.* (1998), Eisenstein and MacDonald (2004), Muraki *et al.* (2004), Finck *et al.* (2010), and Nandi *et al.* (2012)] showing that Coulomb drag is not only sensitive to the magnetic field, but in fact the drag resistivity can be greatly enhanced once the field is applied.

In single-layer measurements, magnetoresistance is usually associated with either (i) multiband systems or (ii) quantum effects. A close analog of the former can be found in graphene-based systems; see Gorbachev *et al.* (2012), Titov *et al.* (2013), and Sec. IV. The latter effects are manifest in strong, quantizing magnetic fields leading to the emergence of a qualitatively different behavior (Girvin and MacDonald, 1997; Eisenstein and MacDonald, 2004) discussed in Sec. VII.

The situation somewhat simplifies if the field is tuned close enough to the point where the Landau levels in the two layers are half filled. In this case, the many-body state in each layer can be viewed as a Fermi liquid of composite fermions (Halperin, Lee, and Read, 1993). A long-range, interlayer interaction between these excitations can lead either to a single-particle drag effect (Sakhi, 1997; Ussishkin and Stern, 1997, 1998; Kim and Millis, 1999) or to novel correlated states; see Sec. VII. Alternative approaches include magneto-drag due to electron-phonon interaction (Badalyan and Kim, 2003), semiclassical theory (Brener and Metzner, 2005), diagrammatic theory in high Landau levels (Bønsager *et al.*, 1996, 1997; von Oppen, Simon, and Stern, 2001; Gornyi, Mirlin, and von Oppen, 2004), self-consistent Hartree approximation (Tso, Geldart, and Vasilopoulos, 1998), and the effect of magnetoplasmons (Khaetskii and Nazarov, 1999; Manolescu and Tanatar, 2002).

#### 1. Hall drag in weak (classical) magnetic field

Recall that the standard single-band Drude theory (2) does not allow for any dependence of the drag resistivity on the magnetic field and, in particular, predicts zero Hall drag; see Eq. (3d). The same conclusion can be reached using diagrammatic perturbation theory (Kamenev and Oreg, 1995). This result is justified by the assumption of energy-independent impurity-scattering time $\tau$. Lifting this assumption (Hu, 1997), one can show that a weak Hall drag signal may appear

$$\rho_D^H \propto sT^4, \qquad s = \frac{\partial\tau(\epsilon)}{\partial\epsilon}\frac{E_F}{\tau(E_F)}. \tag{49}$$

As argued by Hu (1997), this effect is hard to observe in conventional semiconductor heterostructures, where intralayer relaxation processes are dominated by electron-electron interaction: in this case the nonequilibrium distribution function quickly relaxes to a drifted Fermi-Dirac distribution and hence the impurity-scattering time is effectively almost independent of energy, i.e., $s \ll 1$.

Hall drag in weak magnetic fields was studied by Patel *et al.* (1997). The experimental device comprised two 180-Å-wide quantum wells separated by 100 Å and exhibited measurable tunneling between the layers, contrary to the assumptions of Hu (1997). Hall drag in graphene (Titov *et al.*, 2013) was attributed to a different mechanism; see Sec. IV. Other observations of Hall drag were performed in the quantum Hall regime (see Sec. VII), where the effect is much stronger (von Oppen, Simon, and Stern, 2001) than Eq. (49).

### 2. Coulomb drag of composite fermions

All of the previous discussion was based on the underlying physical picture of weakly interacting fermions. Typically, this picture becomes invalid in a strong, quantizing magnetic field. The only exception to this statement is the peculiar state at the half-filled Landau level. This state can be described as a Fermi liquid of composite fermions (Halperin, Lee, and Read, 1993). Each composite fermion is an electron with two attached flux quanta (Jain, 1989) that interacts with the others both electrostatically and by means of a Chern-Simons interaction.

Composite fermions can be characterized by linear-response functions similar to those of electrons. In particular, their respective single-layer resistivities are related to each other by (Halperin, Lee, and Read, 1993)

$$\hat{\rho}_{el} = \hat{\rho}_{cf} + \frac{2h}{e^2}\begin{pmatrix} 0 & 1 \\ -1 & 0 \end{pmatrix}. \tag{50}$$

If one is interested in the relation between conductivities of the electrons and composite fermions, then one has to invert the resistivity matrices in Eq. (50). Clearly, the electronic conductivity is not identical to that of the composite fermions.

Extending Eq. (50) to the case of a double-layer system, one obtains a similar relation for the $4 \times 4$ resistivity matrices (Ussishkin and Stern, 1997). If the interlayer interaction is weak enough, so that composite fermions in a given layer are not sensitive to the Chern-Simons field of the other layer, then similarly to Eq. (50), longitudinal resistivities of the electrons and composite fermions are the same and hence

$$\rho_D^{el} = \rho_D^{cf}. \tag{51}$$

Again, conductivities (in particular, drag conductivities) of electrons and composite fermions are not equivalent.

The quantity measured in drag experiments is the electronic drag resistivity $\rho_D^{el}$, Eq. (13). Given the equality (51), one can calculate either $\rho_D^{cf}$ or $\rho_D^{el}$. The former approach was developed by Kim and Millis (1999), while the latter was considered by Ussishkin and Stern (1997). Both calculations are based on the standard lowest-order perturbation theory and yield similar results (albeit with a rather different interpretation[12]). The calculation of Kim and Millis (1999) consisted of evaluating Eq. (15) for composite fermions and using the correspondence (51). Alternatively, one can treat the problem (Ussishkin and Stern, 1997) in purely electronic terms assuming that interlayer interaction is dominated by the direct Coulomb coupling [the assumption which justifies Eq. (51)]. At the same time, single-layer electronic response functions (such as $\mathrm{Im}\Pi^R$) can be calculated within the composite-fermion approach of Halperin, Lee, and Read (1993).

Within RPA (including the response of composite fermions to the external, Coulomb, and Chern-Simons potentials) and in the limit $q \ll k_F$, $\omega \ll v_F q$, the electronic density-density response function (the polarization operator) is given by (Halperin, Lee, and Read, 1993)

$$\Pi^R(\boldsymbol{q},\omega) = \frac{dn}{d\mu}\frac{q^3}{q^3 - 8\pi i\omega k_F(dn/d\mu)}, \tag{52}$$

where $dn/d\mu$ is the thermodynamic compressibility of the $\nu = 1/2$ state. At large momenta, $\mathrm{Im}\Pi^{-1} \propto q^{-3}$; consequently, the momentum integration in Eq. (15) is dominated (Ussishkin and Stern, 1997) by the region $q \approx k_F(T/T_0)^{1/3}$ [i.e., determined by poles of the interlayer interaction, rather than Eq. (6)]. As a result, the temperature dependence of the drag resistivity is weaker than in the absence of magnetic field (Stern and Ussishkin, 1997; Ussishkin and Stern, 1997)

$$\rho_D = 0.825(h/e^2)(T/T_0)^{4/3}, \tag{53}$$

where the characteristic temperature depends on the carrier density $n$, interlayer spacing $d$, dielectric constant $\varepsilon$, and thermodynamic compressibility

$$T_0 = \frac{\pi e^2 n d}{\varepsilon}\left[1 + \frac{\varepsilon}{2\pi e^2 d}\left(\frac{dn}{d\mu}\right)^{-1}\right].$$

The same temperature dependence was reported by Sakhi (1997) and Kim and Millis (1999).

For realistic parameter values similar to those of the experiment of Lilly *et al.* (1998), the drag resistivity (53) is much larger than the zero-field result (21). This fact is associated with the smallness of the typical momenta involved in the interlayer scattering processes and slow relaxation of density fluctuations in the $\nu = 1/2$ state.

The effect of disorder on drag in the $\nu = 1/2$ state was considered by Stern and Ussishkin (1997). In the diffusive regime, the polarization operator is given by the standard form of Eq. (30) and hence the drag resistivity is given by Eq. (34), albeit with a different diffusion coefficient than the same system would have in the absence of magnetic field. The result

[12]The subquadratic temperature dependence (53) of the drag resistivity at $\nu = 1/2$ was interpreted by Kim and Millis (1999) as a signature of the non-Fermi-liquid nature of composite fermions. In particular, it was related to the similar power law in the self-energy of the composite fermions leading to the $\omega \sim q^3$ scaling of the typical frequencies.

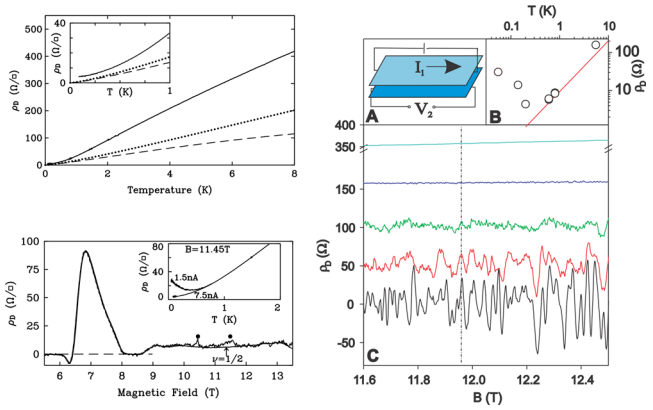


FIG. 12. Coulomb drag measurements at $\nu = 1/2$. Left panel: The top plot shows the experimental $\rho_D(T)$ (solid line) compared to the theory of Stern and Ussishkin (1997); the bottom plot shows the field dependence. The inset shows $\rho_D$ at $B = 11.45$ T for two values of the driving current. From Lilly *et al.*, 1998. Right panel: (A) circuit schematic; (B) $\rho_D(T)$ (dots) vs Eq. (53); (C) $\rho_D(B)$ for different temperatures $T = 0.05$–$5.6$ K. The vertical line corresponds to the $B$ field at which the points plotted in (B) were measured. From Price, Savchenko, and Ritchie, 2010.

is much larger than at $B = 0$. In the diffusive regime, this follows from the observation that the longitudinal conductivity (or the diffusive constant, which encodes all microscopic details) at $\nu = 1/2$ is much smaller than at $B = 0$.

Although this theory is qualitatively similar to the experimental observations (Lilly *et al.*, 1998) (e.g., drag at $\nu = 1/2$ is much larger than at $B = 0$; the temperature dependence in clean samples is subquadratic), theoretical calculations significantly underestimate the overall value of $\rho_D$ as compared to the experiment of Lilly *et al.* (1998). Yang (1998) suggested that the reason for the discrepancy is that the interlayer separation in the samples of Lilly *et al.* (1998) was close to the critical value, where the system forms an incompressible interlayer state (for a detailed discussion of correlated states, see Sec. VII). An alternative suggestion by Ussishkin and Stern (1998) attributed the unexplained features of the experiment (including the extrapolated nonvanishing drag at $T = 0$) to pairing fluctuations of composite fermions. The two scenarios could be distinguished by measuring Hall drag, which vanishes in the latter theory. Finally, the anomalous temperature dependence shown in the inset of the lower left panel in Fig. 12 appears to be qualitatively similar to the effect of mesoscopic fluctuations of Coulomb drag; see Fig. 13. A later experiment (Price, Savchenko, and Ritchie, 2010) reported both the magnitude and temperature dependence of Eq. (53) to be in good agreement with the measured data.

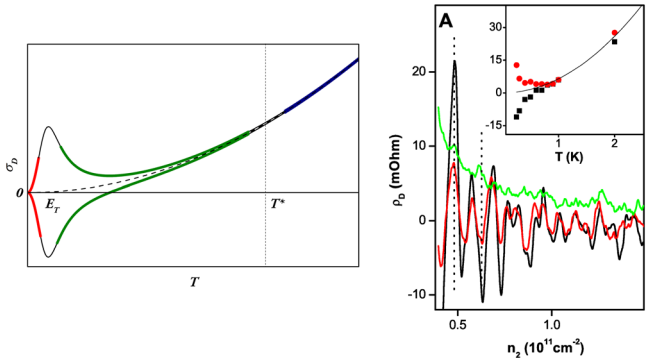


FIG. 13. Left: Qualitative picture of the typical measured drag signal. At high enough temperatures $T > T^*$ the average drag conductivity (35) is representative, $\sigma_D \propto T^2$, with positive coefficient. Below $T^*$ (left of the dotted line), fluctuations dominate and the sign of the measured signal becomes random, i.e., dependent on a particular configuration of disorder. For $T < T^*$ the temperature dependence weakens to $\sigma_D \propto 1/\sqrt{T}$. At very low (most likely, experimentally inaccessible) temperatures $T < E_T \ll T^*$, the quadratic temperature dependence is restored, but with a random coefficient as fluctuations in the effectively 0D system are much stronger than the average; see Eq. (58). Right: Measured drag resistance as a function of carrier density in the passive layer for $T = 1$, 0.4, 0.24 K (from top to bottom). Inset: The temperature dependence of the same data for the two values of $n_2$ denoted by vertical dotted lines in the main plot. The line indicates the $T^2$ dependence. From Price *et al.*, 2007.

## III. MESOSCOPIC FLUCTUATIONS OF COULOMB DRAG

Universal conductance fluctuations (Altshuler, Lee, and Webb, 1991) are quantum interference effects which are manifestations of the wave nature of electrons. As the same electrons are responsible for Coulomb drag, it is natural to expect that the drag resistivity also exhibits mesoscopic fluctuations. The drag fluctuations were first studied theoretically by Narozhny and Aleiner (2000) and Mortensen, Flensberg, and Jauho (2001, 2002a) and then observed experimentally by Price *et al.* (2007, 2008), Price, Savchenko, and Ritchie (2010), and Kim *et al.* (2011).

In a disordered system, it is impossible to track each individual impurity and one uses a statistical approach. Impurities are described by a distribution function and each physical quantity is treated as being random. Observables correspond to average values of the random physical quantities with respect to the distribution of impurities. If a system is large enough, it can be viewed as a combination of smaller parts, which become statistically independent if they are separated by distances larger than any relaxation length. Then instead of averaging over a statistical ensemble, one can average over the volume of one large system.

In the problem of electronic transport, averaging over the system volume can be understood as averaging over all possible paths that an electron can take moving between points $A$ and $B$ (Altshuler and Aronov, 1985; Altshuler, Lee, and Webb, 1991; Aleiner, Altshuler, and Gershenson, 1999). Such paths can cover all of the system volume and thus experience all possible local impurity configurations, making the average over the system equivalent to ensemble averaging.

Consider two paths between points $A$ and $B$. The total transmission probability is determined by the absolute value of the sum of the corresponding quantum amplitudes (Altshuler and Lee, 1988; Altshuler, Lee, and Webb, 1991):

$$W = |A_1 + A_2|^2 = |A_1|^2 + |A_2|^2 + 2|A_1||A_2|\cos(\varphi_1 - \varphi_2),$$

where $\varphi_{1(2)}$ are the quantum-mechanical phases that an electron accumulates along the paths. Typically, the phases $\varphi_{1(2)}$ are random (or incoherent). As a result, the interference term vanishes upon averaging over all possible paths (or impurity configurations), leading to the semiclassical sum of transition probabilities[13]

$$\langle \cos(\varphi_1 - \varphi_2)\rangle = 0 \Rightarrow W = W_1 + W_2,$$
$$W_{1(2)} = |A_{1(2)}|^2.$$

Random quantities can be characterized not only by their average value, but also by higher moments of their statistical distribution, which may be sensitive to the interference term even if the phases $\varphi_{1(2)}$ are still random. Indeed, fluctuations of the transition probability

$$\langle [W - \langle W\rangle]^2\rangle = 4W_1W_2\langle \cos^2(\varphi_1 - \varphi_2)\rangle = 2W_1W_2$$

are completely determined by the interference term.

Fluctuations of the transmission probability result in fluctuations of transport coefficients. The effect of such fluctuations can be observed only in small enough samples (Altshuler, Lee, and Webb, 1991). Indeed, in order to justify the concept of the phase associated with a given electronic path, the length of the path should be less than a typical inelastic relaxation length $L_\varphi$, otherwise coherence would be lost before the electron reaches point $B$ (Anderson, Abrahams, and Ramakrishnan, 1979). At the same time, the path length should be larger than the mean-free path in the system (otherwise electron motion along the path would be deterministic). Therefore, typical paths (and hence, the sample sizes) should be characterized by intermediate lengths $L$:

$$\ell \ll L \ll L_\varphi.$$

Fluctuations observed at such length scales are known as "mesoscopic fluctuations" (Altshuler, Lee, and Webb, 1991).

### A. Drag fluctuations in conventional diffusive samples

Mesoscopic fluctuations of the usual conductance (Altshuler, Lee, and Webb, 1991) are known as the "universal conductance fluctuations" (UCFs). The universality is manifest when $T \ll E_T$, where $E_T$ is the Thouless energy of the sample (i.e., in small samples or at low temperatures; in the diffusive regime $E_T = D/L^2 = g/(2\pi\nu L^2)$, with $g$ the dimensionless conductance and $\nu$, the DOS). Then the fluctuations are characterized by the universal value

$$\delta\sigma \simeq \frac{e^2}{\hbar}, \qquad \langle \delta G^2\rangle \approx \frac{e^4}{h^2}, \qquad \sqrt{\frac{\langle \delta G^2\rangle}{\langle G\rangle^2}} \simeq \frac{1}{g(L)}, \tag{54}$$

where $G = ge^2/h$ is the conductance of the system. The latter equality emphasizes the fact that the dimensionless conductance is a function of the system size.

In larger samples, $\langle \delta G^2\rangle$ is a function of temperature and the sample size. Arguments leading to Eq. (54) are valid only for coherent samples (Altshuler, Lee, and Webb, 1991). At larger length scales $L \gg L_\varphi$ the coherence is lost, and the disorder averaging should be performed by dividing the sample into patches of the size $L_\varphi$. Individual self-coherent patches (54) can be combined as a network of random conductors. This yields (in dimension $d$)

$$\langle \delta G^2(L)\rangle \simeq \langle \delta G^2(L_\varphi)\rangle (L_\varphi/L)^d. \tag{55}$$

The patches of the size $L_\varphi$ remain self-coherent as long as $T \ll E_T(L_\varphi)$. At higher temperatures, thermal averaging should be performed up to energies of order $T$, suppressing the conductance fluctuations

$$\langle \delta G^2(L_\varphi)\rangle \simeq (e^2/h)^2 E_T(L_\varphi)/T.$$

The conductance fluctuations of the sample become

$$\langle \delta G^2[L; T > E_T(L_\varphi)]\rangle \simeq (e^2/h)^2 (L_\varphi/L)^d \hbar/(T\tau_\varphi), \tag{56}$$

where $\tau_\varphi = E_T^{-1}(L_\varphi)$ is the dephasing time (Altshuler *et al.*, 1980).

The fluctuations (56) are observable only in mesoscopic samples. Assuming the samples to be "metallic," $g \gg 1$, the UCFs (54) yield only a small correction to the average value of conductance. For example, in the experiment of Price *et al.* (2007) the single-layer resistance fluctuates by about 200 mΩ around the average of about 500 Ω.

Now we apply these arguments to Coulomb drag (Narozhny and Aleiner, 2000). The drag conductivity depends on (i) the phase space available to electron-hole excitations; (ii) matrix elements of the interlayer interaction; and (iii) electron-hole asymmetry, expressed through the energy dependence of the density of states (or the density dependence of the single-layer Drude conductivity). This can be schematically summarized by

$$\sigma_D \simeq \frac{e^2}{\hbar}\left(\frac{\partial}{\partial\mu}\ln g\right)^2 \times \begin{pmatrix}\text{phase}\\ \text{volume}\end{pmatrix} \times \begin{pmatrix}\text{matrix}\\ \text{element}\end{pmatrix}. \tag{57}$$

The average drag conductivity [cf. Eqs. (34) and (35)] can then be understood (up to the logarithmic factor) by estimating the phase volume by $T^2$, the matrix element by $(\varkappa d)^{-2}$ (coming from static screening), and the factor of the electron-hole asymmetry by $E_F^{-2}$.

Fluctuations of the drag conductivity can also be estimated with the help of Eq. (57). Consider first the lowest temperatures $T \ll E_T$, where the sample is effectively zero dimensional (0D). The phase space is then limited only by temperature, yielding the usual factor of $T^2$. The factor of the electron-hole asymmetry in Eq. (57) is a random quantity with the typical value $\sim E_T^{-2}$, since the Thouless energy is the typical scale of mesoscopic effects. Interaction matrix elements in 0D are independent of energy (Aleiner, Altshuler,

[13] In special cases of coherent paths (for instance, time-reversed paths) the phase difference is exactly zero. Then the interference term does not vanish and leads to quantum corrections to semiclassical transport properties, such as the weak localization correction (Altshuler and Aronov, 1985; Altshuler, Lee, and Webb, 1991).

and Gershenson, 1999); fluctuations are determined by off-diagonal elements that contain a small factor of $g^{-2}$. As a result, one finds the variance of the drag conductivity that strongly exceeds the average

$$\delta\sigma_D \sim \frac{e^2}{\hbar}\frac{T^2}{g^2E_T^2}, \qquad \frac{\sqrt{\langle\delta\sigma_D^2\rangle}}{\langle\sigma_D\rangle} \simeq \frac{E_F^2}{g^2E_T^2} \simeq \frac{L^4}{\ell^4} \gg 1. \tag{58}$$

The quadratic temperature dependence of the variance of the drag conductivity (Narozhny and Aleiner, 2000) for mesoscopic samples ($L \ll L_\varphi$, $T \ll E_T$) was also obtained in the context of quantum circuits [see Sec. V and Levchenko and Kamenev (2008a)] and within the random matrix theory (Mortensen, Flensberg, and Jauho, 2001, 2002b).

In order to extend the 0D argument to larger samples $L \gg L_\varphi$, we again divide the system into patches of the size $L_\varphi$. Since the patches are largely uncorrelated (due to the loss of phase coherence), they can be combined as a network of random conductors; see Eq. (55). Each patch can be analyzed similarly to the 0D case. However, now the interaction matrix elements become energy dependent on the scales larger than $E_T$, decreasing with the transmitted energy $\omega$ as $|M|^2 \sim \omega^{-2}$. Thus the energy transfer is limited by the Thouless energy of the patch $\omega \sim E_T(L_\varphi) = \tau_\varphi^{-1}$, rather than temperature. As a result, the phase space is limited by $T\tau_\varphi^{-1}$, rather than the usual $T^2$. The fluctuations of the density of states (which determine the factor of electron-hole asymmetry) should now be calculated on the scale of temperature rather than the Thouless energy. This suppresses the fluctuations in each layer by the factor of $\sqrt{E_T(L_\varphi)/T}$. Combining the above estimates, we find

$$\delta\sigma_D(L_\varphi) \sim \frac{e^2}{\hbar}\frac{T\tau_\varphi^{-1}}{g^2E_T^2(L_\varphi)}\frac{E_T(L_\varphi)}{T} \sim \frac{e^2}{\hbar g^2}, \tag{59}$$

which is $T$ independent, in contrast to the 0D result (58).

Finally the Coulomb drag fluctuations in 2D samples can be estimated by combining Eqs. (55) and (59):

$$\langle\delta\sigma_D^2(L)\rangle \sim \frac{e^4}{\hbar^2g^4}\frac{L_\varphi^2}{L^2} \sim \frac{e^4}{\hbar^2g^4}E_T(L)\tau_\varphi \propto \frac{1}{T}. \tag{60}$$

The temperature dependence of the fluctuations (60) is contained in the dephasing time $\tau_\varphi \sim g/T$ (Altshuler and Aronov, 1985). At high enough temperatures $T \gg T^*$, the fluctuations are small [the average value of $\sigma_D$ of Eq. (35) is representative], but for $T \ll T^*$ fluctuations dominate; see Fig. 13. The crossover temperature $T^*$ can be found by setting the relative fluctuation to unity

$$T^* \sim E_F(g^2nL^2)^{-1/5}.$$

The fluctuation-dominated regime is characterized by typical values of $\sigma_D$ determined by Eq. (60) rather than the average. In particular, the temperature dependence of the measured drag conductivity in this regime appears almost saturating as $\sigma_D \propto 1/\sqrt{T}$. The value of the prefactor in this expression is sample dependent and has a random sign. If temperature is decreased further, then eventually (although probably only in theory) one can reach the regime where $T < E_T$. Then the sample will become effectively zero dimensional and the quadratic temperature dependence $\sigma_D \propto T^2$ will be restored. In this regime of lowest temperatures, fluctuations greatly exceed the average [see Eq. (58)] and therefore the coefficient in the quadratic temperature dependence will be random (with random sign). The temperature dependence of a typical drag signal is sketched in the left panel of Fig. 13 [cf. the inset in the right panel of Fig. 13; see also the inset in the lower left panel of Fig. 12 and the discussion of the data of Lilly *et al.* (1998) in Sec. III.C].

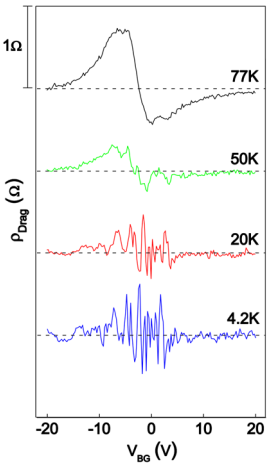


FIG. 14. Mesoscopic fluctuations of Coulomb drag in graphene. At low temperatures the fluctuations fully obscure the average drag. The curves are shifted for clarity; the horizontal dashed lines indicate 0Ω for each curve. From Kim *et al.*, 2011.

This qualitative picture is in full agreement with microscopic calculations (Narozhny and Aleiner, 2000). The average square of the drag conductivity has the form

$$\langle\sigma_D^{\alpha\beta}\sigma_D^{\alpha'\beta'}\rangle = (\delta^{\alpha\alpha'}\delta^{\beta\beta'} + \delta^{\alpha\beta'}\delta^{\alpha'\beta})\langle\sigma_D^2\rangle, \tag{61a}$$

$$\langle\sigma_D^2\rangle = \frac{e^4}{\hbar^2}\frac{\gamma}{18\pi^3}\left(\frac{32\ln 2 - 14}{3}\right)\frac{E_T\tau_\varphi \ln \varkappa d}{g^4(\varkappa d)^3}, \tag{61b}$$

where $\gamma = 1.0086$. Comparing Eq. (61) with the average drag conductivity in the diffusive regime (35), one finds the crossover temperature $T^* = E_F(16\pi g^2nL^2)^{-1/5}$.

For heterostructures used by Gramila *et al.* (1991) and Lilly *et al.* (1998), the value of $T^*$ can be estimated as $T^* \approx 0.2$ K, which is below the temperature range of these experiments. Hence, the average drag coefficients (34) and (35) were sufficient to account for the observed effect with no trace of the random sign predicted by Eqs. (61).

More recently, drag fluctuations were observed in diffusive graphene-based double-layer samples (Kim *et al.*, 2011; Kim and Tutuc, 2012); see Fig. 14. The temperature dependence $\delta\sigma_D \propto T^{-1/2}$ [following from Eq. (61) and the assumption that the main phase-breaking mechanism in the device is electron-electron scattering (Altshuler and Aronov, 1985)] appears to be in agreement with the experimental data. Other aspects of these experiments are specific to graphene. The fluctuations appear to be more pronounced in the vicinity of the charge

neutrality point. However, at the time of writing, a theory of drag fluctuations in graphene has not been developed. There is also no explanation for the most puzzling feature of the data reported in Kim and Tutuc (2012) showing an apparent violation of Onsager reciprocity as the drag fluctuations depend only on the charge density in the passive layer and not in the active layer.

The result (61) is valid for homogeneous 2D diffusive samples in the absence of magnetic field. The randomness (i.e., the sample to sample variation) of the sign of the effect should be contrasted with the deterministic sign change of the drag resistivity suggested for bilayer systems with in-plane periodic potential modulation (Alkauskas *et al.*, 2002). Drag signals of both signs have been observed in vertically integrated 1D quantum wires (Laroche *et al.*, 2011). While the observed effect has been argued (Büttiker and Sánchez, 2011) to have a mesoscopic origin (Mortensen, Flensberg, and Jauho, 2001) dominated by charge fluctuations (Levchenko and Kamenev, 2008a; Sánchez *et al.*, 2010), the data appear to be not random, but reproducible. Very similar data were obtained in the subsequent experiment (Laroche *et al.*, 2014) and interpreted with the help of the Luttinger liquid theory (Pustilnik *et al.*, 2003) (see Sec. VI).

In closing this section, we note that strong fluctuations of Coulomb drag ultimately follow from strong fluctuations of the nonlinear susceptibility. The fact that the fluctuations of the drag resistivity exceed the average is related to the overall smallness of the drag effect due to electron-hole symmetry. A related phenomenon is the fluctuations of the electroacoustic current (see footnote 7) determined by the same nonlinear susceptibility.

### B. Giant fluctuations of Coulomb drag

The predictions of the fluctuation theory (Narozhny and Aleiner, 2000) were put to the test in the dedicated experiment (Price *et al.*, 2007). Both the UCF and drag fluctuations were measured in the same structure. The observed UCFs have shown the usual behavior (Altshuler, Lee, and Webb, 1991). A direct comparison of the correlation fields for the UCF and drag fluctuations confirmed that both effects depend on the same coherence length $L_\varphi$ (Aleiner, Altshuler, and Gershenson, 1999) and have the same quantum origin. Surprisingly, the observed giant drag fluctuations (Price *et al.*, 2007) greatly exceeded the original prediction (Narozhny and Aleiner, 2000). This discrepancy was attributed to the fact that the experiment was performed in the ballistic regime (Zala, Narozhny, and Aleiner, 2001; Narozhny, Zala, and Aleiner, 2002).

Let us remind the reader (see Sec. II) that the drag measurements difference between diffusive and ballistic samples is in the relation between the mean-free path $\ell$ and interlayer separation $d$. The latter sets the upper limit for the interlayer momentum transfer due to the exponential decay of the Coulomb interaction (5). Thus, if the mean-free path is small $\ell \ll d$, then $q \ll d^{-1} \ll \ell^{-1}$ and the effect is dominated by the diffusive motion of charge carriers. In cleaner samples with $\ell \gg d$, both small $q \ll \ell^{-1}$ and large $\ell^{-1} \ll q \ll d^{-1}$ momentum transfers are possible. The conventional statement, that in such samples Coulomb drag is dominated by ballistically moving carriers (Kamenev and Oreg, 1995), follows from observing that processes with large momentum transfers yield a much larger drag resistivity Eq. (21) compared with the diffusive result (34); see Eq. (36).

Coherence properties of electrons are also sensitive to the nature of their motion. The dephasing time $\tau_\varphi$ is a manifestation of inelastic electron-electron scattering (Altshuler and Aronov, 1985; Aleiner, Altshuler, and Gershenson, 1999). The conventional theory of interaction effects in electronic systems (Altshuler and Aronov, 1985) yields the following estimate for the dephasing time in diffusive systems:

$$\tau_\varphi^{-1}(T\tau \ll 1) \sim (T \ln g)/g. \tag{62a}$$

At higher temperatures, transport is dominated by processes with one or few successive impurity scatterings. In this ballistic regime (Zala, Narozhny, and Aleiner, 2001), the dephasing time exhibits somewhat stronger temperature dependence (Narozhny, Zala, and Aleiner, 2002)

$$\tau_\varphi^{-1}(T\tau \gg 1) \sim (T^2/E_F)\ln(2E_F/T). \tag{62b}$$

In Eqs. (62a) and (62b) the parameter distinguishing the diffusive and ballistic regimes is $T\tau$ which is independent of the interlayer separation. This is to be expected since the theory leading to Eqs. (62a) and (62b) was devoted to two-dimensional systems and not bilayers.

The effect of the external magnetic field on the single-layer conductance fluctuations analyzed by Price *et al.* (2007) demonstrates the expected crossover between the ballistic and diffusive results:

$$\tau_\varphi^{-1} \propto \begin{cases} T, & T\tau \lesssim 1, \\ T^2, & T\tau \gtrsim 1. \end{cases} \tag{62c}$$

The same sample where Coulomb drag is dominated by the ballistic motion of electrons with large interlayer momentum transfers $\ell^{-1} \ll q \ll d^{-1}$ may exhibit *both* the diffusive and ballistic behaviors of single-layer transport properties, e.g., of the dephasing time (62).

A similar crossover was observed also in the drag fluctuations that exhibited strikingly different temperature dependence at large and small $T\tau$ (Price *et al.*, 2007):

$$\langle \delta\sigma_D^2 \rangle \propto \begin{cases} T^{-1}, & T\tau \lesssim 1, \\ T^{-4}, & T\tau \gtrsim 1. \end{cases} \tag{63}$$

The crossover temperature in Eq. (63) was found to be about the same as in Eq. (62). This coincidence raised the question of whether the large magnitude of the observed drag fluctuations and their unexpected temperature dependence (63) had the same origin that would involve large momentum transfers $\ell^{-1} \ll q \ll d^{-1}$ [given that the small momentum transfers lead to Eq. (61)].

Scattering processes characterized by large momentum transfers $q \gg 1/\ell$ involve two electrons at a distance that is smaller than the average impurity separation. Thus, the effect should be determined by *local* electron properties. Local properties, such as the local DOS, are known to exhibit

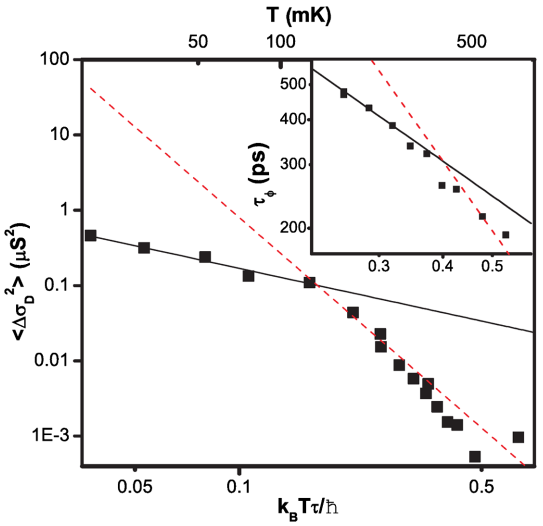


FIG. 15. Drag fluctuations in ballistic samples. The lines represent the asymptotic power laws; see Eq. (63). The inset shows the measured dephasing time. The lines in the inset represent the power laws from Eq. (62). Adapted from Price *et al.*, 2007.

mesoscopic fluctuations stronger than those of the global properties (responsible for drag fluctuations in the diffusive regime). In particular, fluctuations of the local DOS are given by (Lerner, 1988)

$$\delta\nu^2 \sim (\nu^2/g)\ln[\max(L_T, L_\varphi)/\ell], \tag{64}$$

where $L_T = \sqrt{D/T}$ is the thermal length.

Contribution of processes with large momentum transfers to drag fluctuations can be estimated using Eqs. (55) and (57). Electron-electron scattering can be described with the help of ballistic expressions discussed in Sec. II.B. As small-angle scattering plays the dominant role, the matrix element of the interlayer interaction is proportional to the ratio of the mean-free path to the interlayer separation $|M|^2 \sim g^{-2}\ell^2/(\varkappa^2 d^4)$. As this interaction is static, the phase space is limited only by $T$. Assuming that the fluctuations of the nonlinear susceptibility are dominated by fluctuations of the local density of states (64), one finds (up to a logarithmic factor)

$$\delta\sigma_D(L_\varphi) \sim \frac{e^2}{\hbar}\frac{T}{gE_T(L_\varphi)}\frac{\ell^2}{\varkappa^2 d^4}, \tag{65}$$

where the thermal smearing was taken into account similarly to Eq. (59). This leads to the estimate for the drag fluctuations in the whole sample (Price *et al.*, 2007)

$$\langle\delta\sigma_D^2\rangle \sim \frac{e^4}{\hbar^2}\frac{\ell^4}{g^2\varkappa^4 d^8}\frac{T^2}{E_T^2(L_\varphi)}\frac{L_\varphi^2}{L^2} \propto T^2\tau_\varphi^3. \tag{66}$$

The result (66) contains two falsifiable predictions: (i) the magnitude and (ii) the temperature dependence of the drag fluctuations. In comparison with Eq. (61), the prefactor in Eq. (65) contains the large factor $\ell^4/d^4$ and moreover $g^2$ instead of $g^4$ in the denominator. Consequently, the drag fluctuations (66) are much stronger than the diffusive prediction. At the same time, using the temperature dependence of the dephasing time (62), one immediately recovers the measured temperature dependence of the drag coefficient (63). The crossover between the two temperature regimes in Eqs. (63) and (66) is illustrated in Fig. 15.

### C. Drag fluctuations at the half-filled Landau level

Mesoscopic fluctuations of Coulomb drag of composite fermions were studied theoretically by Narozhny, Aleiner, and Stern (2001) and experimentally by Price, Savchenko, and Ritchie (2010). Despite the significant increase in the magnitude of drag of composite fermions relative to that of normal electrons (Lilly *et al.*, 1998; Jörger, Dietsche *et al.*, 2000; Zelakiewicz *et al.*, 2000; Muraki *et al.*, 2004) the fluctuations of the drag resistivity can still exceed the average, resulting in an alternating sign of the measured drag resistivity.

Qualitatively, one can estimate the fluctuation effects using Eq. (25). Similarly to the $B = 0$ case, drag fluctuations stem from the fluctuations of the nonlinear susceptibility. In the diffusive regime, $\langle\mathbf{\Gamma}\rangle$ is given by Eq. (28) with the polarization operator having the standard form (30), although with a different diffusion constant (Stern and Ussishkin, 1997). In contrast to the $B = 0$ case, the $\nu = 1/2$ state is characterized by a large Hall conductivity. This leads to the nonlinear susceptibility being approximately orthogonal to the transferred momentum $\boldsymbol{q}$ [unlike Eq. (31)].

Fluctuations of $\mathbf{\Gamma}$ (and thus of the drag resistivity) result from mesoscopic fluctuations of $\partial\sigma/\partial n$. Other parameters such as the compressibility and the diffusion constant can be taken at their average values (their fluctuations are much smaller than the averages). To estimate fluctuations of $\partial\sigma/\partial n$, one can express the conductivity in terms of the response functions of composite fermions using Eq. (50). On average, the conductivity matrix of composite fermions is diagonal. Assuming the large dimensionless conductance of composite fermions $g_{cf} \gg 1$, the electronic longitudinal conductivity is inversely proportional to $g_{cf}$, meaning *smallness* of the electronic dimensionless conductance

$$g \approx 1/(4g_{cf}) \ll 1. \tag{67}$$

This is the reason one needs to perform calculations in the composite-fermion basis: the $B = 0$ theory of Sec. III.A is justified by the small parameter $1/g$.

Adapting the $B = 0$ theory to the case of composite fermions, Narozhny, Aleiner, and Stern (2001) found the fluctuations of the nonlinear susceptibility (28) of a coherent sample of size $L$ in the $\nu = 1/2$ state to be large

$$\delta\Gamma \sim iq\frac{e}{h}\frac{L^2}{g_{cf}^2}\mathrm{Im}\Pi^R, \qquad \frac{\langle\delta\Gamma^2\rangle}{\langle\Gamma^\gamma\rangle^2} \sim \frac{k_F^4 L^4}{g_{cf}^4} \gg 1, \tag{68}$$

similar to Eq. (58). This is already an observable conclusion: in a fully coherent sample in the diffusive regime, fluctuations of the acoustoelectric current (determined by the same nonlinear susceptibility) are much larger than its average. The result Eq. (68) is justified as long as the thermal $L_T^{cf} \equiv$

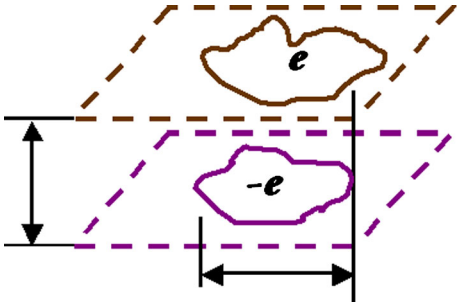


FIG. 16. The phase-breaking mechanism at $\nu = 1/2$. A random flux in the system can be generated by charge-density fluctuations with the opposite signs of excess local charges in the two layers.

$\sqrt{\hbar D^{cf}/T}$ and phase-breaking $L_\varphi^{cf}$ length scales of composite fermions are much larger than $L$.

For larger samples, the global phase coherence is lost and one has to employ the averaging procedure described in Sec. III.A. The system can be divided into $L^2/(L_\varphi^{cf})^2$ self-coherent patches of the size of the phase-breaking length of composite fermions $L_\varphi^{cf}$. Summing up contributions of all patches according to Eq. (55), one finds

$$\langle \rho_D^2 \rangle = \frac{h^2}{e^4}\frac{1}{g_{cf}^4(\kappa d)^2}\left(\frac{L_\varphi^{cf}}{L}\right)^2 \min\left[1, \alpha_1\left(\frac{g_{cf}^2 T\tau_\varphi^{cf}}{\kappa d\hbar}\right)^2\right] \times \min\left[\alpha_3, \alpha_2(T\tau_\varphi^{cf}/\hbar)^2\right], \tag{69}$$

where $\alpha_3 \approx 0.2(32/9\pi) = 0.23$ and the coefficients $\alpha_{1,2}$ are of the order of unity (Narozhny, Aleiner, and Stern, 2001).

The magnitude of the mesoscopic fluctuations depends on the precise source of phase breaking, but their temperature dependence is robust: all generic models of phase breaking in two dimensions (Altshuler and Aronov, 1985) lead to $1/\tau_\varphi \propto T$ in the diffusive regime. In the $\nu = 1/2$ state phase breaking comes from the *quasielastic* scattering of composite fermions off the thermal quasistatic fluctuations of the Chern-Simons magnetic field. This mechanism can be illustrated using a cartoon shown in Fig. 16. Consider a density fluctuation where the excess charges in the two layers have opposite signs. Such a fluctuation is accompanied by a random flux that interacts with the composite fermions leading to the loss of coherence. The energy of this fluctuation is of the order of $T$. It can also be estimated as the energy of a simple capacitor $2\pi e^2 d/[\varepsilon(L_\varphi^{cf})^2] \simeq T$, where $\varepsilon$ is the bulk dielectric constant and $L_\varphi^{cf}$ is the typical size of the density fluctuation with the electron number of the order of unity creating the random flux of approximately $\Phi_0$. As a result,

$$1/\tau_\varphi^{cf} \simeq g_{cf} T/(\varkappa d). \tag{70}$$

Substituting the above estimate into Eq. (69), one finds (assuming $g^{cf} \gg \varkappa d$)

$$\langle \rho_D^2 \rangle \simeq \frac{h^2}{e^4}\frac{2\pi e^2 d}{T\varepsilon L^2 g_{cf}^6}.$$

Using realistic parameters (Lilly *et al.*, 1998) (i.e., $L \simeq 100\ \mu$m, $d = 300$ Å, $T = 0.6K$, $R = 3k\Omega/\square$ leading to $g_{cf} \approx 8$, and $\langle \rho_D \rangle = 15\Omega/\square$), the magnitude of the drag fluctuations can be estimated as $\delta\rho_D \approx 0.3\ \Omega$, which is much smaller than the experimental data of Lilly *et al.* (1998); see the lower left panel of Fig. 12. That experiment remains poorly understood. For lower temperatures and smaller samples, the theory predicts stronger fluctuations (i.e., exceeding the average). Such strong fluctuations were observed by Price, Savchenko, and Ritchie (2010), albeit again with a substantially larger magnitude that follows from the above estimate; see Fig. 17.

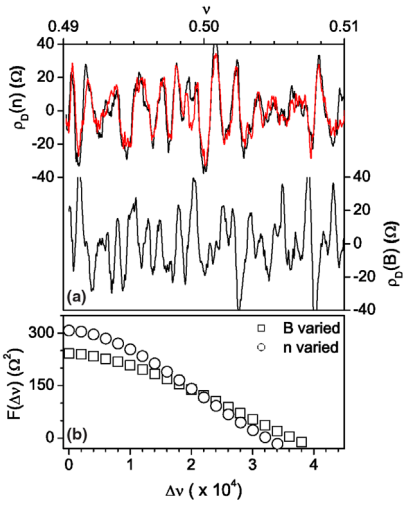


FIG. 17. Mesoscopic fluctuations of Coulomb drag at $\nu = 1/2$, $T = 50$ mK. Upper panel: Comparison of $\delta\rho_D$ as a function of the filling fraction $\nu$ obtained by varying either the carrier density or magnetic field. The gray (red) curve shows a different measurement run demonstrating the reproducibility of the fluctuations. Similarity of the periods of $\rho_D(n)$ and $\rho_D(B)$ is the proof of composite-fermion drag. Lower panel: Autocorrelation function of the fluctuations shown in the upper panel. Squares represent $\rho_D(B)$ and circles represent $\rho_D(n)$. From Price, Savchenko, and Ritchie, 2010.

The dephasing time due to the quasielastic scattering of composite fermions on thermal fluctuations of the Chern-Simons field appears to be shorter than the temperature scale $T\tau_\varphi^{cf} \ll 1$. This does not create any additional complication since most of the phase breaking results from scattering off the Chern-Simons field fluctuations whose dynamics (with characteristic frequency $T/g_{cf}$) is very slow compared to $\tau_\varphi^{cf}$, but fast compared to the time of the experiment. Field fluctuations which are static on the scale of the experiment time affect the mesoscopic fluctuations only by affecting $g_{cf}$. Field fluctuations that are faster than that scale make the potential landscape seen by the composite fermions time dependent and lead to a suppression of the mesoscopic fluctuations by partial ensemble averaging.

Consider the correlation function

$$\langle \rho_D(B)\rho_D(B+\delta B)\rangle - \langle \rho_D(B)\rangle\langle \rho_D(B+\delta B)\rangle = F_1\left(\frac{\delta B}{B^*}\right),$$

with the field $B$ near the $\nu = 1/2$ value. An experimental study of the decay of this correlation function is a way to

measure $L_\varphi^{cf}$: the characteristic magnetic field of the decay is $B^* \sim (L_\varphi^{cf})^{-2}\Phi_0$. The decay of this correlator as a function of density

$$\langle \rho_D(n)\rho_D(n+\delta n)\rangle - \langle \rho_D(n)\rangle\langle \rho_D(n+\delta n)\rangle = F_2\left(\frac{\delta n}{n^*}\right)$$

also yields $L_\varphi^{cf}$: the characteristic density change $n^*$ at which it decays is expected to correspond to half of an electron in a phase coherent region, i.e., $n^* = (L_\varphi^{cf})^{-2}/2$. This statement holds as long as the composite-fermion cyclotron radius is much larger than its mean-free path, i.e., for $|\nu - 1/2| < (2g_{cf})^{-1}$.

The ratio of the above characteristic field $B^*$ to the characteristic density $n^*$ yields two flux quanta

$$\frac{B^*}{n^*} \simeq 2\Phi_0. \tag{71}$$

This should be contrasted to the zero-field case, where

$$B^* \to \frac{\Phi_0}{L_\varphi^2}, \qquad n^* \to \frac{k_F \ell}{L_\varphi^2} \Rightarrow \frac{B^*}{n^*} \simeq \frac{\Phi_0}{g}.$$

At $B = 0$ the electrons do not carry any attached flux. Therefore the characteristic density $n^*$ corresponds to a change in the chemical potential of the order of $\tau_\varphi^{-1}$. Consequently, observation of the ratio (71) in a laboratory experiment serves as a verification of the concept of the flux attachment and the fact that charge carriers in the system are indeed composite fermions.

In single-layer measurements of mesoscopic fluctuations, the ratio (71) was reported by Kvon *et al.* (1997). In double-layer systems, mesoscopic fluctuations of Coulomb drag were investigated by Price, Savchenko, and Ritchie (2010), where it was shown that the fluctuations of drag resistivity obtained either by varying the magnetic field (with $n = \text{const}$) or by varying the carrier density (holding $B$ constant) exhibit the same characteristic scale (or a "period"), if plotted as a function of the filling factor $\nu = nh/eB$; see Fig. 17. The similarity of the two periods is equivalent to the ratio (71).

## IV. DRAG IN GRAPHENE-BASED DOUBLE-LAYER DEVICES

The physical picture of frictional drag outlined in the preceding sections is based on the following assumptions: (i) each of the layers is in a Fermi-liquid state, which at the very least means $\mu_{1(2)} \gg T$; (ii) the electron-electron interaction does not contribute to the intralayer transport scattering time; and (iii) the interlayer Coulomb interaction is assumed to be weak enough, $\alpha = e^2/v_F \ll 1$, such that $\rho_D$ is determined by the lowest-order perturbation theory (Jauho and Smith, 1993; Zheng and MacDonald, 1993; Flensberg and Hu, 1994; Flensberg *et al.*, 1995; Kamenev and Oreg, 1995) leading to Eq. (15). Most of the experiments in semiconductor devices (Eisenstein, 1992; Rojo, 1999) were performed on samples with high carrier density, where $\mu_{1(2)} \gg T$ [with the notable exception of Pillarisetty *et al.* (2002)].

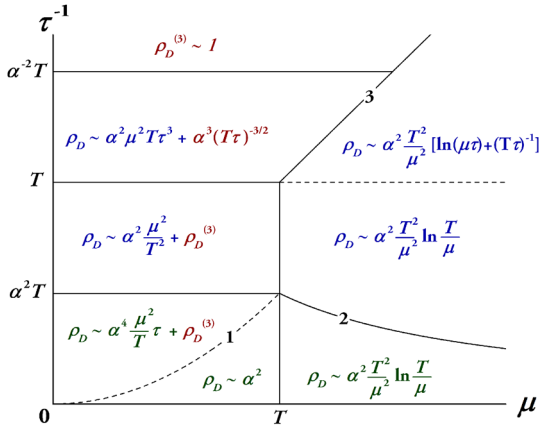


FIG. 18. The parameter regimes and the resulting drag coefficient in graphene for identical layers $\mu \ll \min(T/\alpha, v/d)$ and uncorrelated disorder. Bottom row (below curve 2, $\tau^{-1} \ll \alpha^2 T^2/\mu$): solutions to the quantum kinetic equation; see Sec. IV.B. Curve 1 ($\tau^{-1} = \alpha^2\mu^2/T$) separates the two regimes in Eq. (104). Middle row ($\alpha^2 T \ll \tau^{-1} \ll T$): the region where the quantum kinetic equation approach overlaps with the perturbation theory (Narozhny *et al.*, 2012). The third-order contribution $\rho_D^{(3)} = \mathcal{O}(\alpha^3)$ yielding nonzero drag at $\mu = 0$ is shown in red. Upper row ($\tau^{-1} \gg T$): the diffusive regime, where $\rho_D^{(3)}$ saturates for $\tau^{-1} \gg T/\alpha^2$). From Schütt *et al.*, 2013.

Lifting one or more of these assumptions leads to significant changes in the drag effect. Recently drag measurements were performed in a system of two parallel graphene sheets (Kim *et al.*, 2011; Gorbachev *et al.*, 2012; Kim and Tutuc, 2012; Titov *et al.*, 2013). This system offers much greater flexibility compared to prior experiments in semiconductor heterostructures. The graphene-based system allows one to scan a wide range of chemical potentials (by electrostatically controlling carrier density) from the Fermi-liquid regime to the charge neutrality (or Dirac) point $\mu_i = 0$. Moreover, using hexagonal boron nitride as a substrate (Ponomarenko *et al.*, 2011; Titov *et al.*, 2013), one can decrease disorder strength in the system and reach the regime, where transport properties of the two layers are dominated by electron-electron interaction $\tau \gg \tau_{ee}$. In addition, modern technology allows for a controlled growth of boron nitride yielding devices with a relatively wide range of the interlayer separations, which can be as low as $d = 1$ nm (corresponding to only three atomic layers). While the experiments (Kim *et al.*, 2011; Gorbachev *et al.*, 2012; Kim and Tutuc, 2012; Titov *et al.*, 2013) were performed at relatively low temperatures $T < v_g/d$ ($v_g$ is the quasiparticle velocity in graphene), the range of temperatures available for these measurements (typically, 4–240 K) is much wider than in earlier studies. In a parallel development, Coulomb drag measurements in graphene double ribbon structures were reported by Chen and Appenzeller (2013).

In graphene one can reach parameter regimes which were inaccessible in semiconductor samples; see Fig. 18: (i) near charge neutrality, the chemical potential may become smaller than temperature $\mu_{1(2)} \ll T$; the electronic system becomes nondegenerate; (ii) low-energy excitations in graphene are characterized by the linear Dirac-like dispersion; there is no

Galilean invariance in the system and transport properties are strongly affected by electron-electron interaction (Schütt *et al.*, 2011; Katsnelson, 2012). Moreover, electrons interact by means of 3D nonrelativistic Coulomb interaction, which breaks the Lorenz invariance of the Dirac Hamiltonian.

Nondegenerate systems were considered in the early work on frictional drag (Pogrebinskii, 1977; Price, 1983; Boiko and Sirenko, 1988; Jacoboni and Price, 1988) in the context of semiconductors, where elementary excitations are typically modeled by quasiparticles with parabolic dispersion. In that case, the electron-electron interaction plays a subleading role in single-layer transport (due to Galilean invariance). In contrast, in ultraclean graphene near the Dirac point single-layer transport is dominated by the electron-electron interaction (Schütt *et al.*, 2011; Narozhny *et al.*, 2012).

The low-temperature degenerate regime $T \ll \mu$ can be achieved by, e.g., electrostatically tuning the carrier density away from charge neutrality. In this case the system is expected to exhibit the same qualitative behavior as the semiconductor devices. Indeed, in ballistic samples and under the additional assumption of the small screening length $\varkappa d \gg 1$, one recovers (Tse, Hu, and Sarma, 2007; Narozhny *et al.*, 2012) the standard expression for the drag resistivity (21), albeit with an extra factor $N = 4$ reflecting higher degeneracy of the single-particle spectrum in graphene. However, this regime might be outside of the experimentally accessible parameter range of drag measurements in graphene-based samples (Kim *et al.*, 2011; Gorbachev *et al.*, 2012; Kim and Tutuc, 2012; Titov *et al.*, 2013).

For weaker doping, the assumption of the small screening length is invalid and the standard result (21) has to be modified (Narozhny *et al.*, 2012). A perturbative treatment can still be developed as long as the transport properties of both layers are dominated by disorder (i.e., $\tau_{ee} \gg \tau$). If electron-electron interaction is weak enough

$$\alpha^2 T\tau \min(1, T/\mu_i) \ll 1, \tag{72}$$

then the drag conductivity is given by the standard expression (25). Close to the Dirac point ($\mu_i \ll T$), this yields $\rho_D \propto \mu_1\mu_2$. At intermediate densities ($\mu \sim T$), the drag coefficient reaches a maximum and then decays toward the asymptotic limit (21). This decay is characterized by a long crossover from the logarithmic behavior at $\mu_i > T$ to the standard result (21) that is achieved only for small screening lengths $\varkappa d \gg 1$. As a result, the density dependence of $\rho_D(\mu_i \gtrsim v_g/d)$ cannot be described by a power law. Partially due to this fact, several conflicting results for $\rho_D$ have been reported in the literature (Tse, Hu, and Sarma, 2007; Hwang, Sensarma, and Sarma, 2011; Katsnelson, 2011; Peres, Santos, and Neto, 2011; Amorim and Peres, 2012; Carrega *et al.*, 2012; Lux and Fritz, 2012; Song and Levitov, 2012, 2013).

### A. Perturbative regime in ballistic samples

The perturbation theory is valid when transport properties of the sample are dominated by potential disorder, such that $\tau \ll \tau_{ee}$; see Eq. (72). In ballistic samples the mean-free path is large compared to the interlayer separation $\ell \gg d$. For experimentally relevant temperature range $T < v_g/d$, the latter condition is compatible with the more standard condition for ballistic transport in disordered systems $T\tau \gg 1$. The resulting parameter range occupies the middle row of the "phase diagram" shown in Fig. 18 between the line $T\tau \simeq 1$ and curve 2.

Perturbative calculations in the ballistic regime can be performed using either the diagrammatic (see Fig. 2) or kinetic equation approach (see Sec. II.B). In both cases, one arrives at an expression similar to Eq. (15), where the nonlinear susceptibility and screened interlayer interaction (and hence the polarization operator) have to be specified for Dirac fermions in graphene.

#### 1. Nonlinear susceptibility in graphene

In contrast to the theory reviewed in Sec. II, here we are interested in a wide range of chemical potentials including the Dirac point $\mu = 0$. The nonlinear susceptibility and polarization operator in graphene for arbitrary $\mu$ and $T$ were derived in Narozhny *et al.* (2012). Assuming the long, energy-independent impurity-scattering time $\tau$ and neglecting intralayer interaction, the nonlinear susceptibility has the form

$$\Gamma(\omega, \boldsymbol{q}) = -2\frac{e\tau \boldsymbol{q}}{\pi} g\left(\frac{\omega}{2T}, \frac{v_g q}{2T}; \frac{\mu}{T}\right), \tag{73}$$

where [with $W = \omega/(2T)$, $Q = v_g q/(2T)$, and $x = \mu/T$]

$$g(W, Q; x) = \begin{cases} \sqrt{\frac{W^2}{Q^2} - 1} \int_0^1 dz \frac{z\sqrt{1-z^2}}{z^2 - W^2/Q^2} I(z; W, Q; x), & |W| > Q, \\ -\sqrt{1 - \frac{W^2}{Q^2}} \int_1^\infty dz \frac{z\sqrt{z^2-1}}{z^2 - W^2/Q^2} I(z; W, Q; x), & |W| < Q, \end{cases} \tag{74}$$

$$I(z; W, Q; x) = \tanh\frac{zQ + W + x}{2} - \tanh\frac{zQ + W - x}{2} + \tanh\frac{zQ - W - x}{2} - \tanh\frac{zQ - W + x}{2}. \tag{75}$$

Under the same assumptions, the polarization operator is given by

$$\Pi^R = \frac{q}{4\pi^2 v_g} \int_0^1 \int_0^1 \frac{dz_1 dz_2}{z_1\sqrt{(1-z_1^2)(1-z_2^2)}} \left[ (z_1^{-2} - 1)\left(\frac{Q}{z_2 Q + W + i\eta} + \frac{Q}{z_2 Q - W - i\eta}\right) J_1(z_1^{-1}, z_2, x) \right.$$
$$\left. + (1 - z_2^2)\left(\frac{Q}{z_1^{-1} Q + W + i\eta} + \frac{Q}{z_1^{-1} Q - W - i\eta}\right) J_2(z_1^{-1}, z_2, x) \right], \tag{76a}$$

where

$$J_{1(2)}(z_1,z_2,x)=\tanh\frac{(z_1+z_2)Q+x}{2}+\tanh\frac{(z_1+z_2)Q-x}{2}\mp\tanh\frac{(z_1-z_2)Q+x}{2}\mp\tanh\frac{(z_1-z_2)Q-x}{2}. \tag{76b}$$

The perturbative calculation amounts to using the polarization operator (76) to determine the effective interlayer interaction (7) and then evaluating the drag conductivity [cf. Eqs. (15) and (25)] (Tse, Hu, and Sarma, 2007)

$$\sigma_D^{\alpha\beta}=\frac{1}{16\pi T}\sum_{\boldsymbol{q}}\int d\omega\frac{|\mathcal{D}_{12}^R|^2}{\sinh^2\omega/(2T)}\Gamma_1^\beta(\omega,\boldsymbol{q})\Gamma_2^\alpha(\omega,\boldsymbol{q}), \tag{77}$$

using the nonlinear susceptibility (73). The drag resistivity is then given by Eq. (13). For arbitrary $\mu$ and $T$ this calculation has to be performed numerically (Peres, Santos, and Neto, 2011; Lux and Fritz, 2012). At the same time, all qualitative features of the drag effect can be elucidated by using simple limiting values.

The nonlinear susceptibility (73) decays exponentially for $q\gg\max(\mu,T)$. In the vicinity of the Dirac point $T\gg\mu$, the integral that determines the function $g(W,Q,x)$ cannot be evaluated in terms of elementary functions. It can be shown, however, that in this case the nonlinear susceptibility is proportional to $\mu/T$ (Narozhny *et al.*, 2012):

$$g(x\ll 1)\propto\mu/T, \tag{78}$$

which could be expected since drag is supposed to vanish—or, more precisely, to change sign—at the Dirac point.

In the degenerate limit $T\ll\mu$, the dimensionless function $g(W,Q,x)$ may be approximated by

$$g(x\gg 1,|W|<Q)\approx\frac{4W}{Q}\sqrt{1-\frac{W^2}{Q^2}\frac{\sinh x}{\cosh Q+\cosh x}}. \tag{79}$$

Furthermore, for $\mu\gg v_Fq\gg\omega\sim T$ (or $Q\gg W$) the nonlinear susceptibility becomes similar to the standard (Kamenev and Oreg, 1995) Fermi-liquid expression for the ballistic regime (17)

$$g(x\gg 1,|W|\ll Q)\approx 4\omega/(v_gq), \tag{80}$$

where the extra factor of 4 corresponds to extra degeneracy of Dirac fermions in graphene (Tse, Hu, and Sarma, 2007; Amorim and Peres, 2012).

The relation (18) between $\mathbf{\Gamma}$ and $\mathrm{Im}\Pi$ is not satisfied in graphene. This follows from a direct comparison between their respective integral representations. In particular, the nonlinear susceptibility (73) vanishes at the Dirac point due to exact electron-hole symmetry $\mathbf{\Gamma}(\mu=0)=0$ (Tse, Hu, and Sarma, 2007), while the polarization operator (76) remains finite $\mathrm{Im}\Pi(\mu=0)\neq 0$ (Schütt *et al.*, 2011).

Similarly to the usual Lindhard function (Lindhard, 1954; Giuliani and Vignale, 2005), the polarization operator in doped graphene has the simple static limit

$$\Pi^R(\omega=T=0)=2k_F/(\pi v_g). \tag{81}$$

At the Dirac point, the result is somewhat different

$$\Pi^R(\mu=\omega=0)=\begin{cases}q/(4v_g), & T\ll v_gq,\\ 4T\ln 2/(\pi v_g^2), & T\gg v_gq.\end{cases} \tag{82}$$

**2. Lowest-order perturbation theory**

We now use the above approximations to find the limiting expressions for the drag resistivity in the perturbative regime (Narozhny *et al.*, 2012).

In the simplest limit $N\alpha\mu\ll T$, the perturbative approach is justified automatically. In this case, the single-layer conductivity is determined by weak impurity scattering and has the form

$$\sigma_0=e^2T\tau h_0(\mu/T), \tag{83a}$$

where

$$h_0(x)=\frac{2}{\pi}\int_{-\infty}^{\infty}\frac{dz|z|}{\cosh^2(z+x/2)}=\frac{2}{\pi}\begin{cases}x, & x\gg 1,\\ 2\ln 2, & x\ll 1.\end{cases} \tag{83b}$$

In this limit screening is ineffective and for $\mu_i,\ T\ll v_g/d$ the interlayer spacing drops out of the problem. Then we may use the bare Coulomb potential (5), while the frequency and momentum integration in Eq. (77) are determined by the nonlinear susceptibility (73).

Close to the double Dirac point $\mu_i\ll T$, the nonlinear susceptibility can be approximated by Eq. (78), while the remaining integration is dominated by frequencies and momenta of order temperature $\omega,\ v_gq\sim T$, yielding a dimensionless coefficient. The resulting drag resistivity is given by

$$\rho_D(\mu_i\ll T)\approx 1.41\alpha^2(\hbar/e^2)\mu_1\mu_2/T^2. \tag{84a}$$

If only one of the layers is tuned close to the Dirac point $\mu_1\ll T\ll\mu_2$, the drag conductivity (77) is independent of the properties of the second layer, as the integration in Eq. (77) is still determined by the region $\omega,\ v_gq\sim T$. The single-layer conductivity in the second layer is still determined by $\mu_2$; see Eq. (83). As a result,

$$\rho_D(\mu_1\ll T\ll\mu_2)\approx 5.8\alpha^2(\hbar/e^2)\mu_1/\mu_2. \tag{84b}$$

In the opposite limit $\mu_i\gg T$, the nonlinear susceptibility is given by Eq. (79). Now the momentum integral in Eq. (77) is logarithmic and is dominated by large values of momentum $Q\gg W$. The ratio of the hyperbolic functions in Eq. (79) is similar to the step function: it is equal to unity for $Q\ll x$ and vanishes at larger values of momentum $Q\gg x$. Therefore $x$ effectively acts as the upper cutoff and the momentum integral can be approximated by a logarithm

$$\int_W^\infty\frac{dQ}{Q}\frac{\sinh^2x}{(\cosh Q+\cosh x)^2}\approx\ln\frac{x}{W}. \tag{84c}$$

Consequently the drag coefficient is similar to the standard results of Sec. II

$$\rho_D(\mu_2 > \mu_1 \gg T) \approx \alpha^2 \frac{\hbar}{e^2} \frac{8\pi^2}{3} \frac{T^2}{\mu_1 \mu_2} \ln \frac{\mu_1}{T}. \tag{84d}$$

This is to be expected, since at low temperatures $T \ll \mu_i$ the phase-space argument yielding the $T^2$ dependence is justified and the electron-hole asymmetry determines the dependence on the chemical potential. The logarithmic factor is beyond such qualitative estimates [the result (84d) was calculated with logarithmic accuracy].

*a. Static screening for vanishing interaction strength*

For a slightly stronger interaction (i.e., smaller dielectric permittivity of the insulating substrate) or slightly larger interlayer spacing the condition $N\alpha\mu_i \ll T$, $\mu_i \ll v_g/d$ breaks down and one needs to take into account static screening. Static screening corresponds to the approximation (81) to the polarization operator. If the interaction strength is still small $\alpha \to 0$, then the interaction can be described by

$$\mathcal{D}_{12}^R = -\frac{2\pi\alpha v_g^2}{v_g q + 2N\alpha\mu} e^{-qd}, \tag{85}$$

where $N = 4$ is due to spin and valley degeneracy. The additional constant in the denominator affects the logarithmic integral (84c). As the chemical potential is being increased away from the Dirac point, the following regimes may be gradually achieved (here we discuss these regimes for the case of identical layers; the generalization to the case of two inequivalent layers is straightforward):

(i) $N\alpha\mu \ll T \ll \mu \ll v_g/d$: This regime is identical to the arguments leading to Eq. (84d).

(ii) $N\alpha\mu \ll T \ll v_g/d \ll \mu$: If the chemical potential is increased beyond the inverse interlayer spacing, then the momentum integration in Eq. (84c) is cut off by $v_g/d$ instead of $\mu$. The logarithmic behavior of the drag conductivity will be modified and $\sigma_D$ no longer depends on the chemical potential

$$\sigma_D \sim \alpha^2 e^2 T^2 \tau^2 \ln[v_g/(Td)]. \tag{86a}$$

(iia) $T \ll N\alpha\mu \ll \mu \ll v_g/d$: In this case one finds instead of Eq. (86a)

$$\sigma_D \sim \alpha^2 e^2 T^2 \tau^2 \ln[1/(N\alpha)]. \tag{86b}$$

(iii) $T \ll N\alpha\mu \ll v_g/d \ll \mu$: Increasing the chemical potential further leads to the regime where the static screening can no longer be neglected. Now the lower integration limit in Eq. (84c) is effectively given by the inverse screening length rather than the frequency. The upper limit is still determined by the interlayer spacing. Therefore the drag conductivity again depends logarithmically on the chemical potential (Katsnelson, 2011)

$$\sigma_D \sim \alpha^2 e^2 T^2 \tau^2 \ln[v_g/N\alpha\mu d], \tag{86c}$$

but now this is a *decreasing* function, indicating the existence of the absolute maximum of the drag conductivity as a function of the chemical potential.

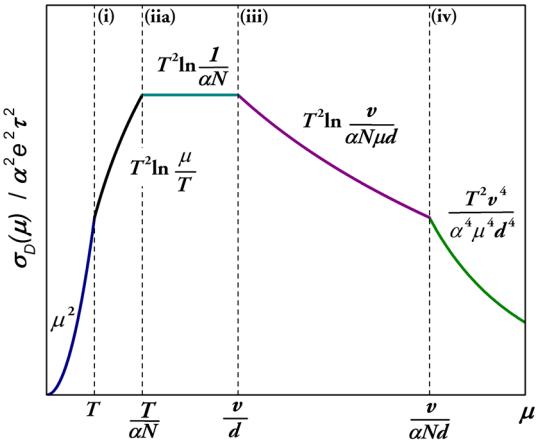


FIG. 19. The drag conductivity (in units of $\alpha^2 e^2 \tau^2$, identical layers) as a function of the chemical potential illustrating the results (86). The colored line shows the quadratic dependence (84a) in the vicinity of the Dirac point. If $T \gg N\alpha v_g/d$, then the region (iia) should be replaced by (ii): the logarithmic dependence $T^2 \ln(1/\alpha)$ should be replaced by $T^2 \ln[v_g/(Td)]$, and the limits $v_g/d$ and $T/(N\alpha)$ should be exchanged. From Narozhny *et al.*, 2012.

(iv) $T \ll v_g/d \ll N\alpha\mu \ll \mu$: Finally, if the chemical potential is so large that the screening length becomes smaller than the interlayer spacing, the momentum integral in Eq. (84c) is no longer logarithmic. As the integration is now dominated by momenta large compared to $T$, the nonlinear susceptibility may be approximated by Eq. (80), leading to the standard Fermi-liquid result

$$\sigma_D = \frac{\zeta(3)}{4} \frac{e^2 \tau^2 T^2}{(k_F d)^2 (\varkappa d)^2}, \qquad \varkappa = 4\alpha k_F, \tag{86d}$$

which differs from that of Kamenev and Oreg (1995) [see Eq. (21)] only by the factor reflecting valley degeneracy in graphene (Tse, Hu, and Sarma, 2007; Katsnelson, 2011; Amorim and Peres, 2012). These results are illustrated in Fig. 19.

*b. Static screening for intermediate interaction strength*

The results (84) and (86) rely on the interaction weakness. For stronger interaction $N\alpha > 1$, (i) the approximation (85) might be unjustified and the full expression (7) for the interaction propagator should be used; (ii) the four regimes (86) may not exist, since it might happen that $T/(N\alpha) \ll T < v_g/(N\alpha d) \ll v_g/d$. In this case, perturbative analysis can still be justified in the degenerate regime $\mu \gg T$, where there are two distinct regimes, (a) $\mu \ll v_g/d$, and (b) $\mu \gg v_g/d$ (Narozhny *et al.*, 2012); the latter regime is usually identified with the Fermi-liquid result (86d). As the single-layer conductivity is still large and dominated by disorder, the condition (72) can be somewhat relaxed:

$$\tau_{ee} \gg \tau \Rightarrow \tau^{-1} \gg \alpha^2 T^2/\mu \Rightarrow \alpha^2 T\tau \ll \mu/T. \tag{87}$$

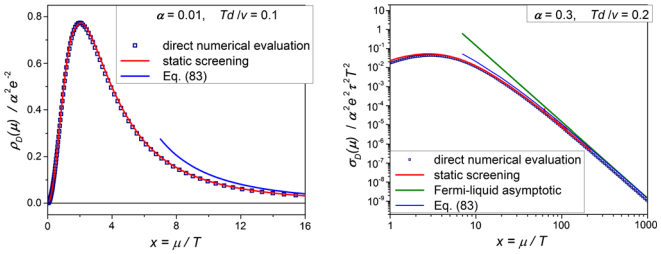


FIG. 20. Results of the numerical evaluation of the drag coefficient in the case of identical layers. The squares represent the calculation of Eq. (25) with the only approximation that the polarization operator in the screened interlayer interaction (7) was evaluated in the absence of disorder. The line on top of the squares corresponds to the same calculation, with the polarization operator replaced by Eq. (81). The asymptotic tail at $\mu/T > 8$ was calculated with the approximate expression (90b), valid for $\mu \gg v_g/d$. Left panel: $\alpha = 0.01$, $Td/v_g = 0.1$. Right panel: $\alpha = 0.3$ and $Td/v_g = 0.2$, log-log scale. The straight line represents the Fermi-liquid result (86d). From Narozhny *et al.*, 2012.

Proceeding under the assumptions of static screening and the ballistic regime (i.e., the dominant contribution to the effect comes from large momenta $v_g q > \omega$), the result of momentum integration is determined by the upper limit and can be assumed independent of $\omega$. The frequency and momentum integrals factorize and neglecting $W/Q$ under the square root in Eq. (79) one finds

$$\sigma_D = \alpha^2 e^2 T^2 \tau^2 f_0\left(\frac{\mu}{T}; \alpha; \frac{Td}{v_g}\right),$$
$$f_0(x;\alpha;\lambda) \approx \frac{32}{3}\int_1^\infty \frac{dQQ^3 e^{-4\lambda Q}}{\{[Q+\tilde{\alpha}(x)]^2 - \tilde{\alpha}(x)^2 e^{-4\lambda Q}\}^2} \times \frac{\sinh^2 x}{(\cosh Q + \cosh x)^2}, \tag{88}$$

where

$$\tilde{\alpha}(x) = N\alpha x/2. \tag{89}$$

The results for weaker interaction, Eqs. (86), can be recovered from Eq. (88) by neglecting terms proportional to $\tilde{\alpha}^2$ in the denominator [which corresponds to approximating the interlayer interaction (7) by Eq. (85)]. In the limit $\mu \gg v_g/d$, the function $f_0$ depends on a single parameter

$$f_0(x\lambda \gg 1) \approx \tilde{f}_0(4\lambda\tilde{\alpha}), \tag{90a}$$

where

$$\tilde{f}_0(y) = \frac{32}{3}\int_0^\infty \frac{dZZ^3 e^{-Z}}{[(Z+y)^2 - y^2 e^{-Z}]^2}. \tag{90b}$$

The function (90b) describes the crossover between the regimes (iii) and (iv) of Eqs. (86) (see Fig. 19). This can be seen by evaluating the integral in the two limits (here $\gamma_0 \approx 0.577\,216$ is the Euler's constant)

TABLE I. Asymptotic expressions for the drag coefficient to the leading order of perturbation theory assuming "realistic" interaction strength $\alpha N \gtrsim 1$, identical layers $n_1 = n_2 = n$, and the experimentally relevant situation $T < v_g/d$. In the opposite regime $T \gg v_g/d$ all results for $\rho_D$ should be divided by $Td/v_g$ (Lux and Fritz, 2012; Narozhny *et al.*, 2012).

| Parameter region | Drag coefficient |
|---|---|
| $\mu \ll T$ | $\rho_D \sim nT^{-2}$ |
| $T \ll \mu \ll v_g/d$ | $\rho_D \sim T^2 n^{-1} \ln(\alpha N n^{1/2} d/v_g)$ |
| $\mu \gg v_g/d$ | $\rho_D = \rho_D^{FL} \sim T^2 n^{-3} d^{-4}$ |

$$\tilde{f}_0(y \ll 1) \approx -32/3(\ln y + \gamma_0 + 11/6), \tag{91a}$$

$$\tilde{f}_0(y \gg 1) \approx 64\zeta(3) y^{-4}. \tag{91b}$$

Numerically, this crossover spans a large interval of values of the chemical potential such that the Fermi-liquid result (86d) is practically unattainable in graphene-based drag measurements (Tutuc, Pillarisetty, and Shayegan, 2009); see Fig. 20.

In experiment one typically measures carrier density rather than the chemical potential (Kim *et al.*, 2011; Gorbachev *et al.*, 2012; Kim and Tutuc, 2012; Titov *et al.*, 2013). In graphene, the electron density is given by

$$n = \int_{-\infty}^{\infty} \frac{d\epsilon|\epsilon|}{\pi v_g^2}\left[\tanh\frac{\epsilon}{2T} - \tanh\frac{\epsilon-\mu}{2T}\right]. \tag{92a}$$

Using the asymptotic expressions

$$n = \frac{1}{\pi v_g^2}\begin{cases} \mu^2, & \mu \gg T, \\ (4\ln 2)\mu T, & \mu \ll T, \end{cases} \tag{92b}$$

one can obtain the qualitative dependence of $\rho_D$ on $n$; see Table I.

The strongly doped, Fermi-liquid regime has attracted the most attention in literature. Most authors report the standard $\rho_D \sim T^2 n^{-3} d^{-4}$ behavior (Tse, Hu, and Sarma, 2007; Hwang, Sensarma, and Sarma, 2011; Katsnelson, 2011; Amorim and Peres, 2012; Carrega *et al.*, 2012; Narozhny *et al.*, 2012) assuming the energy-independent impurity-scattering time.

### 3. Energy-dependent scattering time

In graphene, the impurity-scattering time strongly depends on the type of disorder and on energy (Katsnelson, 2012). In particular, for Coulomb scatterers (Ando, 2006; Cheianov and Fal'ko, 2006; Nomura and MacDonald, 2006, 2007) or strong short-range impurities (Ostrovsky, Gornyi, and Mirlin, 2006)

$$\tau(\epsilon) = \tau_0^2|\epsilon|. \tag{93a}$$

For weak short-ranged disorder (Shon and Ando, 1998)

$$\tau(\epsilon) = \gamma/|\epsilon|. \tag{93b}$$

Moreover, quenched disorder in graphene experiences logarithmic renormalization (Aleiner and Efetov, 2006).

Drag in the presence of Coulomb impurities was first considered by Hwang, Sensarma, and Sarma (2011) and Peres, Santos, and Neto (2011). Both papers reported a stronger dependence of the drag coefficient on the carrier density and interlayer separation $\rho_D \sim T^2 n^{-4} d^{-6}$. This result was later disputed by Amorim *et al.* (2012), Carrega *et al.* (2012), and Narozhny *et al.* (2012). They showed that the energy (or momentum) dependence of $\tau$ is qualitatively irrelevant for the asymptotic behavior of $\rho_D$. In the degenerate limit, microscopic calculations lead to the same results with $\tau(\mu)$ substituted in place of $\tau$. Close to the neutrality point, the drag coefficient acquires an additional logarithmic factor

$$\rho_D(\mu_i \ll T) \sim \alpha^2(\hbar/e^2)(\mu_1\mu_2/T^2)\ln T\tau(T). \tag{94}$$

#### 4. Plasmon contribution

The dynamically screened interaction propagator contains plasmon poles that may (see Sec. II.B) affect the resulting drag resistivity. Theoretically, plasmons were studied in graphene monolayers (at $T = 0$) by Wunsch *et al.* (2006), Hwang and Das Sarma (2007), and Schütt *et al.* (2011) and in double-layer graphene systems by Badalyan and Peeters (2012), Profumo *et al.* (2012), and Stauber and Gómez-Santos (2012). Renormalization of the plasmon spectrum due to electron-electron interaction was considered by Abedinpour *et al.* (2011). Experimentally, plasmons were observed in graphene on $SiO_2$ substrate (Fei *et al.*, 2011, 2012), graphene-insulator stacks (Yan, X. Li *et al.*, 2012), and in graphene microribbon arrays (Ju *et al.*, 2011). Bound states of plasmons with charge carriers, the so-called "plasmarons," were observed by Bostwick *et al.* (2010) and Walter *et al.* (2011). Plasmons subjected to high magnetic field were studied by Yan, Z. Li *et al.* (2012). For reviews of graphene plasmonics see Grigorenko, Polini, and Novoselov (2012) and Luo *et al.* (2013). More recently, plasmonic excitations in Coulomb coupled $N$-layer graphene structures were studied by Zhu, Badalyan, and Peeters (2013).

Within this perturbative approach, i.e., Eq. (72), and for low enough temperatures $\mu, T \ll v_g/d$, the plasmon contribution to drag is subleading (Narozhny *et al.*, 2012). The plasmon pole appears in the region $\omega > v_g q$. Similarly to the situation in semiconductor devices (Sec. II.B), double-layer graphene systems admit an acoustic ($\omega \sim q$) and an optical ($\omega \sim \sqrt{q}$) plasmon mode (Das Sarma and Madhukar, 1981; Principi *et al.*, 2012). In the case where the plasmon decay rate is small (as determined by either weak Coulomb interaction or weak disorder), one can use the $\delta$-function approximation to the interlayer interaction propagator (Flensberg and Hu, 1995). The corresponding contribution to the drag conductivity contains a small factor $g^2|D|^2 \sim \alpha^3$ for small momenta $v_g q \sim \alpha T$ (or $\alpha^4$ for $v_g q \sim T$). If the energy dependence of the scattering time is taken into account, the small parameter is $\alpha^2 T\tau$; see Eq. (72).

This conclusion is illustrated in Fig. 20 showing a comparison between the full numerical evaluation of the perturbative drag coefficient using Eqs. (7), (73), (76), and (77) and the same calculation within the approximation of static screening (85). Numerical modeling of experimental samples, see Figs. 21 and 22, includes the plasmon contribution automatically by using the dynamically screened interaction propagator (7).

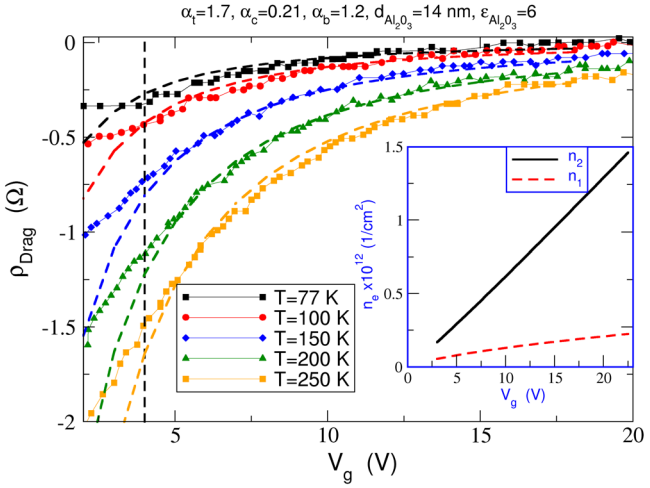


FIG. 21. Results of the numerical evaluation (lines) of the drag coefficient and comparison with the data (symbols) of Kim *et al.* (2011). The interlayer spacing ($d = 14$ nm) and dielectric constants of the insulating material were chosen to represent the experimental device. Inset: the relation of the carrier densities and gate voltage, obtained from the electrostatic model of the sample. From Peres, Santos, and Neto, 2011.

At the same time, a quantitative description of experiments, especially in devices with wider interlayer spacing, might be significantly affected by such aspects as inhomogeneous dielectric background (Badalyan and Peeters, 2012; Carrega *et al.*, 2012) and hybridization between phonon and plasmon modes (Amorim *et al.*, 2012). Plasmon-mediated drag between graphene wave guides was suggested by Shylau and Jauho (2014).

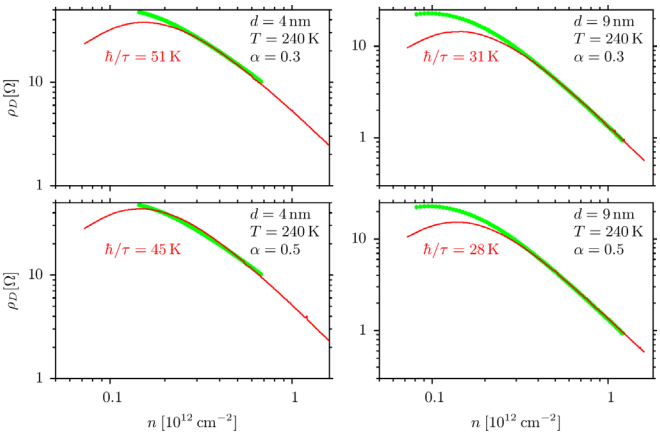


FIG. 22. Results of the numerical evaluation (Titov, Narozhny, and Gornyi, 2013) of the drag coefficient (red line) and the experimental data (green dots) (Ponomarenko, 2013) in the case of identical layers. The values of $T = 240$ K and $d$ are taken from the experiment. The only fitting parameter is the energy-independent impurity-scattering time (once the value of $\alpha_g$ is chosen). The polarization operator was calculated at $T = 240$ K and in the presence of disorder (in the ballistic regime).

#### 5. Drag between massless and massive fermions

Graphene-based double-layer devices can be used to observe Coulomb drag between massless and massive particles by coupling Dirac fermions in monolayer graphene to quasiparticles with parabolic dispersion in either bilayer graphene (Scharf and Matos-Abiague, 2012) or a usual 2DEG (Principi *et al.*, 2012; Scharf and Matos-Abiague, 2012). Experimental realizations were reported by Fisichella *et al.* (2014) and Gamucci *et al.* (2014).

Theoretical analysis of Principi *et al.* (2012) and Scharf and Matos-Abiague (2012) is based on the standard expression (77). Both works focus on the low-temperature, degenerate regime $T \ll \mu$. As expected, in the case of strong screening $\varkappa d \gg 1$, both works reproduce the standard result (21). For $\varkappa d \ll 1$, the resulting drag coefficient is still quadratic in temperature, but contains also a logarithmic factor reminiscent of Eqs. (86). Principi *et al.* (2012) reported a $d$-independent drag in the special case $k_g = k_{2D}$ (which implies a density mismatch between the layers due to the difference in the degeneracies of single-particle states). In the low-density limit $n \to 0$ this yields $\rho_D \propto n^{-1}$, similar to the results of Carrega *et al.* (2012); see also Table I. On the other hand, Scharf and Matos-Abiague (2012) reported $\rho_D \propto n^{-2}$ in the limit $d \to 0$ and for $n_g = 2n_{2D}$. Such discrepancies in the asymptotic behavior of $\rho_D$ may appear due to the complicated structure of the nonlinear susceptibility in graphene; see Eqs. (86) and Fig. 19.

The predicted $T^2$ dependence is observed in experiment (Gamucci *et al.*, 2014) in the $10 < T < 40$ K range, although with the smaller magnitude. At higher temperatures, a violation of Onsager reciprocity was observed. This was attributed to the interlayer current. Most interestingly, at lower temperatures $T < 10$ K, the measured drag shows a marked upturn that may indicate a phase transition at $T_c \sim 10 - 100$ mK; see Sec. VII.B.

The system of coupled Dirac and Schrödinger quasiparticles was also considered by Balram, Hutasoit, and Jain (2014), where it was found that interspecies interaction plays a significant role in determining collective (plasmon) modes.

#### 6. Numerical evaluation of the drag coefficient

The previous discussion demonstrates that already at the perturbative level the drag conductivity (77) exhibits multiple asymptotic dependences. Consequently, virtually every paper on the subject presents results of a numerical evaluation of Eq. (77). In contrast to the earlier work on semiconductor devices (see Sec. II), most authors focus on the density (or chemical potential) dependence rather than on the $T$ dependence. The overall shape of $\rho_D(n)$ curves is qualitatively the same in all calculations. At the Dirac point, drag vanishes, $\rho_D(n = 0) = 0$ [this conclusion does not agree with the experiments of Gorbachev *et al.* (2012) and Titov *et al.* (2013), see below]. Deep in the degenerate (or low-temperature) regime $T \ll \mu$, $\varkappa d \gg 1$, the drag coefficient reaches the standard decaying result (21). Therefore, for intermediate densities there has to be a maximum, roughly at $\mu \sim T$. The corresponding shape is shown in Fig. 20.

Peres, Santos, and Neto (2011) presented detailed numerical calculations aimed at describing the experimental findings of Kim *et al.* (2011); see Fig. 21. This calculation included electrostatic modeling of the device (which included two insulators $SiO_2$ and $Al_2O_3$), dynamically screened (within RPA) electron-electron interaction and the realistic model of Coulomb impurities. For doped graphene layers, the results of the calculation show excellent agreement with the data.

Theoretical modeling of ultraclean graphene double layers (using boron nitride as a substrate as well as insulating spacer) based on the theory of Narozhny *et al.* (2012) was performed by Titov, Narozhny, and Gornyi (2013); see Fig. 22. In this calculation, the polarization operator was calculated at the experimental temperature in the presence of disorder, in contrast to the $T = 0$, free-electron expression (76). The use of full, dynamically screened Coulomb interaction ensured that all plasmon-related features were automatically taken into account. Choosing realistic values (Kozikov *et al.*, 2010; Peres, Santos, and Neto, 2011) for the effective coupling constant, the only fitting parameter in this calculation was the impurity-scattering time $\tau$, which was taken to be energy independent similar to the earlier discussion. Such a calculation was also able to reproduce the data (Ponomarenko, 2013) in the doped regime.

The results shown in Figs. 21 and 22 confirm the applicability of the perturbative approach to Coulomb drag in doped graphene. In contrast to similar calculations aimed at semiconductor devices (see Sec. II), these theories are able to reach quantitative agreement with the experimental data with the minimum of fitting parameters. This implies that frictional drag in graphene is dominated by Coulomb interaction, with phonons playing only a subleading role. The latter conclusion can be expected, given that electrons in graphene are physically confined to move in a two-dimensional plane and the rigidity of the crystal lattice (Katsnelson, 2012).

### B. Hydrodynamic regime

The perturbation theory outlined in Sec. IV.A can be justified either in the case of weak interaction $\alpha \ll 1$ or in the degenerate regime $\mu \gg T$; see Eq. (72). At the same time, the applicability condition (72) involves the impurity-scattering time $\tau$: the perturbation theory fails if the system is "too clean," or in other words if electronic transport is dominated not by disorder, but rather by the electron-electron interaction. The latter affects transport properties of graphene due to the absence of Galilean invariance: the velocity of Dirac fermions $\boldsymbol{v} = v_g^2 \boldsymbol{p}/\epsilon$ is independent of the absolute value of the momentum and therefore total momentum conservation does not prevent velocity (or current) relaxation. As a result, electron-electron scattering is characterized by its own transport relaxation time, which may become smaller than the scattering time due to potential disorder $\tau_{ee} \ll \tau$.

"Ultraclean" graphene double layers were discussed by Schütt *et al.* (2013), Titov *et al.* (2013), and Narozhny *et al.* (2015) within the framework of the quantum kinetic equation. In principle, solving the kinetic equation in a strongly interacting system is a formidable problem that cannot be solved in general terms using presently available analytic methods. However, in graphene, one can take advantage of the

kinematic peculiarity specific to Dirac fermions. Indeed, the scattering of particles with almost collinear momenta is enhanced since the momentum and energy conservation laws coincide. This restricts kinematics of the Dirac fermions (Fritz *et al.*, 2008; Kashuba, 2008; Schütt *et al.*, 2011) and leads to the singularity in the collision integral. This singularity leads to the fast thermalization of particles within a given direction and allows one to derive macroscopic, or hydrodynamic, equations that generalize Eq. (2) for interacting Dirac fermions. In monolayer graphene, this approach was discussed by Fritz *et al.* (2008), Kashuba (2008), Müller and Sachdev (2008), Foster and Aleiner (2009), and Svintsov *et al.* (2012). An alternative macroscopic approach to Coulomb drag in graphene[14] was suggested by Song and Levitov (2012, 2013) and Song, Abanin, and Levitov (2013).

### 1. Collinear scattering singularity

Singular behavior of the collision integrals in the case of collinear scattering of the Dirac fermions (Arnold, Moore, and Yaffe, 2000; Fritz *et al.*, 2008; Kashuba, 2008; Müller, Schmalian, and Fritz, 2009; Schütt *et al.*, 2013) is central to the hydrodynamic approach to transport in graphene.

The general form of the kinetic equation in layer $i$ is given by Eq. (9) with the addition of the intralayer collision integral. If the system is weakly perturbed from equilibrium, then the distribution function can be written in the form (10). Weak deviations from equilibrium are associated with the smallness of the nonequilibrium correction $h$, allowing one to linearize the collision integrals (Lifshitz and Pitaevskii, 1981). The linearized form of the collision integrals is given by

$$\mathcal{I}_{ij} = \sum_{1,1',2'} w_{12,1'2'} f^{(0)}_{j,1} f^{(0)}_{i,2} [1 - f^{(0)}_{j,1'}][1 - f^{(0)}_{i,2'}] \times [h_{j,1'} + h_{i,2'} - h_{j,1} - h_{i,2}], \tag{95a}$$

where the function

$$w_{1,2;1',2'} = |\langle 1,2|U|1',2'\rangle|^2 (2\pi)^3 \delta(\epsilon_1 + \epsilon_2 - \epsilon_{1'} - \epsilon_{2'}) \times \delta(\boldsymbol{k}_1 + \boldsymbol{k}_2 - \boldsymbol{k}'_1 - \boldsymbol{k}'_2) \tag{95b}$$

determines the probability of scattering from states $1'$, $2'$ into states 1, 2 (within the Fermi golden-rule approximation). Here $\langle 1,2|U|1',2'\rangle$ is the interaction matrix element. The indices $i$, $j = 1, 2$ denote the two layers.[15]

In graphene, the interaction matrix elements are most conveniently expressed in the basis of the eigenstates of the Dirac Hamiltonian $|\epsilon, \boldsymbol{e}_{\boldsymbol{v}}\rangle$ labeled by their energy $\epsilon$ and the unit vector $\boldsymbol{e}_{\boldsymbol{v}} = \boldsymbol{v}/v_g$ pointing in the direction of velocity (for a given spin and valley projection):

$$|\langle 1,2|U|1',2'\rangle|^2 = |U(\boldsymbol{q})|^2 \frac{1 + \boldsymbol{e}^{(1)}_{\boldsymbol{v}} \boldsymbol{e}^{(1')}_{\boldsymbol{v}}}{2} \frac{1 + \boldsymbol{e}^{(2)}_{\boldsymbol{v}} \boldsymbol{e}^{(2')}_{\boldsymbol{v}}}{2}. \tag{96}$$

Here $\boldsymbol{q} = \boldsymbol{k}_1 - \boldsymbol{k}'_1$ is the transferred momentum and the two fractions are the "Dirac factors" (Katsnelson, 2012). Now one can separate quantities related to the initial and final states in the function $w_{12,1'2'}$ by using the identities

$$\delta(\epsilon_1 + \epsilon_2 - \epsilon'_1 - \epsilon'_2) = \int d\omega \delta(\epsilon_1 - \epsilon'_1 + \omega)\delta(\epsilon_2 - \epsilon'_2 - \omega),$$

$$\delta(\boldsymbol{k}_1 + \boldsymbol{k}_2 - \boldsymbol{k}'_1 - \boldsymbol{k}'_2) = \int d^2q \delta(\boldsymbol{k}_1 - \boldsymbol{k}'_1 + \boldsymbol{q})\delta(\boldsymbol{k}_2 - \boldsymbol{k}'_2 - \boldsymbol{q}).$$

The $\delta$ functions yield $\epsilon'_1 = v_g|\boldsymbol{k}_1 + \boldsymbol{q}|$ and hence allow one to sum over the states $1'$ and $2'$ in the collision integral (95). Each of these sums results in a diverging factor[16]:

$$\sum_{1'} \propto \frac{1}{\sqrt{v_g^2 q^2 - \omega^2}}. \tag{97}$$

One can see that the divergence corresponds to collinear scattering by examining the angle $\varphi_{\boldsymbol{k}_1\boldsymbol{q}}$ at the light cone:

$$\cos\varphi_{\boldsymbol{k}_1\boldsymbol{q}}(\omega = v_g q) = 1 \Rightarrow \varphi_{\boldsymbol{k}_1\boldsymbol{q}} = 0 \quad (\text{or } \pi).$$

Hence, the argument of one of these $\delta$ functions vanishes: $\epsilon'_1 = \epsilon_1 + \omega$. A similar conclusion follows for the momentum $\boldsymbol{k}_2$. Thus, all momenta are collinear.

Physically, the divergence (97) represents the fact that for the linear spectrum the energy and momentum-conservation laws coincide. Consequently, any relaxation rate obtained by integrating the collision integral (95) over the state 2 will be logarithmically divergent. In order to regularize this divergence, one has to go beyond the golden-rule approximation and take into account renormalization of the spectrum (Abrikosov and Beneslavskii, 1971; González, Guinea, and Vozmediano, 1999; Son, 2007). This leads (Arnold, Moore, and Yaffe, 2000; Fritz *et al.*, 2008) to the appearance of a large factor $|\ln(\alpha)| \gg 1$ in generic relaxation rates in graphene. In disordered graphene, this singularity is also cut off by disorder-induced broadening of the momentum-conservation $\delta$ function (Narozhny *et al.*, 2012).

### 2. Macroscopic linear-response theory in graphene

The collinear scattering singularity (97) allows for an approximate, yet nonperturbative solution of the kinetic equation in graphene (Fritz *et al.*, 2008; Kashuba, 2008; Schütt *et al.*, 2013; Narozhny *et al.*, 2015). The idea is to find zero modes of the collision integral and build macroscopic equations for the corresponding currents.

The standard perturbative description of Coulomb drag is based on the energy-independent approximation for the

[14]The theory of Song and Levitov (2012, 2013) and Song, Abanin, and Levitov (2013) relies on correlations of the disorder potential in the two layers; see Sec. IV.F.

[15]In the perturbative approach of Sec. II.B, the kinetic equation (9) contained only the interlayer collision integral. Therefore, one could associate the states 1 and 2 with the active and passive layers and avoid extra layer indices.

[16]In Sec. IV.A, the nonlinear susceptibility (73) did not exhibit this divergence due to an accidental cancellation that is specific to the particular case of energy-independent impurity-scattering time. In a more general situation the cancellation does not occur and as a result the rate $\tau_D^{-1}$ contains an extra logarithmic factor; see Eq. (94).

nonequilibrium distribution function (10). This constant solution of the kinetic equation describes the single zero mode of the intralayer collision integral corresponding to conservation of the electric charge (or the number of particles). Macroscopic charge flow is described by the electric current (12). Integrating the kinetic equation, one finds the macroscopic equation for $\boldsymbol{j}$ equivalent to the Drude theory; see Eqs. (2). Such a solution is justified by the condition (72), which means that the collision integral in the kinetic equation is dominated by disorder.

In contrast, in ultraclean graphene the collision integral is dominated by Coulomb interaction. Using the collinear scattering singularity [i.e., for $|\ln(\alpha)| \gg 1$], one can neglect all but the zero modes of $\mathcal{I}$ [treated as an integral operator acting on $h_i(\epsilon)$]. In practice, this means retaining only those terms in the power series of the distribution function $h_i$ which correspond to either zero modes of the collision integral or to its eigenmodes with nondivergent eigenvalues. Fritz *et al.* (2008), Kashuba (2008), and Schütt *et al.* (2013) developed the following two-mode approximation:

$$h_i = (\boldsymbol{a}_0^{(i)} + \boldsymbol{a}_1^{(i)}\epsilon)\boldsymbol{v}. \tag{98}$$

The vectors $\boldsymbol{a}_i$ can be expressed in terms of the two macroscopic currents in graphene, the electric current (12) and the energy current

$$\boldsymbol{Q}_i = \sum \epsilon \boldsymbol{v}\delta f_i. \tag{99}$$

The appearance of inequivalent currents is the essential feature of graphene physics. In general, the collision integral has three nondecaying eigenmodes; hence Narozhny *et al.* (2015) used the three-mode approximation:

$$h_i = (\boldsymbol{a}_0^{(i)} + \boldsymbol{a}_s^{(i)}\mathrm{sign}(\epsilon) + \boldsymbol{a}_1^{(i)}\epsilon)\boldsymbol{v}. \tag{100}$$

The $\mathrm{sign}(\epsilon)$ mode is described by the imbalance current (Foster and Aleiner, 2009)

$$\boldsymbol{P}_i = \sum \mathrm{sign}(\epsilon)\boldsymbol{v}\delta f_i. \tag{101}$$

Integrating the kinetic equation with the help of either of these approximations for the nonequilibrium distribution function, one obtains macroscopic equations for the currents $\boldsymbol{j}$, $\boldsymbol{Q}$, and $\boldsymbol{P}$ that generalize Ohm's law for graphene.[17] Solutions of these equations yield linear-response transport coefficients. Note that this approach does not rely on the Kubo formula. In particular, the drag coefficient can be obtained without the use of the perturbative expressions (15) or (77).

The simplest macroscopic equation describes the energy current. In an infinite sample, where all quantities are homogeneous, the equation reads (Schütt *et al.*, 2013)

$$e v_g^2 n\boldsymbol{E} + (v_g^2/c)[\boldsymbol{j}\times\boldsymbol{B}] = \boldsymbol{Q}/\tau, \tag{102}$$

where $n$ is the carrier density in graphene (92). The collision integral does not contribute to Eq. (102) due to energy conservation. In the limit $\mu \gg T$, all currents are equivalent, such that $\boldsymbol{j}(\mu \gg T) \approx (e/\mu)\boldsymbol{Q}(\mu \gg T)$, and Eq. (102) becomes equivalent to the Ohm's law (26). In this limit, the Galilean invariance is restored, all relaxation rates due to electron-electron interaction vanish, and all three macroscopic equations become equivalent.

At the charge neutrality point $n = 0$, Eq. (102) yields $(v_g^2/c)[\boldsymbol{j}\times\boldsymbol{B}] = \boldsymbol{Q}/\tau$. This simple-looking relation illustrates all the essential qualitative features of linear-response transport in graphene. First, in the absence of disorder $\tau \to \infty$, the equation becomes senseless, at least when the system is subjected to external magnetic field. Physically, this means that in the absence of disorder the assumption of the steady state in an infinite system becomes invalid: under external bias, the energy current increases indefinitely. Second, if the system is stabilized by disorder, but $\boldsymbol{B} = 0$, then one finds $\boldsymbol{Q} = 0$. Finally, if the system is subjected to an external magnetic field, the electric and energy currents are orthogonal $\boldsymbol{j}\perp\boldsymbol{Q}$. This leads to the appearance of *classical, positive* magnetoresistance (Müller and Sachdev, 2008; Narozhny *et al.*, 2015)

$$\delta R(B;\mu = 0) \propto (v_g^4\tau/c^2)B^2/T^3, \tag{103}$$

as well as magnetodrag in graphene; see Sec. IV.D. These results are in sharp contrast with the standard Drude theory; see Eqs. (3).

### 3. Coulomb drag in weakly disordered graphene

Close to charge neutrality and in the presence of weak, uncorrelated disorder $\alpha^2 T\tau \gg 1$ (i.e., $\tau^{-1} \ll \tau_{ee}^{-1}$), the drag resistivity in the absence of magnetic field was found by Schütt *et al.* (2013) and has the form

$$\rho_D(\mu_i \ll T) \approx 2.87\frac{h}{e^2}\frac{\alpha^2\mu_1\mu_2}{\mu_1^2+\mu_2^2+0.49T/(\alpha^2\tau)}. \tag{104}$$

As long as any (even infinitesimal) disorder is present, $\rho_D$ vanishes at the double Dirac point $\rho_D(\mu_1 = \mu_2 = 0) = 0$ and grows sharply in its immediate vicinity; see Fig. 23. If only one of the layers is tuned to the Dirac point (median lines in Fig. 23), the drag resistivity always vanishes

$$\rho_D(\mu_1 = 0, \mu_2 \neq 0) = \rho_D(\mu_1 \neq 0, \mu_2 = 0) = 0.$$

If one varies the carrier density in one of the layers through the Dirac point, then the drag resistivity changes sign. In the color maps in Fig. 23 this is represented by the color change between neighboring quadrants. The same sign patterns of the drag resistivity (in zero magnetic field) were observed in the experiments of Kim *et al.* (2011), Gorbachev *et al.* (2012), and Kim and Tutuc (2012).

At the double Dirac point in the absence of disorder, one finds (for $\boldsymbol{B} = 0$) $\rho_D(\mu_1 = \mu_2 = 0) \sim \alpha_g^2 h/e^2$. This peculiar feature is shown in Fig. 23 by the black curve in the lower left panel. It is, however, unlikely that this result is relevant to the nonzero drag resistivity at the Dirac point observed by Gorbachev *et al.* (2012). A possible explanation for this

[17] The full three-mode equations are too cumbersome to reproduce here; see Narozhny *et al.* (2015).

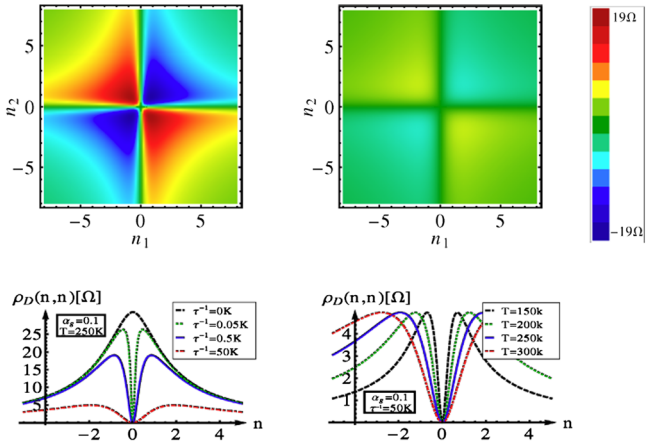


FIG. 23. Leading-order drag coefficient in the ballistic regime as a function of carrier densities (in units of $10^{11}$ cm$^{-2}$) for $d = 9$ nm. Left: $\rho_D$ at $T = 250$ K; the upper panel refers to ultraclean graphene $\tau^{-1} = 0.5$ K; the lower left panel shows the evolution of $\rho_D$ with increasing disorder from $\tau^{-1} = 0$ to $\tau^{-1} = 50$ K. Right: $\rho_D$ for $\tau^{-1} = 50$ K; the lower panel shows $\rho_D$ for $T = 150$, 200, 250, and 300 K. From Schütt *et al.*, 2013.

observation is provided by the higher-order effects (Schütt *et al.*, 2013).

For intermediate disorder strength $\alpha^2 T \ll \tau^{-1} \ll T$, the applicability region of the hydrodynamic approach overlaps with that of the conventional perturbation theory reviewed in Sec. IV.A and one recovers perturbative results; see Fig. 18.

Finally, let us stress the novel qualitative feature of the hydrodynamic approach: the electron-hole asymmetry does not play a definitive role in the drag effect. Indeed, the drag rate $\tau_D^{-1}$ dominates the observable effect only under the standard assumptions of the Fermi-liquid behavior in the two layers. On the contrary, in the vicinity of the Dirac point in graphene, another scattering process, the interplay of fast interlayer energy and current relaxation which is insensitive to the electron-hole asymmetry, becomes important. Further examples to such novel behavior are presented in Sec. IV.D.

### C. Diffusive regime

In strongly disordered graphene samples or, equivalently, at the lowest temperatures $T\tau \ll 1$, the electron motion becomes diffusive. In this regime, the standard perturbative approach based on Eq. (77) is applicable. In particular, the polarization operator has the standard form (30). The nonlinear susceptibility can be found using the argument leading to Eq. (28). In graphene close to the Dirac point $\mu \ll T \ll \tau^{-1}$, the derivative of the longitudinal conductivity with respect to the carrier density is independent of the precise nature of disorder and is given by (Schütt *et al.*, 2013)

$$\partial\sigma/\partial n \sim n v^4 \tau^4.$$

In contrast to the theory reviewed in Sec. II, in graphene the Thomas-Fermi screening length is much longer than the interlayer spacing $\varkappa d \ll 1$; hence one finds the following expression for the drag resistivity:

$$\rho_D(\mu_i \ll T \ll \tau^{-1}) \sim (h/e^2)\alpha^2 \mu_1 \mu_2 T \tau^3, \qquad (105)$$

vanishing at $\mu_i = 0$ due to the electron-hole symmetry.

In the degenerate regime $\mu \gg T$, one recovers the usual quadratic temperature dependence of the drag resistivity. The behavior of $\rho_D$ in the diffusive regime is summarized in Fig. 18 (the upper row). The Fermi-liquid result (34) is recovered only in the academic limit of strong screening $\varkappa d \gg 1$. This regime is not shown in Fig. 18 since in graphene it can be reached only at the extreme values of the chemical potential; see Fig. 20.

Calculations of the lowest-order drag resistivity in the diffusive regime are essentially the same in any system; see Sec. II.C. As shown in Fig. 18, the behavior of $\rho_D$ at the lowest temperatures may be dominated by higher-order drag effects.

### D. Giant magnetodrag in graphene

Although the effect of classical magnetoresistance in multiband systems is well known in semiconductor physics (Seeger, 2002), the equivalent effect in Coulomb drag was only recently observed in graphene-based devices (Gorbachev *et al.*, 2012; Titov *et al.*, 2013). One of the reasons is that the majority of earlier drag measurements were performed in double-well semiconductor heterostructures. Then each of the layers is represented by a two-dimensional electron gas that is formed by electrons occupying the lowest level in the quantum well at the interface between two semiconductors in the device. In contrast to graphene, the conductance and valence bands touch at the Dirac point and, as a result, both electrons and holes participate in transport phenomena at low doping.

The experimental data on magnetodrag in graphene (Gorbachev *et al.*, 2012) is shown in Fig. 24.[18] There are two outstanding features in Fig. 24. At high carrier densities (or in the degenerate regime), the effect of the magnetic field is relatively weak. This observation is consistent with the expectation that transport properties of doped graphene are dominated by one of the two bands (the contribution of the other being exponentially suppressed). In the vicinity of the Dirac point both types of carriers contribute to transport. Moreover, the leading contribution to drag at zero field vanishes right at the neutrality point due to the exact electron-hole symmetry of the Dirac spectrum. Once the magnetic field is applied, the system develops a drag signal which is no longer determined by electron-hole asymmetry. As a result, the drag resistivity near the Dirac point in the presence of weak magnetic field is much higher than the maximum value in zero field; see, e.g., Fig. 22.

The classical, two-band mechanism of magnetodrag in graphene at charge neutrality can be readily illustrated in the case, where the system size is much larger than any characteristic length scale, such that the two graphene sheets may be considered effectively infinite. In this case (see

[18]Note that Gorbachev *et al.* (2012) adopted an alternative definition of the drag resistivity $\rho_{xx}^D = E_{2x}/j_{1x}$. Therefore in this section we discuss the off-diagonal resistivity $\rho_{xx}^{12} = E_{2x}/j_{1x}$ rather than $\rho_D$ that is defined in the rest of the paper with the opposite sign.

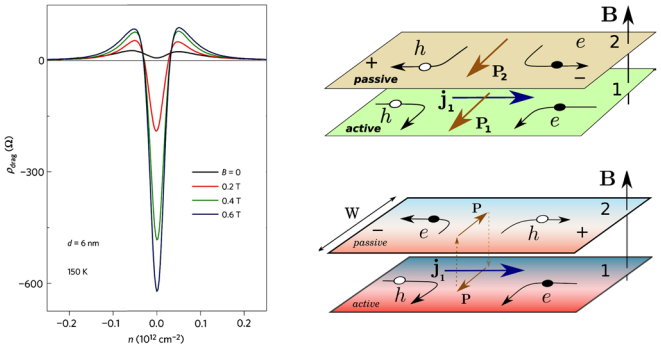


FIG. 24. Left: Off-diagonal resistivity $\rho_{xx}^{12}$ in magnetic field, measured in a graphene-based double-layer device. The two graphene sheets are kept at "opposite" carrier densities $n_1 = -n_2 = n$ and $T = 150$ K. From Gorbachev *et al.*, 2012. Right: Mechanism of magnetodrag at charge neutrality. Upper panel: In an infinite system quasiparticle currents in the two layers (denoted by $\boldsymbol{P}_i$) flow in the same direction, leading to positive $\rho_{xx}^{12}$. Lower panel: In a thermally isolated system no net quasiparticle flow is possible; the quasiparticle currents in the two layers have opposite directions yielding negative $\rho_{xx}^{12}$. From Titov *et al.*, 2013.

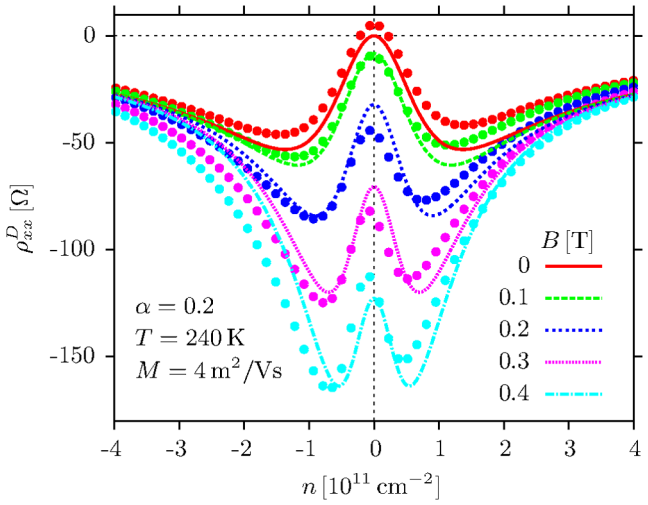


FIG. 25. Off-diagonal resistivity $\rho_{xx}^{12}$ in magnetic field, measured in a graphene-based double-layer device. Both graphene sheets are kept at the same carrier density $n_1 = n_2 = n$ and at $T = 240$ K. Solid symbols represent the experimental data. From Titov *et al.*, 2013.

Fig. 24), the driving current in the active layer $\boldsymbol{j}_1$ corresponds to the counterpropagating flow of electrons and holes with zero total momentum (due to the exact electron-hole symmetry). Once the weak magnetic field is applied, electrons and holes are deflected by the Lorentz force and drift in the same direction. The resulting quasiparticle flow $\boldsymbol{P}_1$ carries a nonzero net momentum in the direction perpendicular to $\boldsymbol{j}_1$. This momentum can be transferred to the passive layer by the interlayer Coulomb interaction inducing the quasiparticle current $\boldsymbol{P}_2$ in the same direction as $\boldsymbol{P}_1$. The Lorentz forces acting on both types of carriers in the passive layer drive the charge flow in the direction opposite to $\boldsymbol{j}_1$. If the passive circuit is open, this current is compensated by a finite drag voltage, yielding a positive drag resistivity (Titov *et al.*, 2013).

This mechanism of magnetodrag at charge neutrality is closely related to the anomalous Nernst effect in single-layer graphene (Müller and Sachdev, 2008; Wei *et al.*, 2009; Zuev, Chang, and Kim, 2009). Indeed, the quasiparticle current is proportional to the heat current at the Dirac point. The fact that the Lorentz force in the electron and hole bands has the opposite sign is also the reason for the vanishing Hall effect at charge neutrality.

Despite being qualitatively clear, this description of magnetodrag yields the induced drag voltage which has the sign opposite to that observed in experiment (Gorbachev *et al.*, 2012; Titov *et al.*, 2013); see Fig. 24. In fact, the *negative* drag in Fig. 24 can appear only if the quasiparticle currents in the two layers $\boldsymbol{P}_1$ and $\boldsymbol{P}_2$ have opposite directions. According to Titov *et al.* (2013) and Narozhny *et al.* (2015), this is what happens in small, mesoscopic samples used in experiment.

Consider the continuity equation for the quasiparticle current $\boldsymbol{P}_1$, including relaxation by electron-hole recombination (Foster and Aleiner, 2009; Titov *et al.*, 2013)

$$\boldsymbol{\nabla P}_1 = -(\rho_1 - \rho_0)/\tau_{\rm ph} - (\rho_1 - \rho_2)/(2\tau_{\rm Q}), \qquad (106)$$

where $\rho_i$ are the quasiparticle densities in the two layers, $\rho_0 = \pi T^2/(3v_g^2)$ is the equilibrium quasiparticle density at the Dirac point, $\tau_{\rm ph}$ describes the energy loss from the system dominated by phonon scattering, and $\tau_Q$ characterizes quasiparticle imbalance relaxation due to interlayer Coulomb interaction. The equation for the passive layer can be obtained by interchanging layer indices. In the absence of quasiparticle recombination, hard-wall boundary conditions at the sample boundaries allow only for the trivial solution. In contrast, taking into account inelastic processes, one finds the nontrivial solution illustrated in Fig. 24: $\boldsymbol{P}_1 = -\boldsymbol{P}_2$.

Combining the continuity equation (106) with the hydrodynamic description of linear-response transport in graphene (with the additional gradient terms that account for inhomogeneity of physical quantities in finite-size systems), one can describe the negative drag observed in experiment (Titov *et al.*, 2013; Narozhny *et al.*, 2015); see Fig. 25. The exponential collapse of theoretical curves at high carrier density is an artifact of the two-mode approximation adopted by Titov *et al.* (2013). The more accurate three-mode approximation (Narozhny *et al.*, 2015) includes thermoelectric effects formulated in terms of energy currents; the corresponding hydrodynamic description yields only the power-law decay of the magnetodrag at $\mu_i \gg T$, in contrast to the exponential collapse shown in Fig. 25. As compared to lower-temperature data (see Fig. 24), the results shown in Fig. 25 exhibit qualitatively new features which can be attributed to higher efficiency of relaxation processes at higher temperature.

### E. Hall drag in graphene

Hall drag measurements in graphene were reported by Titov *et al.* (2013). These experiments were performed at relatively high temperatures $T = 160$–$240$ K, where macroscopic coherence is not expected to exist. While disorder effects in graphene are often attributed to Coulomb scatterers

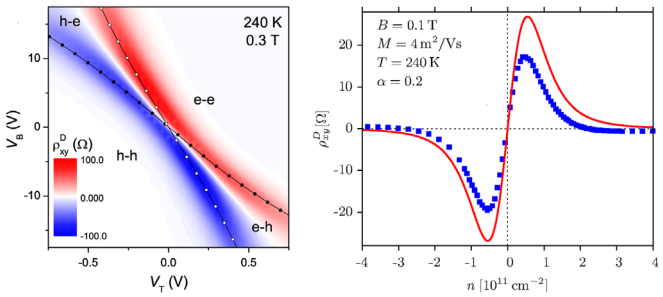


FIG. 26. Left panel: Hall drag resistivity in graphene as a function of gate voltages controlling carrier densities in the two layers. The white diagonal area corresponds to vanishing Hall drag for $n_1 = -n_2$. The lines track positions of maxima in single-layer resistivity in top (open symbols) and bottom (solid symbols) layers. Right panel: Hall drag resistivity as a function of carrier density for $n_1 = n_2 = n$. Blue squares represent the experimental data. The red curve represents the theoretical prediction. From Titov *et al.*, 2013.

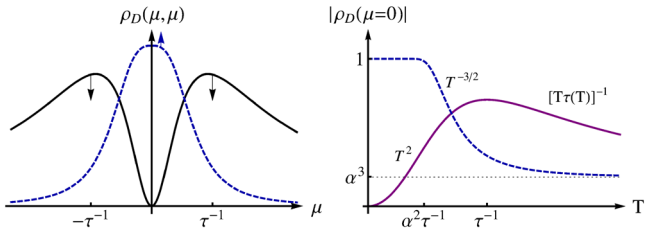


FIG. 27. Schematic view of the drag resistivity at low temperatures. The dashed line illustrates the third-order drag effect. Left panel: The black solid line represents the lowest-order contribution to drag. The arrows indicate the tendency of the two terms with the decrease of temperature $T \to 0$. Right panel: The purple solid line represents the contribution of correlated disorder. From Schütt *et al.*, 2013.

characterized by mean-free time that is linear in energy, the measured Hall drag resistivity is not small as would follow from a mechanism similar to that suggested by Hu (1997) and von Oppen, Simon, and Stern (2001).

Instead, double-layer graphene samples demonstrate a much simpler, yet still strong effect based on the coexistence of electron and hole liquids in each layer (Foster and Aleiner, 2009). Consequently, the observed Hall drag resistance, Fig. 26, is large when one of the layers is close to the neutrality point and vanishes if two layers have the same charge densities with opposite signs (a white line running from the top left to bottom right corner in the left panel of Fig. 26).

Hall drag effect in graphene can be understood with the help of the hydrodynamic theory (Titov *et al.*, 2013; Narozhny *et al.*, 2015). Indeed, given the presence of two noncollinear currents in the model, it is not surprising to see the nonzero Hall drag away from the Dirac point, where both the conventional Hall effect and Hall drag change sign together with the carrier density and thus have to vanish.[19] Hall drag also has to vanish in the degenerate regime where only one band contributes to transport and the standard single-band theory (2) holds. However, this regime lies outside of the parameter range of the experiment (Titov *et al.*, 2013). Thus, some Hall drag signal is observed at all densities, but $\rho^D_{xy}$ decays to rather small values as the density increases beyond $n \simeq 1\times10^{11}\,\mathrm{cm}^{-2}$. Interestingly enough, the data show a sign change of $\rho^D_{xy}$ at $n \approx \pm 2\times 10^{11}\,\mathrm{cm}^{-2}$. This rather weak effect requires a more accurate consideration.

The right panel of Fig. 26 shows the results of the hydrodynamic theory alongside experimental data. This calculation was performed without any fitting (Titov *et al.*, 2013). The value of the impurity-scattering time $\tau$ was determined from the measured single-layer resistivity. The effective interaction parameter was estimated by the most plausible value for graphene on hexagonal boron nitride, $\alpha_g \approx 0.2$ [see, e.g., Kozikov *et al.* (2010) and Reed *et al.* (2010) for general considerations and the experimental evidence for possible values of $\alpha_g$].

### F. Higher-order effects in graphene

All theories of Coulomb drag in graphene discussed so far were concerned with the leading-order contribution of the interlayer interaction. Indeed, even the nonperturbative results of the hydrodynamic approach were obtained by solving the kinetic equation with the collision integral (95), where the transition probability was estimated using the Fermi golden rule. All such theories predict vanishing drag at the point of exact electron-hole symmetry [with the exception of the academic case of pure graphene, see Eq. (104) and Fig. 23].

However, measurements (Gorbachev *et al.*, 2012; Titov *et al.*, 2013) reveal nonzero drag at the double Dirac point; see Fig. 24. At the time of writing, there is no consensus in the community regarding the origin of this effect. At the same time, higher-order processes (see Sec. II.D) are known to be insensitive to the electron-hole symmetry and thus may provide a plausible explanation (Titov *et al.*, 2013).

#### 1. Third-order drag in graphene

The third-order drag effect in graphene was considered by Schütt *et al.* (2013). The principle results are shown in Fig. 18. A schematic illustration of the relative strength of the second- and third-order contributions is given in the left panel of Fig. 27.

The third-order drag resistivity in the diffusive regime can be found similarly to the conventional case; see Sec. II.D. All microscopic details are masked by the diffusive nature of electronic motion. However, due to the relatively weak screening and the possibility to tune the carrier density to the Dirac point, one finds a richer physical picture with multiple parameter regimes.

The standard Fermi-liquid regime (Levchenko and Kamenev, 2008b) corresponds to the condition

$$N\varkappa \gg \max\{d^{-1}, \sqrt{T/D}\},$$

[19] A similar two-fluid model was used by Song, Abanin, and Levitov (2013) to explain Hall drag in terms of the "energy-driven drag mechanism." Indeed, if one omits the interlayer frictional force, one would still find nonzero Hall drag due to the interlayer energy relaxation.

where $N = 4$ describes spin and valley degeneracy of quasiparticle states in graphene. Here the temperature-independent result (40) is reproduced, although with the extra factors of $N$

$$\rho_D^{(3)} \sim (h/e^2)N^{-5}g^{-3}(\varkappa d)^{-2}. \tag{107}$$

At higher temperatures, one can achieve a different, high-temperature regime with

$$d^{-1} \ll N\varkappa \ll \sqrt{T/D}.$$

In this case, the resulting drag resistivity decays rapidly

$$\rho_D^{(3)} \sim \frac{h}{e^2}\frac{1}{g^3}\frac{1}{(N\varkappa d)^2}\left(\frac{D\varkappa^2}{T}\right)^{3/2}. \tag{108}$$

The experiment of Gorbachev *et al.* (2012) was performed on samples with the small interlayer spacing. In the limit $\varkappa d \ll 1$, one finds three different temperature regimes.

Close to the Dirac point and at lowest temperatures, the drag resistivity is temperature independent:

$$\rho_D^{(3)}(\mu \ll T; T\tau \ll \alpha^2) \sim h/e^2. \tag{109}$$

Note that this result is also independent of the strength of the Coulomb interaction $\alpha$.

At somewhat higher temperatures (or, equivalently, for slightly weaker disorder strength), the third-order contribution decays as a function of temperature

$$\rho_D^{(3)}(\mu \ll T \ll \tau^{-1} \ll \alpha^{-2}T) \sim (h/e^2)(\alpha^2 T\tau)^{-3/2}. \tag{110}$$

These results are illustrated in the right panel in Fig. 27.

Away from the Dirac point, the third-order contribution decays as a function of the chemical potential (or, equivalently, carrier density) and quickly becomes subleading, see the left panel in Fig. 27:

$$\rho_D^{(3)}(\mu\tau \gg \max[1, \alpha^{-1}(T\tau)^{1/2}]) \sim \frac{h}{e^2}\frac{1}{(\mu\tau)^3}. \tag{111}$$

As a result, $\rho_D^{(3)}$ may be detectable only at low temperatures and in the vicinity of the Dirac point.

While estimating $\rho_D^{(3)}(\mu = 0)$, the single-layer conductivity was assumed to be of the order of the quantum conductance $\sigma \sim e^2/h$, i.e., discarding localization effects. Indeed, single-layer measurements on high-quality samples show temperature-independent conductivity down to 30 mK (Tan *et al.*, 2007) [possibly due to the specific character of impurities in graphene (Ostrovsky, Gornyi, and Mirlin, 2007)].

For weak disorder or higher temperature the diffusive approximation fails. Drag in vicinity of the Dirac point can then be described by the quantum kinetic equation approach. The previously reviewed results, e.g., Eq. (104), were obtained by approximating the collision integrals with the help of the Fermi golden rule; see Eq. (95b). However, taking into account next-order matrix elements yields a nonzero contribution, similar to the third-order result $\rho_D^{(3)}$.

Taking into account the second-order matrix element, one can generalize the golden-rule expression (96) by using the combination

$$|U_{12}^{(1)} + U_{12}^{(2)}|^2 \simeq |U_{12}^{(1)}|^2 + 2\mathrm{Re}\{U_{12}^{(1)}[U_{12}^{(2)}]^*\}. \tag{112}$$

Since $U_{12}^{(1)} \propto \alpha$ and $U_{12}^{(2)} \propto \alpha^2$, all relaxation rates will now get an additional contribution of the order of $\alpha^3$. In particular, the drag rate $\tau_D^{-1}$ gets a contribution that is independent of the carrier density

$$\tau_D^{-1} \sim \alpha^2 N(\mu/T)^2 + \alpha^3 NT, \tag{113}$$

which dominates near the Dirac point. In this case, one may neglect the conventional, second-order drag contribution; the result is (Schütt *et al.*, 2013)

$$\rho_D \sim \frac{h}{e^2}\frac{\alpha^3 T + \alpha^4\mu^2\tau N}{T + \alpha^2\mu^2\tau N}, \qquad \mu \ll \alpha^{1/2}T, \qquad T\tau \gg 1.$$

Exactly at the Dirac point this yields

$$\rho_D \sim (h/e^2)\alpha^3. \tag{114}$$

This result is illustrated in the right panel of Fig. 27 by the horizontal asymptote at $T\tau \gg 1$.

### 2. Interlayer disorder correlations

Within the conventional theory, charge carriers in each layer scatter off an independent disorder potential. This picture is clearly applicable to the cases where impurities are mostly concentrated in the substrate insulator sandwiching the double-layer structure. In the case of the standard double-well heterostructures (Solomon *et al.*, 1989; Gramila *et al.*, 1991; Eisenstein, 1992; Hill *et al.*, 1997; Lilly *et al.*, 1998), the random potential originates in the delta-doped layers providing charge carriers. These layers are typically located on the outer sides of the double-well structure. In graphene, the disorder potential is often attributed to the insulating substrate, in particular, to $SiO_2$. Indeed, in graphene-based samples of Kim *et al.* (2011) and Kim and Tutuc (2012), graphene monolayers are exfoliated onto a thick $SiO_2$ dielectric, while the interlayer spacer consists of 14-mm-thick $Al_2O_3$. In such a structure, the impurity potential created by the silicon oxide is likely to affect only the nearest monolayer.

In contrast, the samples of Gorbachev *et al.* (2012) consisted of graphene-hexagonal-boron-nitride heterostructures, where the interlayer spacer contains only a few atomic layers of the same insulator (boron nitride) that is used as a substrate. In this case, the impurity potential originating from the interlayer spacer would be equally felt by carriers in both graphene layers. Another scenario for disorder correlation (Gorbachev *et al.*, 2012; Song and Levitov, 2012) involves interactions between charge-density inhomogeneities forming due to impurity potential in the two layers.

The effect of the correlated disorder in the drag measurements is insensitive to the electron-hole symmetry (Gornyi, Yashenkin, and Khveshchenko, 1999; Hu, 2000a), and thus may also provide an explanation (Song and Levitov, 2012;

Schütt *et al.*, 2013) for the observed nonzero drag in graphene at the Dirac point (Gorbachev *et al.*, 2012).

At high temperatures $T\tau \gg 1$, the effect of the correlated disorder can be described by the skeleton diagram similar to the third-order drag contribution; see the right panel of Fig. 7. Interlayer disorder correlations can be incorporated into the scattering amplitude, but now instead of the second-order matrix element in Eq. (112), one has to introduce an interlayer disorder scattering rate $1/T\tau_{12}$. The resulting drag rate $\tau_D^{-1}$ is given by

$$1/\tau_D^{\rm corr} \sim \alpha^2 T/(T\tau_{12}) = \alpha^2/\tau_{12},$$

corresponding to the drag resistivity

$$\rho_D^{\rm corr} \sim \alpha^2/(T\tau_{12}),$$

which overcomes the third-order drag contribution $\rho_D^{(3)} \sim \alpha^3$ at $1/\tau_{12} > \alpha T$. This happens in the perturbative regime ($1/\tau > \alpha^2 T$ for moderately correlated disorder, $\tau_{12} \sim \tau$), where the correlated-disorder contribution can be calculated diagrammatically.

Macroscopic inhomogeneities can be described in terms of macroscopic spatial fluctuations $\delta\mu_i$ in chemical potentials of the two layers (Song and Levitov, 2012), characterized by the correlation function

$$F_{ij}^{(\mu)}(\boldsymbol{r}-\boldsymbol{r}') = \langle \delta\mu_i(\boldsymbol{r})\delta\mu_j(\boldsymbol{r}')\rangle \neq 0. \tag{115}$$

Assuming the spatial scale of the fluctuations to be much larger than all characteristic scales related to the particle scattering, one can solve the hydrodynamic equations locally, yielding the local drag rate

$$1/\tau_D(\boldsymbol{r}) \sim \alpha^2 N \mu_1(\boldsymbol{r})\mu_2(\boldsymbol{r})/T. \tag{116}$$

Averaging over the small fluctuations of the correlated chemical potentials, one arrives (Schütt *et al.*, 2013) at the correction to the universal third-order result (114),

$$\Delta\rho_D(\mu=0) \sim \frac{h}{e^2}\frac{\alpha^2 F_{12}^{(\mu)}(0)}{T^2}(1+\alpha^2 N T\tau). \tag{117}$$

Finally, in the ultraclean limit

$$1/\tau \ll \alpha^2 N F_{ii}^{(0)}/T, \tag{118}$$

one can approximate the local drag resistivity by an analog of Eq. (104):

$$\Delta\rho_D(\boldsymbol{r};\mu=0) \sim \frac{h}{e^2}\alpha^2\frac{\delta\mu_1\delta\mu_2}{\delta\mu_1\delta\mu_1+\delta\mu_2\delta\mu_2}. \tag{119}$$

In particular, for perfectly correlated chemical potentials $\delta\mu_1(\mathbf{r}) = \delta\mu_2(\mathbf{r})$, the fluctuation drops out from Eq. (119) and the local resistivity turns out to be independent of $\boldsymbol{r}$. In a more general case, the averaging over fluctuations becomes nontrivial, but this affects only the numerical prefactor in the final result. Thus, the correlated large-scale fluctuations of the chemical potentials in the layers in effect shift curve 1 in Fig. 18 upward, extending the validity of the fully equilibrated result,

$$\rho_D \sim (h/e^2)\alpha^2, \tag{120}$$

to the case of finite disorder, Eq. (118), at the Dirac point. This implies that in the case of correlated inhomogeneities the disorder-induced dip in the lower left panel of Fig. 23 develops only for sufficiently strong disorder.

## V. COULOMB DRAG AT THE NANOSCALE

The effects of Coulomb interaction are especially pronounced at the nanoscale. In quantum dot devices one can utilize the Coulomb-modified Fano resonance to detect the electric charge (Johnson *et al.*, 2004). A two-level pulse technique was used to detect individual electron spin (Elzerman *et al.*, 2004). Quantum dots were also used as high-frequency noise detectors (Onac *et al.*, 2006). Transport measurements on adjacent but electrically isolated quantum point contacts (QPCs) exhibit a counterflow of electrons [i.e., detector current flowing in the direction opposite to the driving current (Khrapai *et al.*, 2007)]. In nanosize CdSe-CdS semiconductor tetrapods (Mauser *et al.*, 2010), Coulomb draglike effects lead to photoluminescent emission.

Theoretically, Coulomb drag in a system of two electrically isolated QPCs was considered by Levchenko and Kamenev (2008a). Within the linear response the drag mechanism was found to be similar to that in the bulk 2D electron systems. Remarkably, already for seemingly modest drive voltages (much smaller than temperature) the system crosses over to the nonlinear regime, where the effect is dominated by the excess shot noise of the drive circuit. Nonlinear transport was also found to be crucial for drag effects in a system of parallel quantum dots (Moldoveanu and Tanatar, 2009). An exciting new development is the proposal to use the drag effects to study transport properties of polaritons in optical cavities and, in particular, their superfluidity (Berman, Kezerashvili, and Lozovik, 2010a, 2010b).

### A. Quantum dots and quantum point contacts

Interactively coupled mesoscopic and nanoscale circuits, such as quantum wires (Debray *et al.*, 2000, 2001; Morimoto *et al.*, 2003; Yamamoto *et al.*, 2006; Laroche *et al.*, 2011), quantum dots (Aguado and Kouwenhoven, 2000; Onac *et al.*, 2006), or point contacts (Khrapai *et al.*, 2006, 2007), provided new fruitful ways of studying Coulomb drag phenomena and revealed a plethora of interesting physics. These devices typically have dimensions smaller than the temperature length $L_T = v_F/T$ and voltage-related length scale $L_V = v_F/eV$ and differ substantially from their two-dimensional quantum-well counterparts in several important ways. (i) The strength of Coulomb interaction is naturally enhanced by reducing the system size that should lead to a more profound dragging effect. (ii) Transmission across the device in the drag (drive) circuit or both can be efficiently controlled by the gate voltages that allow one to open quantum conduction channels one by one. (iii) The electron-hole symmetry in such devices

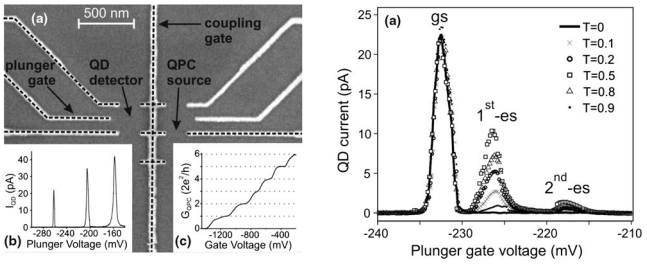


FIG. 28. Left panel: Inset (a) represents a scanning electron micrograph of the gate structure defined on top of the semiconductor heterostructure. The gates highlighted by dashed lines are used to define a quantum dot (QD) on the left and a quantum point contact (QPC) on the right. Inset (b) shows current $I_{\rm QD}$ vs plunger gate voltage, whereas inset (c) displays QPC conductance $G_{\rm QPC}$ as a function of the gate voltage. In such a device the QPC is used as a noise generator and the QD as a detector. The right panel shows the current through the QD, as a function of the plunger gate voltage, under the influence of shot noise generated by the QPC with characteristic peaks. From Onac *et al.*, 2006.

is broken much stronger than in bulk systems. In mesoscopic devices this is due to random configurations of impurities, while in the quantum nanocircuits the effect is due to the energy dependence of transmission coefficients in the Landauer picture of transport (Landauer, 1957, 1970; Büttiker *et al.*, 1985). (iv) Because of these reasons, the quantum circuits may be easily driven out of the linear-response domain and the corresponding voltage scale is parametrically smaller than the temperature. (v) Ultimately, the mere mechanism of drag in the nonlinear regime is different and governed by the quantum noise fluctuations.

The most peculiar feature of the observed Coulomb drag in such systems was that the drag current exhibited maxima for specific values of the gate voltage, where the drive circuit was tuned to an opening of another conductance channel; see Fig. 28. This hinted at the importance of the electron shot noise in the drive circuit, which was known to exhibit a qualitatively similar behavior (Lesovik, 1989; Reznikov *et al.*, 1995). Indeed, electron current shot noise power is proportional to the product of the transmission and reflection coefficients that is peaked between the conductance plateaus. It was argued early on that drag may be interpreted as a rectification of nearly equilibrium classical thermal fluctuations in the drive circuit (Kamenev and Oreg, 1995). The extension of this idea to rectification of the quantum shot noise was plausible and happened to be correct in a certain regime. The subtlety of this picture was that such a rectification is possible due only to electron-hole asymmetry in both circuits; otherwise, drag currents of electrons and holes cancel each other. The mismatch between transmission probabilities of electron and hole excitations is maximal at the verge of an opening of the new conduction channel, which implies that spikes of drag conductance may originate from the asymmetry alone rather than from shot noise.

In order to get insight into these delicate details consider the linear-response regime when drag conductance $g_D$ can be expressed as follows (Levchenko and Kamenev, 2008a):

$$g_D = \int \frac{d\omega}{8\pi T} \frac{|Z_{12}(\omega)|^2}{\omega^2} \frac{\Gamma_1(\omega)\Gamma_2(\omega)}{\sinh^2(\omega/2T)}. \tag{121}$$

Here $Z_{12}(\omega)$ is the interactively induced transimpedance relating local fluctuating currents and voltages between the circuits (Geigenmüller and Nazarov, 1991). The corresponding rectification coefficients are given explicitly by

$$\Gamma_i(\omega) = \frac{2e}{R_Q} \sum_n \int d\epsilon [f(\epsilon_-) - f(\epsilon_+)][|\mathbf{t}_{in}(\epsilon_+)|^2 - |\mathbf{t}_{in}(\epsilon_-)|^2], \tag{122}$$

where $R_Q = 2\pi\hbar/e^2$ is the quantum of resistance, $\epsilon_\pm = \epsilon \pm \omega/2$, $f(\epsilon)$ is the Fermi distribution function, and $|\mathbf{t}_{in}|^2$ is the energy-dependent transmission coefficient in the transversal channel $n$ of the circuit $i = 1, 2$. This expression admits a transparent interpretation: potential fluctuations with frequency $\omega$, say on the left of the quantum point contact, create electron-hole pairs with energies $\epsilon_\pm$ on the branch of right moving particles. Consequently, the electrons can pass through the quantum point contact with the probability $|\mathbf{t}_{in}(\epsilon_+)|^2$, while the holes with the probability $|\mathbf{t}_{in}(\epsilon_-)|^2$. The difference between the two gives the net current flowing across the contact while the Fermi functions in Eq. (122) take care of the statistical occupation of participating scattering states. Note that, unlike in the Landauer formula for conductance of a single quantum point contact where transmissions can be treated as being energy independent, the energy dependence of these probabilities in the drag formula is crucial in order to have the asymmetry between electrons and holes, and thus nonzero rectification $\Gamma_i(\omega)$. A particular functional dependence of $\Gamma$ on frequency depends on a model and details of device circuitry. It is instructive to focus on a limit of a single partially open channel in a smooth adiabatic quantum point contact. One may think then of the potential scattering barrier across it as being practically parabolic. In such a case its transmission probability is given by

$$|\mathbf{t}_{in}(\epsilon)|^2 = \{\exp[(eV_{gi} - \epsilon)/\Delta_i] + 1\}^{-1}, \tag{123}$$

where $\Delta_i$ is an energy scale associated with the curvature of the parabolic barrier in the point contact $i$, while gate voltages $V_{gi}$ move the top of the barrier relative to the Fermi energy within each of the point contacts. This form of transmission was used to explain quantum point contact conductance quantization (Glazman *et al.*, 1988) and it turns out to be useful in the application to the Coulomb drag problem. For the low-temperature limit $T \ll \Delta_i$ using Eq. (123) in Eq. (122) and carrying out energy integration yields

$$\Gamma_i(\omega) = \frac{2e\Delta_i}{R_Q} \ln\left[\frac{\cosh(eV_{gi}/\Delta_i) + \cosh(\omega/\Delta_i)}{\cosh(eV_{gi}/\Delta_i) + 1}\right]. \tag{124}$$

In the opposite limit when $T \gg \Delta_i$ one should replace $\Delta_i \to T$. One should notice that for small frequency $\Gamma_i \propto \omega^2$, whereas transimpedance $Z_{12}(\omega)$ is practically independent of frequency in this limit since its characteristic scale is typically set by the inverse $RC$ time of circuits. Assuming that $T \ll \max\{\Delta_i, \tau_{RC}^{-1}\}$ one arrives at

$$\frac{g_D}{g_Q}=\frac{\pi^2u^2}{6}\frac{T^2}{\Delta_1\Delta_2}\frac{1}{\cosh^2(eV_{g1}/\Delta_1)\cosh^2(eV_{g2}/\Delta_2)}, \tag{125}$$

where $u=Z_{12}(0)/R_Q$. The resulting expression for the drag conductance exhibits peaks as a function of gate voltage in drag or drive quantum point contact. Yet at this level it has nothing to do with the shot noise peaks, but rather reflects rectification of near-equilibrium thermal fluctuations (hence proportionality to $T^2$) along with the electron-hole asymmetry (hence a nonmonotonic dependence on $V_{gi}$). However, one should realize that the crossover to the nonlinear regime of transport in such devices can occur at rather low voltages $eV^*\sim T^2/\Delta_i$ such that Eq. (121) becomes inapplicable already at $V>V^*$. More general considerations by Levchenko and Kamenev (2008a), Chudnovskiy (2009), and Sánchez *et al.* (2010) revealed that for the out of equilibrium nonlinear regime the drag current is due to the rectification of the quantum shot noise and hence proportional to the Fano factor $\sum_n|\mathbf{t}_{ni}|^2[1-|\mathbf{t}_{ni}|^2]$. It again exhibits a generic nonmonotonic behavior of drag with multiple peaks but for an entirely different reason independent of the asymmetry factor. Nonlinear transport was also found to be crucial for drag effects in a system of parallel quantum dots (Moldoveanu and Tanatar, 2009).

Drag phenomena in quantum circuits can be naturally connected to our earlier discussion of drag in mesoscopic systems in Sec. III. Indeed, one or both circuits may be represented by a multichannel quasi-one-dimensional (or two-dimensional) mesoscopic sample. In this case $\sum_n|\mathbf{t}_n(\epsilon)|^2=g(\epsilon)$ is a dimensionless (in units of $R_Q^{-1}$) conductance of the sample as a function of its Fermi energy. As discussed earlier, such conductance exhibits universal fluctuations, that is $g(\epsilon)=g+\delta g(\epsilon)$, where $g\gg1$ is an average conductance and $\delta g(\epsilon)\sim1$ is a sample and energy-dependent fluctuating part. Since the characteristic scale of the energy dependence of the fluctuating part is the Thouless energy $E_T$ one naturally finds from Eq. (122) that corresponding mesoscopic fluctuations of the rectification coefficient are of the order

$$\Gamma(\omega)\sim\pm\frac{e}{R_Q}\frac{\omega^2}{E_T}. \tag{126}$$

This result ultimately leads to the an estimate of the variance of drag in the form of Eq. (58).

Quantum Coulomb drag circuits provide a rich platform to explore nanoscale transport far beyond ideas of using them for high-frequency noise sensing. In particular, a different drag effect may also be observed in the absence of any drive current if one nanocircuit is made hotter than the other—the cold circuit is expected to rectify the thermal charge fluctuations of the hot circuit (Sothmann *et al.*, 2012). Furthermore, interactively coupled devices provide unique tools to test nonlinear fluctuation-dissipation relations and its closely related Onsager symmetry relations in the far from equilibrium conditions when detailed balance is explicitly broken (Sánchez *et al.*, 2010; Bulnes Cuetara *et al.*, 2013).

Other intriguing examples include nanosize CdSe-CdS semiconductor tetapods (Mauser *et al.*, 2010), where Coulomb draglike effects lead to photoluminescent emission. As an alternative to optical probes, electrical readout of a single electron spin becomes possible in Coulomb draglike devices of interactively coupled QPC and QD (Elzerman *et al.*, 2004).

### B. Optical cavities

The Coulomb interaction is not exclusive to electrons and can couple any charges. Moreover, even neutral, composite objects may interact with charges by means of an effective "polarization" or "charge-dipole" interaction (Margenau and Kestner, 1969), which ultimately stems from the Coulomb interaction between an external charge and individual charged constituents of the composite object. In particular, long-ranged interactions between spatially separated electrons and polaritons may lead to interesting drag effects (Kulakovskii and Lozovik, 2004; Berman, Kezerashvili, and Lozovik, 2010a, 2010b) that can be used, e.g., for designing electrically controlled optical switches (Berman, Kezerashvili, and Kolmakov, 2014).

Two-dimensional excitonic polaritons have been the subject of intensive research (Kasprzak *et al.*, 2006; Balili *et al.*, 2007; Snoke, 2008; Amo *et al.*, 2009). These excitations appear as a result of resonant exciton-photon interaction in a system consisting of an optical microcavity and a quantum well embedded within the cavity. The lower polariton branch is characterized by extremely small effective mass raising the possibility of achieving the Bose-Einstein condensation and superfluidity at relatively high temperatures (Balili *et al.*, 2007; Littlewood, 2007).

The optically excited excitons in microcavities should not be confused with the spontaneously formed excitons in double quantum wells discussed in Sec. VII.A. In particular, these excitons can be excited by laser pumping in the single quantum well embedded within the cavity. Now, if a second quantum well is added to the device (Berman, Kezerashvili, and Lozovik, 2010a), then the Coulomb interaction binding electrons and holes into excitons can be screened (Finkelstein, Shtrikman, and Bar-Joseph, 1995; Gubarev *et al.*, 2000) by a 2DEG populating the second well. As a result, the excitonic binding energy is reduced and as the density of the 2DEG approaches a certain critical value, the excitons may disappear altogether. The excitonic collapse manifests itself through disappearance of the corresponding line in the photoluminescence spectrum.

Keeping the electron density below the critical value, one obtains a system containing coexisting, spatially separated excitons and electrons. The effective interaction between electrons and excitons was considered by Lozovik and Nikitkov (1999). This interaction leads to mutual friction between the two systems that can be observed by selectively exciting one of them by external probes.

By focusing laser pumping on a particular region within the cavity, one can generate a gradient of exciton and polariton densities. These gradients induce a flow of both polaritons and excitons. The long-range interaction between

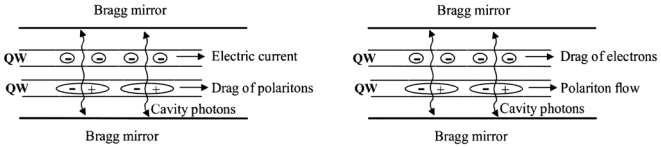


FIG. 29. Left: Quasiparticle flow in the cavity polariton subsystem induced by the electric current in the 2DEG at low temperatures. Right: Electric current in the 2DEG induced by the optically excited flow in the polariton subsystem. From Berman, Kezerashvili, and Lozovik, 2010b.

the excitons (or the exciton component of the polaritons) may transfer energy and momentum to the electronic system in the second quantum well, generating an electric current or inducing voltage, similar to the standard drag effect discussed in Sec. II.

Alternatively, one can drive a current through the 2DEG. In this case, the mutual friction will lead to the appearance of the exciton flow. These excitons are entangled with cavity photons and their flow will create a flow of polaritons. In other words, the long-ranged electron-exciton interaction allows one to effectively "move" the cavity photons by applying electric current to the 2DEG (Berman, Kezerashvili, and Lozovik, 2010a, 2010b). The drag effects in microcavities are schematically illustrated in Fig. 29.

Recently, Berman, Kezerashvili, and Kolmakov (2014) proposed to use the drag effect in optical cavities for building an electrically controlled optical switch; see Fig. 30. The polaritons are assumed to be created at a constant rate by external laser pumping. The wedgelike shape of the microcavity is chosen in order to create a force driving the polaritons along the cavity toward the Y junction. Without the drag effect, the polariton flux is distributed equally between the two branches of the junction. Driving an electric current

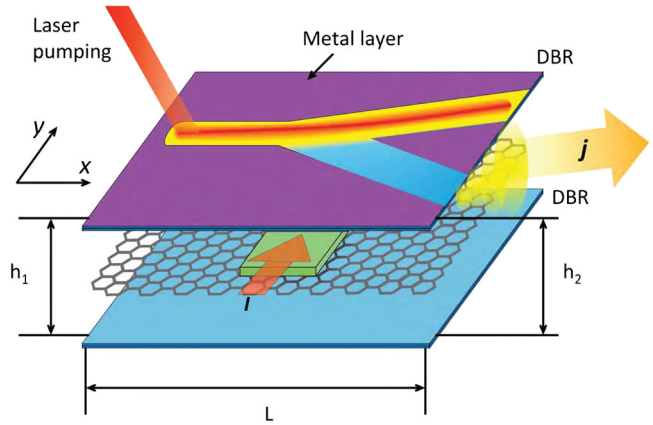


FIG. 30. The wedge-shaped microcavity formed by two distributed Bragg reflectors (DBR) that encompasses the embedded quantum wells. The excitons are located in the quantum well (gray) between the reflectors. A metal layer deposited on the upper DBR creates a Y-shaped potential energy landscape for the polaritons. The driving current runs perpendicularly to the stem of the channel in the quantum well. From Berman, Kezerashvili, and Kolmakov, 2014.

through a second quantum well results in a drag force in the junction region that effectively redistributes the polaritons flux between the branches. Berman, Kezerashvili, and Kolmakov (2014) found that for realistic parameters of the device one can achieve 90% accuracy of the switching of the polariton flow.

## VI. COULOMB DRAG BETWEEN PARALLEL NANOWIRES

It is well known that the physics of electrons confined to one spatial dimension (1D) is dominated by interactions. Coulomb drag between two closely spaced but electrically isolated quantum wires was used to observe Wigner crystallization (Yamamoto *et al.*, 2002, 2006, 2012) and Luttinger liquid effects (Debray *et al.*, 2001; Laroche *et al.*, 2008, 2014). The effect was also used to study 1D subbands in quasi-1D wires (Debray *et al.*, 2000; Laroche *et al.*, 2011).

Early theoretical work on drag between 1D systems (Hu and Flensberg, 1996; Gurevich, Pevzner, and Fenton, 1998; Raichev and Vasilopoulos, 1999, 2000a, 2000b; Gurevich and Muradov, 2000, 2005) was based on the Fermi-liquid approach and targeted multiple-channel wires at high enough temperatures, where electron correlation effects (other than screening) are not important. Tanatar (1998) considered the role of disorder. It is, however, well known that the Fermi-liquid theory fails for purely 1D systems, i.e., single-channel wires (Giamarchi, 2004), quasi-1D wires with single 1D subband occupancy (Laroche *et al.*, 2014), and systems comprising a small number of coupled 1D channels. Coulomb drag between two Luttinger liquids with a pointlike interaction region was discussed by Flensberg (1998) and Komnik and Egger (2001). Nazarov and Averin (1998) considered two independent Luttinger liquids coupled by interwire backscattering. Schlottmann (2004a, 2004b) used Bethe-ansatz methods to solve the problem of two wires coupled by a particular $\delta$-function potential. Especially interesting is the prediction of the Mott-insulator–type state corresponding to the formation of two interlocked charge-density waves (CDW) in quantum wires (Klesse and Stern, 2000; Fuchs, Klesse, and Stern, 2005) [see also Furuya, Matsuura, and Ogata (2015)].

A theory of Coulomb drag based on the Tomonaga-Luttinger liquid (TLL) theory (Tomonaga, 1950; Luttinger, 1963; Haldane, 1981a, 1981b) predicts a behavior that qualitatively deviates from that in higher dimensions. Below a certain crossover scale $T^*$, the drag resistivity between *infinitely long quantum wires of equal electron density* is predicted to increase exponentially with decreasing temperature (Klesse and Stern, 2000)

$$\rho_D \sim \rho_T \exp(\Delta/T). \tag{127}$$

The energy gap $\Delta$ and crossover temperature $T^*$ are complicated functions of the interwire distance $d$, width of wires $w$, effective Bohr radius $a_B$ of the host material, and electron density $n$. For widely separated wires ($k_F d \gg 1$) they are exponentially suppressed

$$\Delta \sim T^* \sim E_F \exp\left[-k_F d/(1-K)\right], \tag{128}$$

and the drag resistivity exhibits the high-temperature power-law behavior[20]

$$\rho_D \sim (h/e^2) k_F \lambda^2 (T/E_F)^{4K-3} \tag{129}$$

for all practically relevant scales. Here $K$ is the TLL interaction parameter in the relative charge sector determined by the difference of the small momentum intrawire and interwire couplings and $\lambda$ is the dimensionless interwire backscattering potential strength.

The physical picture behind Eq. (127) is that at low temperatures $T < T^*$ the electrons in both wires form a zigzag-ordered interlocked CDW. Then a relative charge displacement can be created only by overcoming a potential barrier, which ultimately translates into transport via activation and consequently into Arrhenius-like behavior of drag.

For short wires, Klesse and Stern (2000) reported a qualitatively different behavior. Here the CDW in one wire may slip as a whole relative to the CDW in the other wire. These instantaneous slips may stem from either thermal fluctuations or tunneling events. The latter leads to the drag resistance that tends to a finite, but exponentially large (in the wire length $L$) value as $T \to 0$. In contrast, Ponomarenko and Averin (2000) found a vanishing drag resistance $\rho_D \sim T^2$, regardless of whether the CDW is formed or not.

For wires with different electron densities, Fuchs, Klesse, and Stern (2005) found that the drag resistance (127) is suppressed by an additional exponential factor $\exp(-|\delta\mu|/T)$, where $\delta\mu = \mu_1 - \mu_2$ is the difference between the chemical potentials $\mu_i$ in the two wires. The high-temperature result (129) also becomes exponentially suppressed as soon as $|\delta\mu|$ exceeds the temperature.

Allowing for a spin degree of freedom adds extra complexity to the problem, since the system might be unstable toward a gap opening in the spin sectors.[21] If this does not happen (or at temperatures exceeding the spin gaps), the system shows the same qualitative behavior as before, but the exponent in Eq. (129) changes to $2K - 1$. However, if the single wires develop spin gaps, the drag resistivity vanishes at $T = 0$ (Klesse and Stern, 2000).

At temperatures above $T^*$, the charge sector is gapless and the system can be described as two coupled wires in the TLL phase. For quasiparticles with linear dispersion the only process contributing to drag is the interwire backscattering characterized by large momentum transfers $q \sim 2k_F$. This process can be described by the usual drag formula (15), where one typically assumes the nonlinear susceptibility to be proportional to the imaginary part of the polarization operator (Pustilnik *et al.*, 2003; Fiete, Hur, and Balents, 2006):

$$\rho_D = \frac{h}{e^2} \int \frac{dq d\omega}{4\pi^3} \frac{q^2 V_q^2}{n^2 T} \frac{[\mathrm{Im}\Pi(q,\omega)]^2}{\sinh^2(\omega/2T)}, \tag{130}$$

where $V_q$ describes the interwire interaction. In the limit $qd \gg 1$, the asymptotic form of $V_q$ is given by $V_q = (e^2/\epsilon)\sqrt{2\pi/(qd)}\exp(-qd)$. The polarization operator for the TLL model is known (Giamarchi, 2004). For spinless fermions, the spectral weight of $2k_F$ density fluctuations is given by

$$\begin{aligned}\mathrm{Im}\Pi(q_\pm,\omega) = -\frac{\sin\pi K}{4\pi^2 u}\left(\frac{2\pi\alpha T}{u}\right)^{2K-2} \\ \times B\left(\frac{K}{2} - \frac{i(\omega - u q_\pm)}{4\pi T}, 1-K\right) \\ \times B\left(\frac{K}{2} - \frac{i(\omega + u q_\pm)}{4\pi T}, 1-K\right),\end{aligned} \tag{131}$$

where $\alpha \sim k_F^{-1}$ is the short-distance cutoff of the TLL theory, $q_\pm = q \pm 2k_F$, $u$ is the renormalized Fermi velocity, and $B(x,y)$ is the Euler beta function. Using Eq. (131) in Eq. (130) one recovers Eq. (129), which was obtained by Klesse and Stern (2000) by means of a renormalization group analysis. In the perturbative approach, the interaction parameter $\lambda$ in Eq. (129) is given by $\lambda = V_{2k_F}/v_F$. This leads to the exponential dependence of $\rho_D$ on distance separating the wires [since $V_{2k_F} \propto \exp(-2k_F d)$]. The regime of spin-incoherent Luttinger liquid and the effect of disorder modify temperature dependence of Eq. (129) (Fiete, Hur, and Balents, 2006). In the weakly interacting limit ($K \simeq 1$) the drag resistivity is expected to grow linearly with temperature (Hu and Flensberg, 1996; Gurevich, Pevzner, and Fenton, 1998).

In recent years, a lot of the attention was devoted to 1D liquids with nonlinear dispersion [for reviews on this topic, see Deshpande *et al.* (2010), Imambekov, Schmidt, and Glazman (2012), and Matveev (2013)]. In the TLL theory, the curvature of the quasiparticle spectrum is described by an irrelevant operator (in the renormalization group sense). However, at high enough temperatures it might lead to important effects and even mask the pure Luttinger behavior. In the context of Coulomb drag (Pustilnik *et al.*, 2003; Aristov, 2007; Rozhkov, 2008; Pereira and Sela, 2010; Dmitriev, Gornyi, and Polyakov, 2012), this is particularly important since nonlinearity of the band kinematically allows drag with small momentum transfer $q \sim T/v_F \ll k_F$.

Analytic calculation of the dynamical structure factor $\mathrm{Im}\Pi(q,\omega)$ for arbitrary interactions and nonlinear dispersion is a major challenge. However, such calculation is readily available in the case of weakly interacting electrons. At finite temperatures, but with the accuracy of the order $T \ll m v_F^2$, the one-loop diagram yields

$$\mathrm{Im}\Pi(q,\omega) = \frac{m}{4k} \frac{\sinh(\omega/2T)}{\cosh(q v_F \xi_+/2T)\cosh(q v_F \xi_-/2T)}, \tag{132}$$

where $\xi_\pm = 2m(\omega - v_F q)/q^2 \pm 1$. It is now tempting to follow the conventional path and use this result for $\mathrm{Im}\Pi$ in the expression for the drag (130) to obtain

$$\rho_D \simeq (h k_F/e^2)(V_0/v_F)^2 (T/E_F)^2, \tag{133}$$

with the conclusion that curvature effects restore the Fermi-liquid behavior of drag in 1D wires; furthermore, the

[20] In 1D, $\rho_D = -\lim_{I_1 \to 0}(1/L) dV_2/dI_1$ is the drag resistivity per unit length (Klesse and Stern, 2000; Pustilnik *et al.*, 2003).

[21] For a comprehensive discussion of ground state properties of capacitively coupled 1D systems, see Giamarchi (2004) and Carr, Narozhny, and Nersesyan (2013).

contribution (133) would dominate over the backscattering component (129) already at temperatures above $T > E_F e^{-4k_F d}$ [in Eq. (133) $V_0$ should be understood as $V_{q\sim T/v_F}$]. At even higher temperatures, $v/d < T < E_F$, the same approach yields a saturating drag resistivity, $\rho_D \sim (\hbar k_F/e^2)(V_0/v_F)^2 \times (v/dE_F)^2$, followed by a falloff $\rho_D \propto 1/T^{3/2}$ at $T > E_F$. For nonidentical wires there appears an additional energy scale $T_\delta = k_F|\delta v|$ describing splitting between symmetric and antisymmetric plasmon modes in the double-wire system, which is determined by the difference between Fermi velocities in the wires $\delta v = v_{F1} - v_{F2}$. Assuming that $T_\delta \ll T_d$, Eq. (133) holds only for $T_\delta < T < T_d$, whereas below $T_\delta$ drag resistivity due to forward scattering decreases as $\rho_D \propto T^5$ with lowering temperature.

However, as shown by Dmitriev, Gornyi, and Polyakov (2012) the conclusions about the forward scattering contribution to drag may be premature. The reason is subtle: Eq. (130) was derived under the tacit assumption that the intralayer relaxation processes due to electron-electron interaction are faster than the interwire momentum transfer. Now, in purely 1D systems relaxation is determined by three-body collisions (Lunde, Flensberg, and Glazman, 2007; Micklitz, Rech, and Matveev, 2010; Levchenko, Ristivojevic, and Micklitz, 2011; Rieder *et al.*, 2014) as inelastic two-body interaction is forbidden by energy and momentum conservation. The same kinematic restrictions require that intrawire backscattering responsible for equilibration involves states deep at the bottom of the band. Because of the Pauli statistics, the probability to find such a state unoccupied is exponentially small. Consequently, the equilibration rate $\tau_{\rm eq}^{-1}$ in 1D is exponentially suppressed, $\tau_{\rm eq}^{-1} \propto e^{-E_F/T}$, and Eqs. (130) and (133) are difficult to justify.

At the same time, interwire backscattering with small momentum transfer $q \sim T/V_F \ll k_F$ is also allowed in 1D systems with nonlinear spectrum. This process involves a pair of scattering states: one near the Fermi level and another at the bottom of the band. Dmitriev, Gornyi, and Polyakov (2012) found a solution of two coupled kinetic equations [cf. Eqs. (9)] yielding the drag resistivity in the form

$$\rho_D \simeq \frac{\hbar k_F}{e^2}\left(\frac{V_0}{v_F}\right)^2 \frac{1}{k_F d}\frac{T_d}{T}\sqrt{\frac{E_F}{T}}e^{-2E_F/T}. \tag{134}$$

By comparing the exponential factors in Eqs. (129) and (134), one can see that backscattering-induced drag friction due to soft collision (namely, collisions with small momentum transfer) dominates over direct backscattering with $2k_F$ momentum transfer at temperatures $T > T_d$. This is despite the fact that the contribution of soft collisions is strongly suppressed compared to Eq. (133).

At even higher temperatures there exists delicate interplay between the relaxation rates of two-particle interwire backscattering with small momentum transfer and triple-body intrawire chirality changing soft collisions that determine the behavior of $\rho_D(T)$. Each of these scattering processes can be described by respective functions $\mathcal{D}_2(T)$ and $\mathcal{D}_3(T)$, which physically correspond to diffusion coefficients in momentum space. Their functional form is not universal and determined by the interaction model considered. Three-particle collisions dominate provided that $\mathcal{D}_3 > \mathcal{D}_2 e^{-E_F/T}$. This condition implicitly defines a new crossover temperature scale $T_c > T_d$ at which Eq. (134) crosses over to (Dmitriev, Gornyi, and Polyakov, 2012)

$$\rho_D \simeq \frac{\hbar}{e^2}\frac{\mathcal{D}_3}{k_F E_F}\left(\frac{E_F}{T}\right)^{3/2} e^{-E_F/T}. \tag{135}$$

Note that in this transport regime $\rho_D$ is suppressed only by a single exponential factor. In the case of short-ranged interaction $\mathcal{D}_3 \propto T^2$, whereas $\mathcal{D}_2$ is temperature independent so that the preexponential factor in Eq. (135) scales with $T$ as $T^{1/2}$. In the case of the Coulomb interaction this scaling is different since $\mathcal{D}_3 \propto T^5$.

Coulomb drag between true 1D systems was recently observed by Laroche *et al.* (2014) in a system of vertically integrated quantum wires where each wire has less than one 1D sub-band occupied. The most striking theoretical prediction, i.e., the upturn in the temperature dependence, was revealed below the crossover temperature $T^* \sim 1.6$ K; see Fig. 31. However, a quantitative comparison between the data and the theoretical results proved to be difficult. Using the experimental estimates for the carrier density $n_{1D} = \sqrt{n_{2D}}$ and interwire distance $d \simeq 40$ nm, one arrives at $k_F d \sim 2$. Then, from Eq. (128) one finds the values for the Luttinger parameter $K \simeq 0.1 - 0.2$ (for samples 3-R and 2-C) corresponding to very strong interaction that is beyond the applicability of the bosonization theory of Klesse and Stern (2000). On the other hand, fitting the high-temperature data to the power-law behavior (129) yields $K \simeq 1.5$. This estimate, however, should be approached with caution, since Eq. (129) was derived for identical wires which is not the case in experiment, where electronic densities in the parent 2D layers differ by about 20%. In that case one expects (Fuchs, Klesse, and Stern, 2005) an exponential suppression of $\rho_D$. All these issues remain to be clarified both theoretically and experimentally.

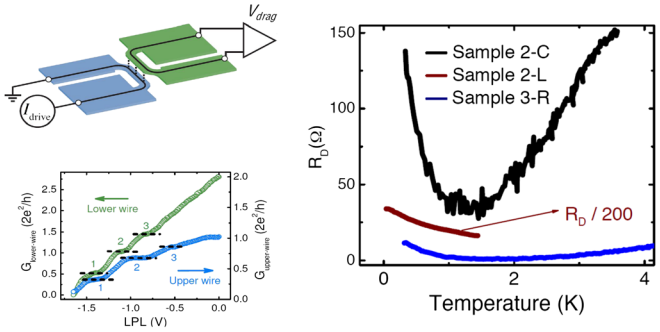


FIG. 31. Left: Measurement schematic (top) and single-wire conductance quantization (bottom). Right: Temperature dependence of the drag signal for three different samples (the magnitude of $\rho_D$ in sample 2-L is divided by 200 for visibility). For samples 2-L and 2-C, the temperature dependence was taken with no more than one 1D subband occupancy in each wire, whereas the number of 1D subbands occupied in sample 3-R is known to be bounded by $0 < N_{\rm drive} \leq 2$ and $0 < N_{\rm drag} \leq 3$. From Laroche *et al.*, 2014.

## VII. NOVEL MANY-BODY STATES IN DOUBLE-LAYER SYSTEMS

When a double-layer system is subjected to a strong magnetic field, the standard theoretical description of Coulomb drag (Jauho and Smith, 1993; Zheng and MacDonald, 1993; Kamenev and Oreg, 1995) fails: in contrast to naive expectations, numerous experiments (Hill *et al.*, 1996, 1998; Patel *et al.*, 1997; Rubel *et al.*, 1997, 1998; Rubel, Fischer, Dietsche, von Klitzing, and Eberl, 1997; Feng *et al.*, 1998; Jörger, Dietsche *et al.*, 2000; Lok, Kraus, Pohlt, Dietsche *et al.*, 2001; Lok, Kraus, Pohlt, Güven *et al.*, 2001; Pillarisetty *et al.*, 2003) show significant dependence of the measured drag resistivity $\rho_D$ on the applied field, especially in the extreme quantum regime (Murphy *et al.*, 1994; Lilly *et al.*, 1998; Nandi *et al.*, 2012).

Further experiments revealed the existence of novel quantum Hall states that are specific to bilayer systems and have no analog in single-layer samples. Early work in this direction was reviewed in Eisenstein (1992, 1997). Remarkably, the bilayer many-body states exhibiting the quantum Hall effect (Murphy *et al.*, 1994) may at the same time support a condensate of indirect (or interlayer) excitons (Wiersma *et al.*, 2007; Finck *et al.*, 2010; Nandi *et al.*, 2012). An interlayer exciton is a bound pair of an electron from one layer and a hole from another layer of the device. The exciton carries no electric charge. Nevertheless, exciton transport (especially in the superfluid state) leads to interesting electrical effects. The experimental situation in the field was reviewed by Eisenstein and MacDonald (2004) and Eisenstein (2014). Here we focus on the manifestations of this exciting new physics in the drag measurements.

### A. Quantum Hall effect in double-layer systems

In a seminal paper, Halperin (1983) suggested a generalization of the Laughlin wave function for the analysis of multicomponent systems. The simplest example of an extra degree of freedom that can be accounted for using this approach is the electron spin. A double-layer system provides another example, which is similar to the spin-1/2 system in some respects and is significantly different in other. The two possible values of the layer index can be represented by the two orientations of a pseudospin (Yang *et al.*, 1994; Stern *et al.*, 2000). However, unlike the real spin, the double-layer system does not possess the SU(2) symmetry due to the difference between the intralayer and interlayer matrix elements of the Coulomb interaction. Consequently, in the double-layer system the energy eigenstates do not have to be eigenstates of the total spin operator $\hat{S}_T$ (Girvin and MacDonald, 1997). As a result, states described by Halperin's wave functions that are not eigenstates of $\hat{S}_T$ may be realized in double layers (Eisenstein *et al.*, 1992; Suen *et al.*, 1992).

In this review we are mostly interested in double-layer systems where tunneling between the two layers is negligible. Such systems support novel many-body quantum Hall states that are specific to bilayers and arise due to the interlayer Coulomb interaction (Chakraborty and Pietiläinen, 1987; Haldane and Rezayi, 1987). Yoshioka, MacDonald, and Girvin (1989) investigated a wide class of such states using Halperin's two-component wave functions (Halperin, 1983). The ground state of the system crucially depends on the ratio of the interlayer separation and magnetic length $d/\ell_0$. For a given filling factor, the magnetic length $\ell_0$ is proportional to the average separation between electrons in one layer. Therefore, the ratio $d/\ell_0$ parametrizes the relative strength of intralayer and interlayer Coulomb interactions. Assuming truly two-dimensional layers (i.e., setting aside complications that arise due to the finite width of the quantum wells in GaAs samples), one finds that the interlayer many-body states are stable for $d/\ell_0 \sim 1$. At large $d$, the interlayer Coulomb interaction is inefficient and then the system behaves as if one connects two quantum Hall samples in parallel (Eisenstein, 1997). This observation can be illustrated with the help of the typical phase diagram shown in Fig. 32 for the case of the total filling factor $\nu_T = 1$ (Murphy *et al.*, 1994). In the opposite limit $d/\ell_0 \to 0$, the system approaches the SU(2)-symmetric point, and thus the Halperin states that are not eigenstates of $\hat{S}_T$ are expected to collapse (Eisenstein, 1997).

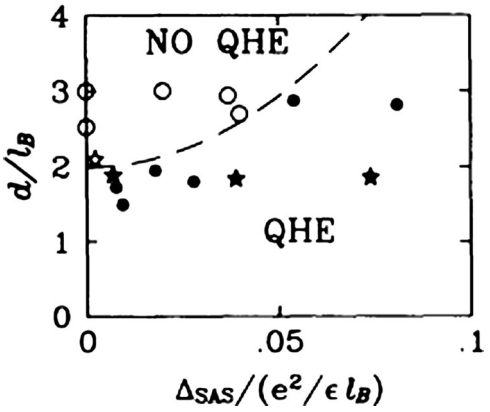


FIG. 32. The quantum Hall effect at $\nu_T = 1$ in double-layer systems. $\Delta_{SAS}$ is the tunnel splitting and $e^2/\epsilon\ell$ is the Coulomb energy. Each symbol corresponds to a particular double-layer sample. Only the samples represented by solid symbols exhibit a quantized Hall plateau at $\nu_T = 1$. The interlayer quantum Hall state exists also in the absence of tunneling. From Murphy *et al.*, 1994.

Double layers at the total filling factor $\nu_T = 1$ and with large interlayer separation (experimentally, $d/\ell_0 \sim 2-4$) behave as two weakly coupled systems of composite fermions (i.e., each layer is at $\nu = 1/2$) while exhibiting strongly enhanced drag as compared to the zero-field case; see Sec. II.G. As the ratio $d/\ell_0$ is decreased, experiments (Kellogg, Spielman *et al.*, 2002; Kellogg *et al.*, 2003) show a gradual development of the Hall drag signal and a nonmonotonic behavior of the longitudinal drag resistivity $\rho_D$. As $d/\ell_0$ approaches the transition into the strongly correlated, many-body state,[22] $\rho_D$ shows strong enhancement, followed by a decrease. In the strongly coupled interlayer $\nu_T = 1$ state

[22]Since the transition between the weakly and strongly coupled quantum Hall states is still poorly understood, one should be speaking in terms of the transition region instead of the precise critical value of $d/\ell_0$.

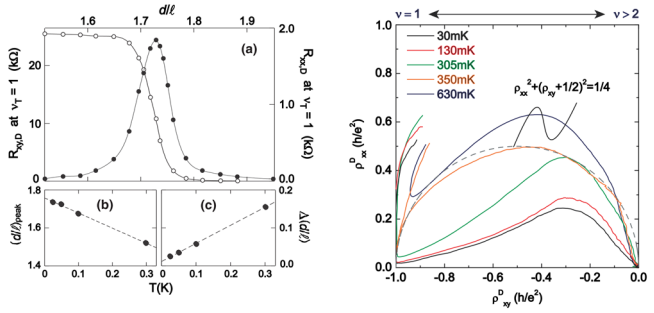


FIG. 33. Left: Hall (open dots) and longitudinal (closed dots) drag resistance at $\nu_T = 1$ and $T = 50$ mK as a function of the ratio $d/\ell_0$. The two lower panels show the temperature dependence of the location and the half-width of the peak in $R^D_{xx}$. The lines are guides for the eye. From Kellogg *et al.*, 2003. Right: Drag resistivity and Hall drag resistivity in units of $h/e^2$ for different temperatures. The end points represent the strong-coupling ($\rho^D_{xy} = -1$) and weak-coupling ($\rho^D_{xy} = 0$) regimes. The dashed line represents Eq. (140). From Tutuc, Pillarisetty, and Shayegan, 2009.

$\rho_D$ practically vanishes. At the same time, the Hall drag resistance develops a quantized plateau; see Fig. 33. Similar behavior was observed by Tutuc, Shayegan, and Huse (2004), Wiersma *et al.* (2004), and Tutuc, Pillarisetty, and Shayegan (2009).

Early theoretical work on drag in quantum Hall states was focused on the nondissipative drag (Renn, 1992; Duan, 1995; Yang, 1998; Yang and MacDonald, 2001). In contrast to the case of the weak magnetic field (see Sec. II.G), a strong, quantized Hall drag has been identified as a signature of the interlayer correlated states. The $2 \times 2$ Hall resistivity matrix (for the two layers) was shown (Renn, 1992; Yang, 1998) to be proportional to the Gram matrix (Conway and Sloane, 1988; Read, 1990) describing topological order in the quantum Hall state (Wen, 1995):

$$\rho^{xy}_{ij} = (h/e^2)K_{ij} \Rightarrow \rho^{xy}_{12} = nh/e^2, \quad n > 0. \tag{136}$$

A similar conclusion was reached by Yang and MacDonald (2001) on general topological grounds.

Kim *et al.* (2001) suggested using the drag resistivity to distinguish between various quantum Hall states in double-layer systems at $\nu_T = 1$. For the compressible (weak-coupling) state at large interlayer separation, the Hall drag resistivity vanishes, while the longitudinal drag is determined by gauge-field fluctuations and is given by Eq. (53). The compressible state exhibits a strong pairing instability (Greiter, Wen, and Wilczek, 1991; Bonesteel, 1993). If Landau-level mixing is substantial (as it often is in experimental samples), the paired state may be described by the $(3, 3, -1)$ Halperin wave function. This state resembles a $p_x + ip_y$ superconductor of composite fermions. As a result, it is expected to exhibit the quantized Hall drag resistivity (136) with $n = -1$.

For smaller interlayer separation ($d \simeq \ell_0$) the system undergoes a transition into an incompressible, correlated "quantum Hall ferromagnet" state described by the (1, 1, 1) Halperin wave function. This state possesses a gapless neutral mode and is characterized by the Hall resistivity (136) with $n = 1$.

The nature of the transition between the compressible, weak-coupling state at large interlayer separation and the incompressible, strong-coupling state at $d \simeq \ell_0$ is not completely understood (Finck *et al.*, 2010; Eisenstein, 2014). Numerical evidence (Schliemann, Girvin, and MacDonald, 2001; Burkov *et al.*, 2002) suggested a first order transition at $T = 0$, which contradicts the experimental observation of gradual development of the quantized Hall drag (Kellogg, Spielman *et al.*, 2002; Kellogg *et al.*, 2003); see Fig. 33. Stern and Halperin (2002) suggested a phenomenological description of the drag resistivity in the transition region. Postulating that in the transition region the system is split into regions of the strong-coupling (1, 1, 1) phase and regions of the weak-coupling compressible phase, they describe the transition as the point where the fraction $f$ of the sample occupied by the (1, 1, 1) phase reaches the percolation threshold $f_c = 1/2$.

In a system of identical layers, the linear-response theory can be formulated in terms of symmetric and antisymmetric states. Denoting the $2 \times 2$ resistivity matrices corresponding to symmetric and antisymmetric currents by $\rho^s$ and $\rho^a$, one finds the drag resistivity as $\rho^D = (\rho^a - \rho^s)/2$.

In the weak-coupling phase at $d \gg \ell_0$, the drag resistivity is very small, $\rho^D \ll \rho^{a(s)}$. Neglecting $\rho^D$, one may approximate the resistivities as (in units of $h/e^2$)

$$\rho^a(d \gg \ell_0) = \rho^s(d \gg \ell_0) = \begin{pmatrix} \epsilon & 2 \\ -2 & \epsilon \end{pmatrix}, \tag{137}$$

where $\epsilon = 1/k_F \ell_{tr} \ll 1$ (within the composite-fermion model), $k_F = 4\pi n$ is the Fermi wave vector, $n$ is the electronic density, and $\ell_{tr}$ is the transport mean-free path. For $T < 1$ K, the experimentally measured values of $\rho^D$ are almost 2 orders of magnitude less than $\epsilon$.

The strong-coupling (1, 1, 1) phase exhibits features of the quantum Hall state for the symmetric currents

$$\rho^s_0(d \lesssim \ell_0) = \begin{pmatrix} 0 & 2 \\ -2 & 0 \end{pmatrix}, \tag{138}$$

while for the antisymmetric currents it is a superfluid (Stern and Halperin, 2002) $\rho^a_0(d \lesssim \ell_0) = 0$.

Analyzing the system close to the transition as a composite system comprising regions of both phases, Stern and Halperin (2002) found a phenomenological expression for the drag resistivity

$$\rho^D_{xx} = \frac{8\epsilon f(1-f)(1-2f)}{\epsilon^2 + 4(1-2f)^2}. \tag{139}$$

As $f$ increases from zero, this drag resistivity grows from zero [or rather, the very small value in the compressible state that is neglected in Eq. (139)] reaching a maximum at $f^* \approx 1/2 - \epsilon/4$ (for small $\epsilon$) and again vanishing at the percolation threshold, in qualitative agreement with the nonmonotonic drag observed by Kellogg, Spielman *et al.* (2002) and Kellogg *et al.* (2003).

Furthermore, using the semicircle law (Dykhne and Ruzin, 1994), it can be shown that to the lowest order in $\epsilon$ the drag resistivities satisfy the following (Stern and Halperin, 2002):

$$(\rho_{xy}^D + 1/2)^2 + (\rho_{xx}^D)^2 = 1/4, \tag{140}$$

yielding vanishing Hall drag for the compressible state ($f = 0$) and the quantized value (136) with $n = -1$ for the (1, 1, 1) state at $f \geq 1/2$. Between the two extremes the negative $\rho_{xy}^D$ varies monotonously. The apparent discrepancy in the sign of $\rho_{xy}^D$ obtained by Stern and Halperin (2002) and Kim *et al.* (2001) seems to stem from the alternative definition of drag resistivities. Similar predictions for transport coefficients, in particular, Eq. (140), but without the explicit phase separation were obtained by Simon, Rezayi, and Milovanovic (2003). An alternative model invoking the coexistence of the two phases was suggested by Spivak and Kivelson (2005).

The semicircle relation (140) was experimentally tested by Tutuc, Pillarisetty, and Shayegan (2009); see Fig. 33. Instead of comparing a number of double-well devices with different interlayer separations (Kellogg *et al.*, 2003), Tutuc, Pillarisetty, and Shayegan (2009) varied the electron density and observed the transition between the strong-coupling state at $\nu_T = 1$ and the weakly coupled state at $\nu_T = 2$. The data at intermediate temperatures $T \approx 300$ K are in a good quantitative agreement with the theory. At the same time, Eq. (140) is only approximate and is expected to hold if the drag resistivity is much larger than the symmetric bilayer resistivity at all fillings. Drag resistivity in the weak-coupling state is also neglected. Given these approximations, the agreement between the data and the phenomenological theory of Stern and Halperin (2002) is satisfactory.

### B. Interlayer exciton formation

Further experiments revealed the most intriguing feature of the strong-coupling quantum Hall state at $\nu_T = 1$: the presence of the exciton condensate capable of neutral superfluid transport (Eisenstein and MacDonald, 2004; Eisenstein, 2014). Originally envisioned for optically generated excitons in bulk semiconductors (Blatt, Böer, and Brandt, 1962; Moskalenko, 1962; Keldysh and Kopaev, 1964; Keldysh and Kozlov, 1968), the phenomenon was also predicted for indirect excitons in double-layer systems (Lozovik and Yudson, 1976; Shevchenko, 1976).

The quantized Hall effect along with the vanishing longitudinal resistivity at $\nu_T = 1$ indicated a gapped spectrum of charged excitations. In these measurements (Eisenstein *et al.*, 1992; Suen *et al.*, 1992; Eisenstein, 2014), electrical currents in the two layers flow in the same direction. In contrast, the condensate couples to antiparallel or counterflowing currents (Kellogg *et al.*, 2004; Tutuc, Shayegan, and Huse, 2004; Wiersma *et al.*, 2004) and manifests itself through vanishing Hall voltage. The simplest explanation for this observation is based on charge neutrality of excitons: as neutral objects, excitons do not experience the Lorentz force and hence no Hall voltage develops when equal, counterpropagating currents are flowing through the two layers.

Another spectacular manifestation of the exciton condensate is the Josephson-like tunneling anomaly (Spielman *et al.*, 2000; Wiersma *et al.*, 2006, 2007; Finck *et al.*, 2008; Tiemann, Dietsche *et al.*, 2008; Yoon *et al.*, 2010) that theoretically was predicted by Wen and Zee (1992) and Park and Das Sarma (2006) and later discussed by Dolcini *et al.* (2010).

Finally, the latest experiments revealing the existence of the exciton condensate utilized the multiple connected Corbino geometry (Tiemann, Dietsche *et al.*, 2008; Tiemann, Lok *et al.*, 2008; Finck *et al.*, 2011; Nandi *et al.*, 2012). For a theoretical discussion of the superfluid flow in the Corbino geometry, see Su and MacDonald (2008). The advantage of the Corbino samples is that they support the exciton flow through the bulk (in contrast to the Hall bar samples where transport is dominated by the edges).

Coulomb drag has played an important role in discovering the interlayer correlated state (Eisenstein, 2014). Quantized Hall drag measured in the simply connected square geometry (Kellogg, Spielman *et al.*, 2002) was one of the first indications of anomalous in-plane transport in double-layer systems at $\nu_T = 1$. Remarkably, the quantized Hall voltage has been found to be the same in both layers. At first glance, this contradicts the boundary conditions of the drag measurement: drag experiments involve passing current through one of the layers and measuring the induced voltage in the other, where no current is allowed to flow. The absence of the current seems to yield the absence of the Lorentz force and hence lead to the standard conclusion that no Hall voltage should be induced in the passive layer; see Sec. II.G. However, this argument does not take into account collective effects. In the presence of the condensate, the driving current can be decomposed into the symmetric and antisymmetric parts (Stern and Halperin, 2002). While the symmetric current carries the electric charge, the antisymmetric (or counterpropagating) current is equivalent to the condensate flow. In the passive layer the two currents cancel each other thus satisfying the boundary condition. At the same time, it is the symmetric, charge-carrying current that can couple to the magnetic field. This current is shared between the layers, yielding the identical quantized Hall voltage across both layers.

Similar arguments lead to the expectation of "perfect" longitudinal drag (Su and MacDonald, 2008): the symmetric current shared between the layers should be responsible not only for the Hall, but also for the longitudinal voltage in the passive layer. This prediction was tested in a dedicated experiment by Nandi *et al.* (2012) using Corbino samples. Deviating from the standard setup, Nandi *et al.* (2012) closed the electric circuit in the passive layer and measured the induced *current*, rather than the voltage. In this case, perfect drag means that the induced current should be the same in magnitude as the driving current passed through the active layer while flowing in the opposite direction. This is exactly what was observed by Nandi *et al.* (2012), at least for small driving currents; see Fig. 34.

The previous arguments neglect the impact of disorder that might affect the presumed dissipationless excitonic transport (Su and MacDonald, 2008) across the bulk of the device (Fertig and Murthy, 2005; Huse, 2005; Fil and Shevchenko, 2007; Lee, Eastham, and Cooper, 2011). Assuming a phenomenological resistance $R_s$ of the excitonic system, one still

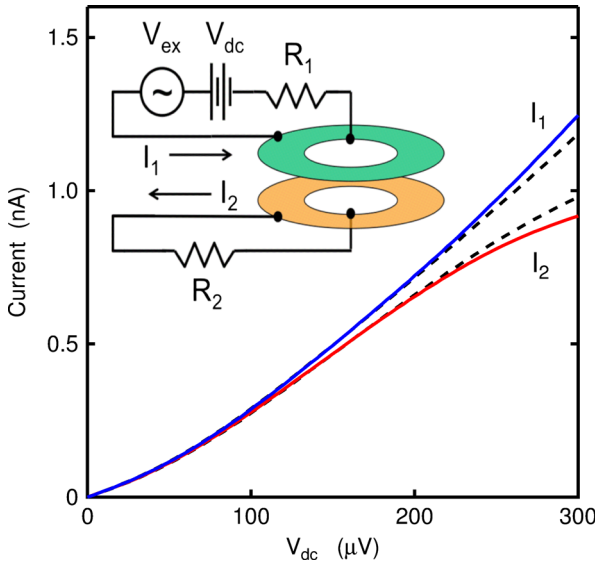


FIG. 34. Corbino Coulomb drag. Solid lines show the drive and drag currents. The measurement was performed at $\nu_T = 1$, $T = 17$ mK, and $d/\ell_0 = 1.5$. Dashed lines represent the results of simulations incorporating estimated series resistances and measured Corbino conductivity. The inset shows the measurement schematic. The resistances $R_i$ comprise both external circuit resistors and the resistances intrinsic to the device. From Nandi *et al.*, 2012.

finds [neglecting the Corbino conductance (Nandi *et al.*, 2012)] perfect drag $I_1 = I_2 = V/(R_1 + R_2 + R_s)$, where $R_i$ represent the net resistances in series with the Corbino sample; see the inset in Fig. 34. As the magnitude of $R_1 + R_2$ is expected to always exceed $2h/e^2$ (Su and MacDonald, 2008; Pesin and MacDonald, 2011), the ability of the experiment to detect small values of $R_s$ is limited. The issue of dissipation in the excitonic system might be clarified by future multiterminal measurements.

So far we discussed experiments on the exciton physics in double-layer systems comprising similar electronic layers (Eisenstein and MacDonald, 2004). It is also possible to create devices with oppositely doped layers, the so-called electron-hole bilayers (Keogh *et al.*, 2005; Das Gupta *et al.*, 2011). Coulomb drag measurements in these systems (Croxall *et al.*, 2008; Seamons *et al.*, 2009) do not provide direct evidence of interlayer coherence, but nevertheless demonstrate an upturn in $\rho_D$ as the temperature is lowered below 1 K. The upturn is seen only in devices with smaller (20 nm) interlayer separation suggesting exciton formation.

A microscopic theory of Coulomb drag in proximity to a phase transition was suggested by Hu (2000b) and Mink *et al.* (2012, 2013). As the system approaches the transition temperature $T_c$ from above, the drag resistivity was found to exhibit a logarithmic divergence

$$\rho_D = \rho_0 + A \ln[T_c/(T - T_c)], \tag{141}$$

where $\rho_0$ and $A$ are two fitting parameters (Gamucci *et al.*, 2014). While qualitatively resembling the upturn observed in electron-hole bilayers (Croxall *et al.*, 2008; Seamons *et al.*, 2009), the theory does not account for either a subsequent downturn at the lowest temperatures or the apparent violation of Onsager reciprocity (Croxall *et al.*, 2008) [although the latter might be related to heating effects (Seamons *et al.*, 2009)]. The theory also does not make falsifiable predictions regarding the dependence of $\rho_D$ on carrier densities in the two layers (Morath *et al.*, 2009) [at higher temperatures, where the data show the standard $T^2$ dependence, the density dependence of $\rho_D$ is stronger than expected on the basis of the Fermi-liquid many-body calculations (Hwang and Das Sarma, 2008b)].

The logarithmic temperature dependence (141) fits well with the upturn in the drag resistivity observed by Gamucci *et al.* (2014) in hybrid devices comprising either a monolayer or bilayer graphene sheet and a GaAs quantum well; see Fig. 35. In fact, the search for exciton physics was one of the main motivations for experimental studies of Coulomb drag in double-layer graphene-based structures (Kim *et al.*, 2011; Gorbachev *et al.*, 2012).

Exciton condensation in graphene has attracted considerable theoretical attention (Aleiner, Kharzeev, and Tsvelik, 2007; Kharitonov and Efetov, 2008, 2010; Lozovik and Sokolik, 2008; Min *et al.*, 2008; Zhang and Joglekar, 2008; Fil and Kravchenko, 2009; Efimkin and Lozovik, 2011; Lozovik, Ogarkov, and Sokolik, 2012; Pikalov and Fil, 2012; Sodemann, Pesin, and MacDonald, 2012; Suprunenko, Cheianov, and Fal'ko, 2012; Abergel *et al.*, 2013). Several contradicting values of the transition temperature in double-layer graphene systems have been reported. The initial estimate (Zhang and Joglekar, 2008; Mink *et al.*, 2012) of $T_c$ close to room temperature appeared to be too optimistic. Screening effects (Kharitonov and Efetov, 2008, 2010) were shown to lead to extremely low values under 1 mk ($T_c \sim 10^{-7} E_F$). More recent investigations involving a detailed analysis of screened Coulomb interaction (Lozovik, Ogarkov, and Sokolik, 2012; Sodemann, Pesin, and MacDonald, 2012; Abergel *et al.*, 2013), multiband pairing (Lozovik, Ogarkov, and Sokolik, 2012; Mink *et al.*, 2012), and pairing with nonzero momentum (Efimkin and Lozovik, 2011) suggested somewhat higher values of $T_c$, making the transition experimentally accessible.

High-temperature coherence and superfluidity was also suggested in thin films of topological insulators (Seradjeh, Moore, and Franz, 2009; Efimkin, Lozovik, and Sokolik, 2012; Mink *et al.*, 2012, 2013).

The effect of exciton condensation on Coulomb drag was numerically investigated in graphene by Zhang and Jin (2013) and analytically in topological insulator films by Efimkin and Lozovik (2013). The latter work focused on the drag effect at temperatures exceeding $T_c$, where the pairing fluctuations are expected to play an important role. In addition to the Maki-Thompson–type contribution (Hu, 2000b; Mink *et al.*, 2012, 2013) to the drag resistivity, Efimkin and Lozovik (2013) analyzed the Aslamazov-Larkin–type contribution and found

$$\delta\rho_D^{\mathrm{AL}} \propto [\ln(T/T_c)]^{-1}. \tag{142}$$

Far away from the transition, the result (142) decays logarithmically, similarly to Eq. (141), but close to the transition exhibits a stronger divergence $\delta\rho_D^{\mathrm{AL}} \propto (T - T_c)^{-1}$.

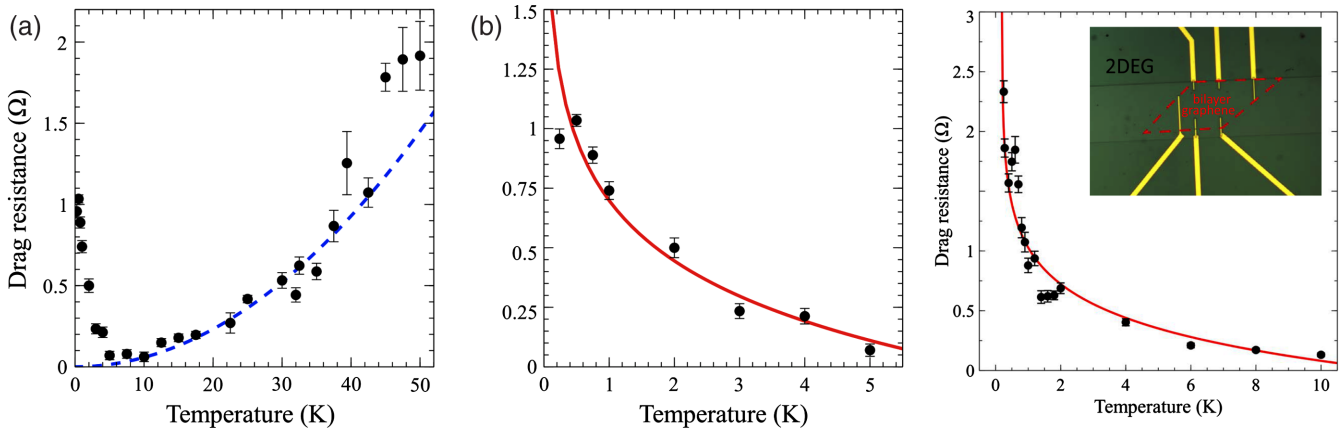


FIG. 35. Coulomb drag in a graphene-2DEG vertical heterostructure. Left: Measured drag resistivity. The dashed line represents the best fit for the standard temperature dependence $R_D = aT^2$, $a = (5.8 \pm 0.3) \times 10^{-4}$ ΩK$^{-2}$. Middle: A fit of the low-$T$ upturn based on Eq. (141). The critical temperature found from the fit is $T_c \sim 10 - 100$ mK. Right: The low-$T$ upturn in a bilayer graphene-2DEG heterostructure. The fit based on Eq. (141) yields $T_c \sim 190$ mK. From Gamucci *et al.*, 2014.

## VIII. OPEN QUESTIONS AND PERSPECTIVES

The physics of the Coulomb drag in double-layer systems is well understood if both layers are in the Fermi-liquid state (Flensberg *et al.*, 1995; Kamenev and Oreg, 1995). The current in the passive layer is created by exciting electron-hole pairs (each pair consisting of an occupied state above the Fermi surface and an empty state below) in a state characterized by finite momentum. The momentum comes from the electron-hole excitations in the active layer created by the driving current. The momentum transfer is due to the interlayer Coulomb interaction. Therefore it follows from the usual phase-space considerations that the drag coefficient is proportional to the square of the temperature $\rho_D \propto T^2$. Remarkably, this simple argument is sufficient to describe the observed low-temperature dependence of $\rho_D$. Deviations from the quadratic dependence at higher temperatures are primarily due to the effect of phonons and plasmons (Rojo, 1999).

The universality of the Landau Fermi-liquid theory (Lifshitz and Pitaevskii, 1981; Altshuler and Aronov, 1985) can be traced to the linearization of the quasiparticle spectrum. Within this approximation all details of the microscopic structure of the system are contained in a limited number of parameters, such as the Fermi velocity and DOS at the Fermi level. Many observable quantities (e.g., the electronic contribution to the specific heat, spin susceptibility, period of the de Haas–van Alphen oscillations, etc.) can be expressed in terms of these parameters and thus exhibit the "universal" behavior (as a function of temperature or external fields). The same arguments can be applied to elementary excitations in strongly doped graphene ($\mu \gg T$), where the Fermi-liquid theory is expected to be applicable.

Coulomb drag belongs to a different class of observables. In conventional semiconductor devices, it reflects the degree of electron-hole asymmetry in the system vanishing in the approximation of linearized spectrum (Kamenev and Oreg, 1995). The drag coefficient is determined by the subleading contribution taking into account the curvature of the quasiparticle spectrum. Indeed, in the passive layer the momentum is transferred equally to electrons and holes so that the resulting state can carry current only in the case of electron-hole asymmetry. Likewise, this asymmetry is necessary for the current-carrying state in the active layer to be characterized by nonzero total momentum. The electron-hole asymmetry manifests itself (Narozhny, Aleiner, and Stern, 2001; von Oppen, Simon, and Stern, 2001) in the energy (or chemical potential) dependence of such quantities as the density of states, single-layer conductivity, and diffusion coefficient. Within the Fermi-liquid theory (Kamenev and Oreg, 1995), the asymmetry is weak, $\partial\sigma_i/\partial\mu_i \approx \sigma_i/\mu_i$, leading to the drag effect that is much weaker than the single-layer conductivity.

Coulomb drag in non-Fermi-liquid systems is much more interesting. In particular, it was used to study novel strongly correlated, many-body states in double quantum wells (Eisenstein, 2014), graphene (Gamucci *et al.*, 2014), quantum wires (Laroche *et al.*, 2014), and optical cavities (Berman, Kezerashvili, and Kolmakov, 2014), where practical applications in optical switches have been suggested. In these systems, drag measurements have proved to be an invaluable tool to study the microscopic structure of complex, interacting many-body systems.

At the same time, our understanding of many of these systems is incomplete. In contrast to the Fermi-liquid theory, many aspects of the strongly correlated many-body states lack a detailed theoretical description. Consequently, their transport properties, including Coulomb drag, can be evaluated only with the help of heuristic or phenomenological models. One can only hope that a proper microscopic theory of these effects will eventually be developed.

This brings us to the list of unresolved questions related to the theory reviewed in this paper and possible direction of the field in the near future.

(i) At low enough temperatures and especially in strong magnetic fields, double-layer systems may host excitonic condensates (Eisenstein, 2014). In monolayer graphene, such condensation is also possible, but for reasonably weak interactions the condensation temperature appears to be rather low (Aleiner, Kharzeev, and Tsvelik, 2007; Kharitonov and Efetov, 2008; Mink *et al.*, 2012). Nevertheless, a possibility of

interlayer correlated states in graphene-based systems [and possibly in hybrid devices involving other materials (Geim and Grigorieva, 2013)] is rather exciting and certainly requires theoretical attention.

(ii) The hydrodynamic approach of Sec. IV.B should be extended to include thermoelectric effects in graphene-based double structures as well as in monolayer and bilayer graphene. As pointed out by Foster and Aleiner (2009) and Narozhny *et al.* (2015), the quasiparticle imbalance in graphene may play a decisive role in thermal transport. Another promising direction may be opened by generalization of the macroscopic linear-response equations to a true, nonlinear hydrodynamics. The relation between the quantum kinetic equation of Zala, Narozhny, and Aleiner (2001) and the hydrodynamic approach [both in graphene (Narozhny *et al.*, 2015) and in 2DEG (Andreev, Kivelson, and Spivak, 2011; Apostolov, Levchenko, and Andreev, 2014)] is also of certain theoretical interest.

(iii) Dirac fermions can be found as low-energy excitations not only in graphene, but also in topological insulators (Bernevig and Hughes, 2013; Shen, 2013). An extension of the present theory of Coulomb drag to various possible system configurations involving topological insulators and/or hybrid devices involving topological insulators, graphene, etc., appears to be very promising (Mink *et al.*, 2012).

(iv) Novel aspects of Luttinger liquid physics and the role of equilibration processes on drag can be further explored with the edge states of quantum Hall systems or topological edge liquids of the quantum spin Hall effect. Some theoretical predictions have already been made (Zyuzin and Fiete, 2010) and recent experimental advances (Roth *et al.*, 2009; Altimiras *et al.*, 2010; König *et al.*, 2013; Du *et al.*, 2015) bring these exciting perspectives within reach.

(v) Mesoscopic fluctuations of Coulomb drag in ballistic samples should be further analyzed on the basis of the microscopic theory. The theory should be further extended to the cases of Dirac fermions in graphene and composite fermions at the half-filled Landau level. Experimental work in this direction was already initiated by Price, Savchenko, and Ritchie (2010) and Kim *et al.* (2011).

(vi) The third-order drag effect (see Sec. IV.F) bears a certain resemblance to the well-known Altshuler-Aronov corrections to single-layer conductivity (Altshuler and Aronov, 1985; Zala, Narozhny, and Aleiner, 2001). Zala, Narozhny, and Aleiner (2001) showed that the dominant contribution to conductivity at low (diffusive regime) and high (ballistic regime) temperatures technically comes from different diagrams describing conceptually similar, but at the same time distinct interference processes. Similarly, we expect that the third-order drag contribution in ballistic regime might be governed by scattering processes which are distinct from those considered by Levchenko and Kamenev (2008a).

We close this review by pointing out the surprising richness of the Coulomb drag problem. The original suggestion of a way to observe interwell interactions in semiconductor heterostructures has developed into a vibrant field of research where technological advances go hand in hand with theoretical developments. New experiments with novel materials keep being devised and stimulate new avenues for theoretical thinking. We are expecting to see further intriguing discoveries being made related to frictional drag in the foreseeable future.

## ACKNOWLEDGMENTS

We thank all of our collaborators for sharing their insights over the years and especially I. L. Aleiner, A. V. Andreev, S. Apostolov, W. Chen, I. V. Gornyi, A. Kamenev, M. I. Katsnelson, A. D. Mirlin, M. Norman, P. M. Ostrovsky, L. Ponomarenko, M. Schütt, A. Stern, M. Titov, and the late A. Savchenko. While writing this review we greatly benefited from discussions with M. Foster, G. Gervais, D. Polyakov, and J. Schmalian. The work of A. L. was supported by NSF Grants No. DMR-1606517 and No. ECCS-1560732, in part by a DAAD grant from German Academic Exchange Services, Office of the Vice Chancellor for Research and Graduate Education with funding from the Wisconsin Alumni Research Foundation, and No. SPP 1459 and No. SPP 1666 of the Deutsche Forschungsgemeinschaft. B. N. N. acknowledges support from the EU Network Grant InterNoM and the Deutsche Forschungsgemeinschaft under Grants No. SCHO 287/7-1 and No. SH 81/2-1.

***NOTE ADDED IN PROOF.***—After the submission of this review to the editorial offices, several important developments occurred.

Drag measurements were performed in the double *bilayer* graphene (BLG) structures (Li *et al.*, 2016; Lee *et al.*, 2016). In contrast to the devices based on monolayer graphene, these new BLG samples exhibit drag response with an inverse sign in the regime of low temperatures and intermediate densities. Careful measurements with BLG devices having different aspect ratios combined with the new nonlocal method of reading off drag voltage showed that the observed data cannot be simply understood using traditional theoretical approaches. Understanding these results remains a challenge for theorists. Magnetodrag and Hall drag measurements in these systems are underway.

Since BLG allows a great degree of tunability of interaction strength, this platform paves the way for the pursuit of new emergent phases in strongly interacting bilayers, such as the elusive exciton condensate. In a parallel development, novel aspects of Coulomb drag in the electron-hole bilayers specific to the formation of excitons have been discussed theoretically by Efimkin and Galitski (2016) in the context of earlier data on GaAs/GaAlAs quantum wells, and by Mou *et al.* (2015) in the context of graphene double layers.

Coulomb drag in one-dimensional electron liquids continues to attract considerable attention. This particular direction is primarily driven by theoretical proposals and ideas such as those discussed by Chou, Levchenko and Foster (2015) and Dmitriev, Gornyi, and Polyakov (2015). Further experimental studies in this field are highly desirable to stimulate further progress. In particular, the recent observation of a helical Luttinger liquid in the edge channels of an InAs/GaSb quantum spin Hall insulator (Li *et al.*, 2015) gives hope that Coulomb drag can be realized in this novel system.

In the context of other nanoscale systems, Coulomb drag has been measured recently in systems of coupled quantum dots (Keller *et al.*, 2016) revealing a cotunneling mediated

drag mechanism. A related theory was reported by Kaasbjerg and Jauho (2016). Measurements on a system of stacked graphene quantum dots (Bischoff *et al.*, 2015) exhibited much richer physics than was previously anticipated (Sánchez *et al.*, 2010). The observed quantum-mechanical detector backaction in the regime of strongly correlated transport is yet to be understood theoretically.

Transport properties of novel materials systems including topological insulator films (Liu, Liu, and Culcer, 2016) and phosphorene based double-layer heterostructures (Saberi-Pouya *et al.*, 2016) have been studied theoretically. The predicted drag effect in these systems is awaiting its experimental verification.

## REFERENCES


Abedinpour, S. H., G. Vignale, A. Principi, M. Polini, W.-K. Tse, and A. H. MacDonald, 2011, Phys. Rev. B **84**, 045429.

Abergel, D. S. L., M. Rodriguez-Vega, E. Rossi, and S. Das Sarma, 2013, Phys. Rev. B **88**, 235402.

Abrahams, E., P. W. Anderson, D. C. Licciardello, and T. V. Ramakrishnan, 1979, Phys. Rev. Lett. **42**, 673.

Abrikosov, A., and S. Beneslavskii, 1971, Zh. Eksp. Teor. Fiz. **59**, 1280 [Sov. Phys. JETP **32**, 699 (1971), http://www.jetp.ac.ru/cgi-bin/e/index/e/32/4/p699?a=list].

Aguado, R., and L. P. Kouwenhoven, 2000, Phys. Rev. Lett. **84**, 1986.

Aleiner, I. L., B. L. Altshuler, and M. E. Gershenson, 1999, Waves Random Media **9**, 201.

Aleiner, I. L., and K. B. Efetov, 2006, Phys. Rev. Lett. **97**, 236801.

Aleiner, I. L., D. E. Kharzeev, and A. M. Tsvelik, 2007, Phys. Rev. B **76**, 195415.

Alkauskas, A., K. Flensberg, B. Y.-K. Hu, and A.-P. Jauho, 2002, Phys. Rev. B **66**, 201304.

Altimiras, C., H. le Sueur, U. Gennser, A. Cavanna, D. Mailly, and F. Pierre, 2010, Nat. Phys. **6**, 34.

Altshuler, B., and A. Aronov, 1979, Zh. Eksp. Teor. Fiz. **77**, 2028 [Sov. Phys. JETP **50**, 968 (1979), http://www.jetp.ac.ru/cgi-bin/e/index/e/50/5/p968?a=list].

Altshuler, B. L., 1985, Pis'ma Zh. Eksp. Teor. Fiz. **41**, 530 [JETP Lett. **41**, 648 (1985), http://www.jetpletters.ac.ru/ps/1470/article_22425.shtml].

Altshuler, B. L., and A. G. Aronov, 1985, in *Electron-Electron Interactions in Disordered Systems*, edited by A. L. Efros and M. Pollak (North-Holland, Amsterdam).

Altshuler, B. L., D. E. Khmel'nitzkii, A. I. Larkin, and P. A. Lee, 1980, Phys. Rev. B **22**, 5142.

Altshuler, B. L., and P. A. Lee, 1988, Phys. Today **41**, 36.

Altshuler, B. L., P. A. Lee, and R. A. Webb, 1991, Eds., *Mesoscopic Phenomena in Solids* (North-Holland, New York).

Amo, A., *et al.*, 2009, Nature (London) **457**, 291.

Amorim, B., and N. M. R. Peres, 2012, J. Phys. Condens. Matter **24**, 335602.

Amorim, B., J. Schiefele, F. Sols, and F. Guinea, 2012, Phys. Rev. B **86**, 125448.

An, S., G. Gopalakrishnan, Y. Shiroyanagi, S. C. Parks, T. J. Gramila, L. N. Pfeiffer, and K. W. West, 2006, Physica (Amsterdam) **34E**, 214.

Anderson, P. W., E. Abrahams, and T. V. Ramakrishnan, 1979, Phys. Rev. Lett. **43**, 718.

Ando, T., 2006, J. Phys. Soc. Jpn. **75**, 074716.

Ando, T., A. B. Fowler, and F. Stern, 1982, Rev. Mod. Phys. **54**, 437.

Andreev, A. V., S. A. Kivelson, and B. Spivak, 2011, Phys. Rev. Lett. **106**, 256804.

Apalkov, V. M., and M. E. Raikh, 2005, Phys. Rev. B **71**, 245109.

Apostolov, S. S., A. Levchenko, and A. V. Andreev, 2014, Phys. Rev. B **89**, 121104.

Aristov, D. N., 2007, Phys. Rev. B **76**, 085327.

Arnold, P., G. D. Moore, and L. G. Yaffe, **2000**, J. High Energy Phys. 11, 001.

Asgari, R., B. Tanatar, and B. Davoudi, 2008, Phys. Rev. B **77**, 115301.

Aslamazov, L. G., and A. I. Larkin, 1968, Fiz. Tverd. Tela (Leningrad) **10**, 1104 [Sov. Phys. Solid State **10**, 875 (1968)].

Badalyan, S. M., and C. S. Kim, 2003, Solid State Commun. **127**, 521.

Badalyan, S. M., C. S. Kim, G. Vignale, and G. Senatore, 2007, Phys. Rev. B **75**, 125321.

Badalyan, S. M., and F. M. Peeters, 2012, Phys. Rev. B **86**, 121405.

Badalyan, S. M., and U. Rössler, 1999, Phys. Rev. B **59**, 5643.

Badalyan, S. M., and G. Vignale, 2009, Phys. Rev. Lett. **103**, 196601.

Baker, J., and A. G. Rojo, 2001, J. Phys. Condens. Matter **13**, 3389.

Baker, J., G. Vignale, and A. G. Rojo, 1999, Phys. Rev. B **60**, 8804.

Balili, R., V. Hartwell, D. Snoke, L. Pfeiffer, and K. West, 2007, Science **316**, 1007.

Balram, A. C., J. A. Hutasoit, and J. K. Jain, 2014, Phys. Rev. B **90**, 045103.

Berk, Y., A. Kamenev, A. Palevski, L. N. Pfeiffer, and K. W. West, 1995, Phys. Rev. B **51**, 2604.

Berman, O. L., R. Kezerashvili, and Y. E. Lozovik, 2010a, Phys. Lett. A **374**, 3681.

Berman, O. L., R. Kezerashvili, and Y. E. Lozovik, 2010b, Phys. Rev. B **82**, 125307.

Berman, O. L., R. Y. Kezerashvili, and G. V. Kolmakov, 2014, ACS Nano **8**, 10437.

Bernevig, A., and T. Hughes, 2013, *Topological Insulators and Topological Superconductors* (Princeton University Press, Princeton, NJ).

Bischoff, D., M. Eich, O. Zilberberg, C. Rössler, T. Ihn, and K. Ensslin, 2015, Nano Lett. **15**, 6003.

Blatt, J. M., K. W. Böer, and W. Brandt, 1962, Phys. Rev. **126**, 1691.

Bloch, F., 1930, Z. Phys. **59**, 208.

Boebinger, G. S., A. Passner, L. N. Pfeiffer, and K. W. West, 1991, Phys. Rev. B **43**, 12673.

Boiko, I. I., and Y. M. Sirenko, 1988, Zh. Tekh. Fiz. **58**, 967 [Sov. Phys. Tech. Phys. **33**, 586 (1988)].

Boiko, I. I., and Y. M. Sirenko, 1990, Phys. Status Solidi B **159**, 805.

Boiko, I. I., P. Vasilopoulos, and Y. M. Sirenko, 1992, Phys. Rev. B **45**, 13538.

Bonesteel, N. E., 1993, Phys. Rev. B **48**, 11484.

Bønsager, M. C., K. Flensberg, B. Y.-K. Hu, and A. P. Jauho, 1996, Phys. Rev. Lett. **77**, 1366.

Bønsager, M. C., K. Flensberg, B. Y.-K. Hu, and A. P. Jauho, 1997, Phys. Rev. B **56**, 10314.

Bønsager, M. C., K. Flensberg, B. Y.-K. Hu, and A. MacDonald, 1998a, Phys. Rev. B **57**, 7085.

Bønsager, M. C., K. Flensberg, B. Y.-K. Hu, and A. MacDonald, 1998b, Physica B (Amsterdam) **249–251**, 864.

Bønsager, M. C., Y. B. Kim, and A. H. MacDonald, 2000, Phys. Rev. B **62**, 10940.

Bostwick, A., F. Speck, T. Seyller, K. Horn, M. Polini, R. Asgari, A. H. MacDonald, and E. Rotenberg, 2010, Science **328**, 999.

Braude, V., and A. Stern, 2001, Phys. Rev. B **64**, 115431.

Brener, S., and W. Metzner, 2005, Pis'ma Zh. Eksp. Teor. Fiz. **81**, 618 [JETP Lett. **81**, 498 (2005), http://www.jetpletters.ac.ru/ps/649/article_10143.shtml].
Bulnes Cuetara, G., M. Esposito, G. Schaller, and P. Gaspard, 2013, Phys. Rev. B **88**, 115134.
Burkov, A., J. Schliemann, A. MacDonald, and S. Girvin, 2002, Physica (Amsterdam) **12E**, 28.
Büttiker, M., Y. Imry, R. Landauer, and S. Pinhas, 1985, Phys. Rev. B **31**, 6207.
Büttiker, M., and R. Sánchez, 2011, Nature Natotechnology **6**, 757.
Cambel, V., and M. Moško, 1993, Semicond. Sci. Technol. **8**, 364.
Carr, S. T., B. N. Narozhny, and A. A. Nersesyan, 2013, Ann. Phys. (Amsterdam) **339**, 22.
Carrega, M., T. Tudorovskiy, A. Principi, M. I. Katsnelson, and M. Polini, 2012, New J. Phys. **14**, 063033.
Chakraborty, T., and P. Pietiläinen, 1987, Phys. Rev. Lett. **59**, 2784.
Cheianov, V. V., and V. I. Fal'ko, 2006, Phys. Rev. Lett. **97**, 226801.
Chen, H. Y., and J. Appenzeller, 2013, Nano Res. **6**, 897.
Chen, W., A. V. Andreev, and A. Levchenko, 2015, Phys. Rev. B **91**, 245405.
Chou, Y.-Z., A. Levchenko, and M. S. Foster, 2015, Phys. Rev. Lett. **115**, 186404.
Chudnovskiy, A. L., 2009, Phys. Rev. B **80**, 081309.
Conway, J. H., and N. J. A. Sloane, 1988, *Sphere Packings, Lattices, and Groups* (Springer-Verlag, New York).
Croxall, A. F., K. Das Gupta, C. A. Nicoll, M. Thangaraj, H. E. Beere, I. Farrer, D. A. Ritchie, and M. Pepper, 2008, Phys. Rev. Lett. **101**, 246801.
Cui, H. L., X. L. Lei, and N. J. M. Horing, 1988, Phys. Rev. B **37**, 8223.
Cuoco, M., W. Saldarriaga, A. Polcari, A. Guarino, O. Moran, E. Baca, A. Vecchione, and P. Romano, 2009, Phys. Rev. B **79**, 014523.
D'Amico, I., and G. Vignale, 2000, Phys. Rev. B **62**, 4853.
Das Gupta, K., A. F. Croxall, J. Waldie, C. A. Nicoll, H. E. Beere, I. Farrer, D. A. Ritchie, and M. Pepper, 2011, Adv. Condens. Matter Phys. **2011**, 727958.
Das Gupta, K., M. Thangaraj, A. Croxall, H. Beere, C. Nicoll, D. Ritchie, and M. Pepper, 2008, Physica (Amsterdam) **40E**, 1693.
Das Sarma, S., and A. Madhukar, 1981, Phys. Rev. B **23**, 805.
Das Sarma, S., and B. A. Mason, 1985, Ann. Phys. (N.Y.) **163**, 78.
Debray, P., P. Vasilopoulos, O. Raichev, R. Perrin, M. Rahman, and W. C. Mitchel, 2000, Physica (Amsterdam) **6E**, 694.
Debray, P., V. Zverev, O. Raichev, R. Klesse, P. Vasilopoulos, and R. S. Newrock, 2001, J. Phys. Condens. Matter **13**, 3389.
Debray, P., V. N. Zverev, V. Gurevich, R. Klesse, and R. S. Newrock, 2002, Semicond. Sci. Technol. **17**, R21.
Deshpande, V. V., M. Bockrath, L. I. Glazman, and A. Yacoby, 2010, Nature (London) **464**, 209.
Dmitriev, A. P., I. V. Gornyi, and D. G. Polyakov, 2015, arXiv:1512.00373.
Dmitriev, A. P., I. V. Gornyi, and D. G. Polyakov, 2012, Phys. Rev. B **86**, 245402.
Dmitriev, I. A., F. Evers, I. V. Gornyi, A. D. Mirlin, D. G. Polyakov, and P. Wölfle, 2008, Phys. Status Solidi B **245**, 239.
Dolcini, F., D. Rainis, F. Taddei, M. Polini, R. Fazio, and A. H. MacDonald, 2010, Phys. Rev. Lett. **104**, 027004.
Donarini, A., R. Ferrari, A. P. Jauho, and L. Molinari, 2003, Phys. Lett. A **312**, 123.
Du, L., I. Knez, G. Sullivan, and R.-R. Du, 2015, Phys. Rev. Lett. **114**, 096802.
Duan, J.-M., 1995, Europhys. Lett. **29**, 489.
Duan, J.-M., and S. Yip, 1993, Phys. Rev. Lett. **70**, 3647.
Duine, R. A., M. Polini, A. Raoux, H. Stoof, and G. Vignale, 2011, New J. Phys. **13**, 045010.
Duine, R. A., M. Polini, H. Stoof, and G. Vignale, 2010, Phys. Rev. Lett. **104**, 220403.
Duine, R. A., and H. T. C. Stoof, 2009, Phys. Rev. Lett. **103**, 170401.
Dykhne, A. M., and I. M. Ruzin, 1994, Phys. Rev. B **50**, 2369.
Efetov, D. K., and P. Kim, 2010, Phys. Rev. Lett. **105**, 256805.
Efimkin, D. K., and V. Galitski, 2016, Phys. Rev. Lett. **116**, 046801.
Efimkin, D. K., and Y. E. Lozovik, 2011, Zh. Eksp. Teor. Fiz. **140**, 1009 [JETP **113**, 880 (2011), http://link.springer.com/article/10.1134/S1063776111130048].
Efimkin, D. K., and Y. E. Lozovik, 2013, Phys. Rev. B **88**, 235420.
Efimkin, D. K., Y. E. Lozovik, and A. A. Sokolik, 2012, Phys. Rev. B **86**, 115436.
Eisenstein, J., 2014, Annu. Rev. Condens. Matter Phys. **5**, 159.
Eisenstein, J. P., 1992, Superlattices Microstruct. **12**, 107.
Eisenstein, J. P., 1997, in *Perspectives in Quantum Hall Effects*, edited by S. Das Sarma and A. Pinczuk (Wiley, New York).
Eisenstein, J. P., G. S. Boebinger, L. N. Pfeiffer, K. W. West, and S. He, 1992, Phys. Rev. Lett. **68**, 1383.
Eisenstein, J. P., and A. H. MacDonald, 2004, Nature (London) **432**, 691.
Elsayad, K., J. P. Carini, and D. Baxter, 2008, Solid State Commun. **148**, 261.
Elzerman, J., R. Hanson, L. W. van Beveren, B. Witkamp, L. Vandersypen, and L. Kouwenhoven, 2004, Nature (London) **430**, 431.
Farina, L. A., K. M. Lewis, C. Kurdak, S. Ghosh, and P. Bhattacharya, 2004, Phys. Rev. B **70**, 153302.
Fei, Z., *et al.*, 2011, Nano Lett. **11**, 4701.
Fei, Z., *et al.*, 2012, Nature (London) **487**, 82.
Feng, X. G., S. Zelakiewicz, H. Noh, T. J. Ragucci, T. J. Gramila, L. N. Pfeiffer, and K. W. West, 1998, Phys. Rev. Lett. **81**, 3219.
Fertig, H. A., and G. Murthy, 2005, Phys. Rev. Lett. **95**, 156802.
Fiete, G. A., K. L. Hur, and L. Balents, 2006, Phys. Rev. B **73**, 165104.
Fil, D. V., and L. Y. Kravchenko, 2009, Low Temp. Phys. **35**, 712.
Fil, D. V., and S. I. Shevchenko, 2007, Low Temp. Phys. **33**, 780.
Finck, A. D. K., A. R. Champagne, J. P. Eisenstein, L. N. Pfeiffer, and K. W. West, 2008, Phys. Rev. B **78**, 075302.
Finck, A. D. K., J. P. Eisenstein, L. N. Pfeiffer, and K. W. West, 2010, Phys. Rev. Lett. **104**, 016801.
Finck, A. D. K., J. P. Eisenstein, L. N. Pfeiffer, and K. W. West, 2011, Phys. Rev. Lett. **106**, 236807.
Finkel'shtein, A. M., 1983, Zh. Eksp. Teor. Fiz. **84**, 168 [Sov. Phys. JETP **57**, 97 (1983), http://www.jetp.ac.ru/cgi-bin/e/index/e/57/1/p97?a=list].
Finkelstein, A. M., 1984, Z. Phys. B **56**, 189.
Finkelstein, G., H. Shtrikman, and I. Bar-Joseph, 1995, Phys. Rev. Lett. **74**, 976.
Fisichella, G., G. Greco, F. Roccaforte, and F. Giannazzo, 2014, Nanoscale **6**, 8671.
Flensberg, K., 1998, Phys. Rev. Lett. **81**, 184.
Flensberg, K., and B. Y.-K. Hu, 1994, Phys. Rev. Lett. **73**, 3572.
Flensberg, K., and B. Y.-K. Hu, 1995, Phys. Rev. B **52**, 14796.
Flensberg, K., B. Y.-K. Hu, A.-P. Jauho, and J. M. Kinaret, 1995, Phys. Rev. B **52**, 14761.
Flensberg, K., T. Stibius Jensen, and N. Asger Mortensen, 2001, Phys. Rev. B **64**, 245308.
Foster, M. S., and I. L. Aleiner, 2009, Phys. Rev. B **79**, 085415.
Frederikse, H. P. R., 1953, Phys. Rev. **92**, 248.
Fritz, L., J. Schmalian, M. Müller, and S. Sachdev, 2008, Phys. Rev. B **78**, 085416.

Fuchs, T., R. Klesse, and A. Stern, 2005, Phys. Rev. B **71**, 045321.
Furuya, S. C., H. Matsuura, and M. Ogata, 2015, arXiv:1503.02499.
Gamucci, A., *et al.*, 2014, Nat. Commun. **5**, 5824.
Geballe, T. H., and G. W. Hull, 1954, Phys. Rev. **94**, 1134.
Geigenmüller, U., and Y. V. Nazarov, 1991, Phys. Rev. B **44**, 10953.
Geim, A. K., and I. V. Grigorieva, 2013, Nature (London) **499**, 419.
Giamarchi, T., 2004, *Quantum Physics in One Dimension* (Oxford University Press, New York).
Giordano, N., and J. D. Monnier, 1994, Phys. Rev. B **50**, 9363.
Girvin, S. M., and A. H. MacDonald, 1997, in *Perspectives in Quantum Hall Effects*, edited by S. Das Sarma and A. Pinczuk (Wiley, New York).
Giuliani, G., and G. Vignale, 2005, *Quantum Theory of the Electron Liquid* (Cambridge University Press, Cambridge, England).
Giuliani, G. F., and J. J. Quinn, 1982, Phys. Rev. B **26**, 4421.
Glazman, L. I., G. B. Lesovik, D. E. Khmel'nitskii, and R. I. Shekhter, 1988, Pis'ma Zh. Eksp. Teor. Fiz. **48**, 218 [JETP Lett. **48**, 238 (1988), http://www.jetpletters.ac.ru/ps/1104/article_16696.shtml].
Glazov, M. M., M. A. Semina, S. M. Badalyan, and G. Vignale, 2011, Phys. Rev. B **84**, 033305.
González, J., F. Guinea, and M. A. H. Vozmediano, 1999, Phys. Rev. B **59**, R2474.
Gorbachev, R. V., *et al.*, 2012, Nat. Phys. **8**, 896.
Gorkov, L. P., A. I. Larkin, and D. E. Khmel'nitzkii, 1979, Pis'ma Zh. Eksp. Teor. Fiz. **30**, 248 [JETP Lett. **30**, 228 (1979), http://www.jetpletters.ac.ru/ps/1364/article_20629.shtml].
Gornyi, I., A. Yashenkin, and D. Khveshchenko, 2000, Physica B (Amsterdam) **284–288**, 1930.
Gornyi, I. V., A. D. Mirlin, and F. von Oppen, 2004, Phys. Rev. B **70**, 245302.
Gornyi, I. V., and B. N. Narozhny, 2014 (unpublished).
Gornyi, I. V., A. G. Yashenkin, and D. V. Khveshchenko, 1999, Phys. Rev. Lett. **83**, 152.
Gramila, T. J., J. P. Eisenstein, A. H. MacDonald, L. N. Pfeiffer, and K. W. West, 1991, Phys. Rev. Lett. **66**, 1216.
Gramila, T. J., J. P. Eisenstein, A. H. MacDonald, L. N. Pfeiffer, and K. W. West, 1992, Surf. Sci. **263**, 446.
Gramila, T. J., J. P. Eisenstein, A. H. MacDonald, L. N. Pfeiffer, and K. W. West, 1993, Phys. Rev. B **47**, 12957.
Gramila, T. J., J. P. Eisenstein, A. H. MacDonald, L. N. Pfeiffer, and K. W. West, 1994, Physica (Amsterdam) **197B**, 442.
Greiter, M., X.-G. Wen, and F. Wilczek, 1991, Phys. Rev. Lett. **66**, 3205.
Grigorenko, A. N., M. Polini, and K. S. Novoselov, 2012, Nat. Photonics **6**, 749.
Grüneisen, E., 1933, Ann. Phys. (Berlin) **408**, 530.
Gubarev, S. I., I. V. Kukushkin, S. V. Tovstonog, M. Y. Akimov, J. Smet, K. von Klitzing, and W. Wegscheider, 2000, Pis'ma Zh. Eksp. Teor. Fiz. **72**, 469, http://www.jetpletters.ac.ru/ps/892/article_13761.shtml [JETP Lett. **72**, 324 (2000)].
Gurevich, L. E., 1946a, Zh. Eksp. Teor. Fiz. **16**, 193 [J. Phys. (USSR) **9**, 857 (1945)].
Gurevich, L. E., 1946b, Zh. Eksp. Teor. Fiz. **16**, 416 [J. Phys. (USSR) **10**, 67 (1946)].
Gurevich, V. L., and M. I. Muradov, 2000, Pis'ma Zh. Eksp. Teor. Fiz. **71**, 164, http://www.jetpletters.ac.ru/ps/901/article_13857.shtml [JETP Lett. **71**, 111 (2000)].
Gurevich, V. L., and M. I. Muradov, 2005, J. Phys. Condens. Matter **17**, 87.
Gurevich, V. L., V. B. Pevzner, and E. W. Fenton, 1998, J. Phys. Condens. Matter **10**, 2551.
Gurevich, Y. G., and O. L. Mashkevich, 1989, Phys. Rep. **181**, 327.
Güven, K., and B. Tanatar, 1997a, Phys. Rev. B **56**, 7535.
Güven, K., and B. Tanatar, 1997b, Solid State Commun. **104**, 439.
Haldane, F., and E. Rezayi, 1987, Bull. Am. Phys. Soc. **32**, 892.
Haldane, F. D. M., 1981a, J. Phys. C **14**, 2585.
Haldane, F. D. M., 1981b, Phys. Rev. Lett. **47**, 1840.
Halperin, B. I., 1983, Helv. Phys. Acta **56**, 75 [http://www.e-periodica.ch/digbib/view?pid=hpa-001:1983:56#87].
Halperin, B. I., P. A. Lee, and N. Read, 1993, Phys. Rev. B **47**, 7312.
Hänsch, W., and G. D. Mahan, 1983, J. Phys. Chem. Solids **44**, 663.
Herring, C., 1954, Phys. Rev. **96**, 1163.
Hill, N. P. R., J. T. Nicholls, E. H. Linfield, M. Pepper, D. A. Ritchie, A. R. Hamilton, and G. A. C. Jones, 1996, J. Phys. Condens. Matter **8**, L557.
Hill, N. P. R., J. T. Nicholls, E. H. Linfield, M. Pepper, D. A. Ritchie, B. Y.-K. Hu, and K. Flensberg, 1998, Physica B (Amsterdam) **249–251**, 868.
Hill, N. P. R., J. T. Nicholls, E. H. Linfield, M. Pepper, D. A. Ritchie, G. A. C. Jones, B. Y.-K. Hu, and K. Flensberg, 1997, Phys. Rev. Lett. **78**, 2204.
Höpfel, R., and J. Shah, 1988, Solid State Electron. **31**, 643.
Höpfel, R. A., J. Shah, P. A. Wolff, and A. C. Gossard, 1986, Phys. Rev. Lett. **56**, 2736.
Hruska, M., and B. Spivak, 2002, Phys. Rev. B **65**, 033315.
Hu, B. Y.-K., 1997, Phys. Scr. **T69**, 170.
Hu, B. Y.-K., 1998, Phys. Rev. B **57**, 12345.
Hu, B. Y.-K., 2000a, Physica (Amsterdam) **6E**, 611.
Hu, B. Y.-K., 2000b, Phys. Rev. Lett. **85**, 820.
Hu, B. Y.-K., and K. Flensberg, 1996, in *Hot Carriers in Semiconductors*, edited by K. Hess (Plenum Press, New York).
Huang, X., G. Bazan, and G. Bernstein, 1995, Phys. Rev. Lett. **74**, 4051.
Huse, D. A., 2005, Phys. Rev. B **72**, 064514.
Hwang, E. H., and S. Das Sarma, 2007, Phys. Rev. B **75**, 205418.
Hwang, E. H., and S. Das Sarma, 2008a, Phys. Rev. B **77**, 115449.
Hwang, E. H., and S. Das Sarma, 2008b, Phys. Rev. B **78**, 075430.
Hwang, E. H., S. D. Sarma, V. Braude, and A. Stern, 2003, Phys. Rev. Lett. **90**, 086801.
Hwang, E. H., R. Sensarma, and S. D. Sarma, 2011, Phys. Rev. B **84**, 245441.
Imambekov, A., T. L. Schmidt, and L. I. Glazman, 2012, Rev. Mod. Phys. **84**, 1253.
Jacoboni, C., and P. J. Price, 1988, Solid State Electron. **31**, 649.
Jain, J. K., 1989, Phys. Rev. Lett. **63**, 199.
Jalabert, R., and S. Das Sarma, 1989, Phys. Rev. B **40**, 9723.
Jauho, A.-P., and H. Smith, 1993, Phys. Rev. B **47**, 4420.
Johnson, A. C., C. M. Marcus, M. P. Hanson, and A. C. Gossard, 2004, Phys. Rev. Lett. **93**, 106803.
Jörger, C., S. J. Cheng, W. Dietsche, R. Gerhardts, P. Specht, K. Eberl, and K. von Klitzing, 2000, Physica (Amsterdam) **6E**, 598.
Jörger, C., S. J. Cheng, H. Rubel, W. Dietsche, R. Gerhardts, P. Specht, K. Eberl, and K. von Klitzing, 2000, Phys. Rev. B **62**, 1572.
Jörger, C., W. Dietsche, W. Wegschneider, and K. Klitzing, 2000, Physica (Amsterdam) **6E**, 586.
Ju, L., *et al.*, 2011, Nat. Nanotechnol. **6**, 630.
Kaasbjerg, K., and A.-P. Jauho, 2016, Phys. Rev. Lett. **116**, 196801.
Kamenev, A., and Y. Oreg, 1995, Phys. Rev. B **52**, 7516.
Kashuba, A. B., 2008, Phys. Rev. B **78**, 085415.
Kasprzak, J., *et al.*, 2006, Nature (London) **443**, 409.
Katsnelson, M. I., 2011, Phys. Rev. B **84**, 041407.
Katsnelson, M. I., 2012, *Graphene* (Cambridge University Press, Cambridge, England).

Keldysh, L. V., and Y. V. Kopaev, 1964, Fiz. Tverd. Tela (Leningrad) **6**, 2791 [Sov. Phys. Solid State **6**, 2219 (1965)].
Keldysh, L. V., and A. N. Kozlov, 1968, Zh. Eksp. Teor. Fiz. **54**, 978 [Sov. Phys. JETP **27**, 521 (1968), http://www.jetp.ac.ru/cgi-bin/e/index/e/27/3/p521?a=list].
Keller, A. J., J. S. Lim, D. Sanchez, R. Lopez, S. Amasha, J. A. Katine, H. Shtrikman, and D. Goldhaber-Gordon, 2016, arXiv:1603.00799.
Kellogg, M., J. P. Eisenstein, L. N. Pfeiffer, and K. W. West, 2002, Solid State Commun. **123**, 515.
Kellogg, M., J. P. Eisenstein, L. N. Pfeiffer, and K. W. West, 2003, Phys. Rev. Lett. **90**, 246801.
Kellogg, M., J. P. Eisenstein, L. N. Pfeiffer, and K. W. West, 2004, Phys. Rev. Lett. **93**, 036801.
Kellogg, M., I. B. Spielman, J. P. Eisenstein, L. N. Pfeiffer, and K. W. West, 2002, Phys. Rev. Lett. **88**, 126804.
Keogh, J. A., K. Das Gupta, H. E. Beere, D. A. Ritchie, and M. Pepper, 2005, Appl. Phys. Lett. **87**, 202104.
Khaetskii, A. V., and Y. V. Nazarov, 1999, Phys. Rev. B **59**, 7551.
Kharitonov, M. Y., and K. B. Efetov, 2008, Phys. Rev. B **78**, 241401.
Kharitonov, M. Y., and K. B. Efetov, 2010, Semicond. Sci. Technol. **25**, 034004.
Khrapai, V. S., S. Ludwig, J. P. Kotthaus, H. P. Tranitz, and W. Wegscheider, 2006, Phys. Rev. Lett. **97**, 176803.
Khrapai, V. S., S. Ludwig, J. P. Kotthaus, H. P. Tranitz, and W. Wegscheider, 2007, Phys. Rev. Lett. **99**, 096803.
Khveshchenko, D. V., 2000, Phys. Rev. B **61**, 7227.
Kim, S., I. Jo, J. Nah, Z. Yao, S. K. Banerjee, and E. Tutuc, 2011, Phys. Rev. B **83**, 161401(R).
Kim, S., and E. Tutuc, 2012, Solid State Commun. **152**, 1283.
Kim, Y. B., and A. J. Millis, 1999, Physica (Amsterdam) **4E**, 171.
Kim, Y. B., C. Nayak, E. Demler, N. Read, and S. D. Sarma, 2001, Phys. Rev. B **63**, 205315.
Klesse, R., and A. Stern, 2000, Phys. Rev. B **62**, 16912.
Komnik, A., and R. Egger, 2001, Eur. Phys. J. B **19**, 271.
König, M., *et al.*, 2013, Phys. Rev. X **3**, 021003.
Kozikov, A. A., A. K. Savchenko, B. N. Narozhny, and A. V. Shytov, 2010, Phys. Rev. B **82**, 075424.
Krishnaswamy, A. E., S. M. Goodnick, and J. Bird, 1999, Microelectron. Eng. **47**, 81.
Kukkonen, C. A., and A. W. Overhauser, 1979, Phys. Rev. B **20**, 550.
Kulakovskii, D. V., and Y. E. Lozovik, 2004, Zh. Eksp. Teor. Fiz. **125**, 1375 [http://www.jetp.ac.ru/cgi-bin/e/index/r/125/6/p1375?a=list] [JETP **98**, 1205 (2004)].
Kvon, Z. D., E. B. Olshanetsky, G. M. Gusev, J. C. Portal, and D. K. Maude, 1997, Phys. Rev. B **56**, 12112.
Laikhtman, B., and P. M. Solomon, 1990, Phys. Rev. B **41**, 9921.
Laikhtman, B., and P. M. Solomon, 2005, Phys. Rev. B **72**, 125338.
Laikhtman, B., and P. M. Solomon, 2006, Solid State Commun. **138**, 143.
Landau, L. D., E. M. Lifshitz, and L. P. Pitaevskii, 1984, *Electrodynamics of Continuous Media* (Pergamon Press, New York).
Landauer, R., 1957, IBM J. Res. Dev. **1**, 223.
Landauer, R., 1970, Philos. Mag. **21**, 863.
Laroche, D., E. S. Bielejec, J. L. Reno, G. Gervais, and M. Lilly, 2008, Physica (Amsterdam) **40E**, 1569.
Laroche, D., G. Gervais, M. P. Lilly, and J. L. Reno, 2011, Nature Natotechnology **6**, 793.
Laroche, D., G. Gervais, M. P. Lilly, and J. L. Reno, 2014, Science **343**, 631.
Lee, D. K. K., P. R. Eastham, and N. R. Cooper, 2011, Adv. Condens. Matter Phys. **2011**, 792125.
Lee, K., J. Xue, D. C. Dillen, K. Watanabe, T. Taniguchi, and E. Tutuc, 2016, arXiv:1603.00757
Lee, P. A., and A. D. Stone, 1985, Phys. Rev. Lett. **55**, 1622.
Lerner, I. V., 1988, Phys. Lett. A **133**, 253.
Lesovik, G. B., 1989, Pis'ma Zh. Eksp. Teor. Fiz. **49**, 513 [JETP Lett. **49**, 592 (1989), http://www.jetpletters.ac.ru/ps/1120/article_16970.shtml].
Levchenko, A., and A. Kamenev, 2008a, Phys. Rev. Lett. **101**, 216806.
Levchenko, A., and A. Kamenev, 2008b, Phys. Rev. Lett. **100**, 026805.
Levchenko, A., and M. R. Norman, 2011, Phys. Rev. B **83**, 100506.
Levchenko, A., Z. Ristivojevic, and T. Micklitz, 2011, Phys. Rev. B **83**, 041303.
Li, J. I. A., T. TaniguchiK. WatanabeJ. HoneA. Levchenko, and C. R. Dean, 2016, arXiv:1602.01039.
Li, T., *et al.*, 2015, Phys. Rev. Lett. **115**, 136804.
Lifshitz, E. M., and L. P. Pitaevskii, 1981, *Physical Kinetics* (Pergamon Press, New York).
Lilly, M. P., J. P. Eisenstein, L. N. Pfeiffer, and K. W. West, 1998, Phys. Rev. Lett. **80**, 1714.
Lindhard, J., 1954, Dan. Mat. Fys. Medd. **28** [http://gymarkiv.sdu.dk/MFM/kdvs/mfm%2020-29/mfm-28-8.pdf].
Littlewood, P., 2007, Science **316**, 989.
Liu, H., W. E. Liu, and D. Culcer, 2016, Physica (Amsterdam) **79E**, 72.
Lok, J. G. S., S. Kraus, W. Dietsche, K. von Klitzing, F. Schwerdt, M. Hauser, W. Wegscheider, and M. Bichler, 2002, Physica (Amsterdam) **12E**, 119.
Lok, J. G. S., S. Kraus, M. Pohlt, W. Dietsche, K. von Klitzing, W. Wegschneider, and M. Bichler, 2001, Phys. Rev. B **63**, 041305(R).
Lok, J. G. S., S. Kraus, M. Pohlt, K. Güven, W. Dietsche, K. von Klitzing, W. Wegschneider, and M. Bichler, 2001, Physica (Amsterdam) **298B**, 135.
Lozovik, Y. E., and M. V. Nikitkov, 1999, Zh. Eksp. Teor. Fiz. **116**, 1440 [http://www.jetp.ac.ru/cgi-bin/e/index/r/116/4/p1440?a=list] [JETP **89**, 775 (1999)].
Lozovik, Y. E., S. L. Ogarkov, and A. A. Sokolik, 2012, Phys. Rev. B **86**, 045429.
Lozovik, Y. E., and A. A. Sokolik, 2008, Pis'ma Zh. Eksp. Teor. Fiz. **87**, 61 [JETP Lett. **87**, 61 (2008), http://www.jetpletters.ac.ru/ps/1830/article_27971.shtml].
Lozovik, Y. E., and V. I. Yudson, 1976, Zh. Eksp. Teor. Fiz. **71**, 738 [Sov. Phys. JETP **44**, 389 (1976), http://www.jetp.ac.ru/cgi-bin/e/index/e/44/2/p389?a=list].
Lunde, A. M., K. Flensberg, and L. I. Glazman, 2006, Phys. Rev. Lett. **97**, 256802.
Lunde, A. M., K. Flensberg, and L. I. Glazman, 2007, Phys. Rev. B **75**, 245418.
Lunde, A. M., K. Flensberg, and A.-P. Jauho, 2005, Phys. Rev. B **71**, 125408.
Lunde, A. M., and A.-P. Jauho, 2004, Semicond. Sci. Technol. **19**, S433.
Lung, F., and D. C. Marinescu, 2011, Physica (Amsterdam) **43E**, 1769.
Luo, X., T. Qiu, W. Lu, and Z. Ni, 2013, Mater. Sci. Eng. R **74**, 351.
Luttinger, J. M., 1963, J. Math. Phys. (N.Y.) **4**, 1154.
Lux, J., and L. Fritz, 2012, Phys. Rev. B **86**, 165446.
Lyo, S. K., 2003, Phys. Rev. B **68**, 045310.
Manolescu, A., and B. Tanatar, 2002, Physica (Amsterdam) **13E**, 80.
Margenau, H., and N. R. Kestner, 1969, *Theory of Intermolecular Forces* (Pergamon Press, New York).

Maslov, D. L., 1992, Phys. Rev. B **45**, 1911.
Matveev, K. A., 2013, Zh. Eksp. Teor. Fiz. **144**, 585 [http://www.jetp.ac.ru/cgi-bin/e/index/r/144/3/p585?a=list] [JETP **117**, 508 (2013)].
Mauser, C., E. D. Como, J. Baldauf, A. L. Rogach, J. Huang, D. Talapin, and J. Feldmann, 2010, Phys. Rev. B **82**, 081306(R).
Micklitz, T., J. Rech, and K. A. Matveev, 2010, Phys. Rev. B **81**, 115313.
Min, H., R. Bistritzer, J.-J. Su, and A. H. MacDonald, 2008, Phys. Rev. B **78**, 121401.
Mink, M. P., H. T. C. Stoof, R. A. Duine, M. Polini, and G. Vignale, 2012, Phys. Rev. Lett. **108**, 186402.
Mink, M. P., H. T. C. Stoof, R. A. Duine, M. Polini, and G. Vignale, 2013, Phys. Rev. B **88**, 235311.
Mishchenko, E. G., M. Y. Reizer, and L. I. Glazman, 2004, Phys. Rev. B **69**, 195302.
Moldoveanu, V., and B. Tanatar, 2009, Europhys. Lett. **86**, 67004.
Morath, C. P., J. A. Seamons, J. L. Reno, and M. P. Lilly, 2009, Phys. Rev. B **79**, 041305(R).
Morimoto, T., Y. Iwase, N. Aoki, T. Sasaki, Y. Ochiai, A. Shailos, J. P. Bird, M. P. Lilly, J. L. Reno, and J. A. Simmons, 2003, Appl. Phys. Lett. **82**, 3952.
Mortensen, N. A., K. Flensberg, and A.-P. Jauho, 2001, Phys. Rev. Lett. **86**, 1841.
Mortensen, N. A., K. Flensberg, and A.-P. Jauho, 2002a, Phys. Rev. B **65**, 085317.
Mortensen, N. A., K. Flensberg, and A.-P. Jauho, 2002b, Phys. Scr. **T101**, 177.
Moskalenko, S. A., 1962, Fiz. Tverd. Tela (Leningrad) **4**, 276 [Sov. Phys. Solid State **4**, 199 (1962)].
Moško, M., V. Cambel, and A. Mošková, 1992, Phys. Rev. B **46**, 5012.
Mosko, M., J.-L. Pelouard, and F. Pardo, 1994, Semicond. Sci. Technol. **9**, 806.
Mott, N. F., and H. Jones, 1936, *The Theory of the Properties of Metals and Alloys* (Clarendon, Oxford).
Mou, X., L. F. Register, and A. H. MacDonald, S. K. Banerjee, 2015, Phys. Rev. B **92**, 235413.
Müller, M., and S. Sachdev, 2008, Phys. Rev. B **78**, 115419.
Müller, M., J. Schmalian, and L. Fritz, 2009, Phys. Rev. Lett. **103**, 025301.
Muraki, K., J. G. S. Lok, S. Kraus, W. Dietsche, K. von Klitzing, D. Schuh, M. Bichler, and W.Wegscheider, 2004, Phys. Rev. Lett. **92**, 246801.
Murphy, S. Q., J. P. Eisenstein, G. S. Boebinger, L. N. Pfeiffer, and K. W. West, 1994, Phys. Rev. Lett. **72**, 728.
Nandi, D., A. D. K. Finck, J. P. Eisenstein, L. N. Pfeiffer, and K. W. West, 2012, Nature (London) **488**, 481.
Narozhny, B. N., 2007, Phys. Rev. B **76**, 153409.
Narozhny, B. N., and I. L. Aleiner, 2000, Phys. Rev. Lett. **84**, 5383.
Narozhny, B. N., I. L. Aleiner, and A. Stern, 2001, Phys. Rev. Lett. **86**, 3610.
Narozhny, B. N., I. V. Gornyi, M. Titov, M. Schütt, and A. D. Mirlin, 2015, Phys. Rev. B **91**, 035414.
Narozhny, B. N., M. Titov, I. V. Gornyi, and P. M. Ostrovsky, 2012, Phys. Rev. B **85**, 195421.
Narozhny, B. N., G. Zala, and I. L. Aleiner, 2002, Phys. Rev. B **65**, 180202.
Nazarov, Y. V., and D. V. Averin, 1998, Phys. Rev. Lett. **81**, 653.
Noh, H., S. Zelakiewicz, X. G. Feng, T. J. Gramila, L. N. Pfeiffer, and K. W. West, 1998, Phys. Rev. B **58**, 12621.
Noh, H., S. Zelakiewicz, T. J. Gramila, L. N. Pfeiffer, and K. W. West, 1999, Phys. Rev. B **59**, 13114.
Nomura, K., and A. H. MacDonald, 2006, Phys. Rev. Lett. **96**, 256602.
Nomura, K., and A. H. MacDonald, 2007, Phys. Rev. Lett. **98**, 076602.
Onac, E., F. Balestro, L. H. W. van Beveren, U. Hartmann, Y. V. Nazarov, and L. P. Kouwenhoven, 2006, Phys. Rev. Lett. **96**, 176601.
Oreg, Y., and B. I. Halperin, 1999, Phys. Rev. B **60**, 5679.
Oreg, Y., and A. Kamenev, 1998, Phys. Rev. Lett. **80**, 2421.
Orgad, D., and S. Levit, 1996, Phys. Rev. B **53**, 7964.
Ostrovsky, P. M., I. V. Gornyi, and A. D. Mirlin, 2006, Phys. Rev. B **74**, 235443.
Ostrovsky, P. M., I. V. Gornyi, and A. D. Mirlin, 2007, Eur. Phys. J. Spec. Top. **148**, 63.
Park, K., and S. Das Sarma, 2006, Phys. Rev. B **74**, 035338.
Patel, N. K., E. H. Linfield, K. M. Brown, M. Pepper, D. A. Ritchie, and G. A. C. Jones, 1997, Semicond. Sci. Technol. **12**, 309.
Pereira, R. G., and E. Sela, 2010, Phys. Rev. B **82**, 115324.
Peres, N. M. R., J. M. B. L. dos Santos, and A. H. C. Neto, 2011, Europhys. Lett. **95**, 18001.
Pesin, D. A., and A. H. MacDonald, 2011, Phys. Rev. B **84**, 075308.
Pikalov, A. A., and D. V. Fil, 2012, Nanoscale Res. Lett. **7**, 145.
Pillarisetty, R., H. Noh, D. C. Tsui, E. P. D. Poortere, E. Tutuc, and M. Shayegan, 2002, Phys. Rev. Lett. **89**, 016805.
Pillarisetty, R., H. Noh, D. C. Tsui, E. P. D. Poortere, E. Tutuc, and M. Shayegan, 2003, Phys. Rev. Lett. **90**, 226801.
Pillarisetty, R., H. Noh, D. C. Tsui, E. P. D. Poortere, E. Tutuc, and M. Shayegan, 2005, Phys. Rev. Lett. **94**, 016807.
Pillarisetty, R., H. Noh, E. Tutuc, E. D. Poortere, D. Tsui, and M. Shayegan, 2004, Physica (Amsterdam) **22E**, 300.
Pillarisetty, R., H. Noh, E. Tutuc, E. P. D. Poortere, K. Lai, D. Tsui, and M. Shayegan, 2005, Phys. Rev. B **71**, 115307.
Pogrebinskii, M. B., 1977, Fiz. Tekh. Poluprovodn. **11**, 637 [Sov. Phys. Semicond. **11**, 372 (1977)].
Ponomarenko, L., *et al.*, 2011, Nat. Phys. **7**, 958.
Ponomarenko, L. A., 2013 (private communication).
Ponomarenko, V. V., and D. V. Averin, 2000, Phys. Rev. Lett. **85**, 4928.
Price, A. S., A. K. Savchenko, G. Allison, and D. A. Ritchie, 2008, Physica (Amsterdam) **40E**, 961.
Price, A. S., A. K. Savchenko, B. N. Narozhny, G. Allison, and D. A. Ritchie, 2007, Science **316**, 99.
Price, A. S., A. K. Savchenko, and D. A. Ritchie, 2010, Phys. Rev. B **81**, 193303.
Price, P. J., 1983, Physica B+C (Amsterdam) **117–118**, 750.
Price, P. J., 1984, Solid State Commun. **51**, 607.
Price, P. J., 1988, in *The Physics of Submicron Semiconductor Devices*, edited by H. Grubin, D. K. Ferry, and C. Jacoboni (Plenum, New York).
Principi, A., M. Carrega, R. Asgari, V. Pellegrini, and M. Polini, 2012, Phys. Rev. B **86**, 085421.
Profumo, R. E. V., R. Asgari, M. Polini, and A. H. MacDonald, 2012, Phys. Rev. B **85**, 085443.
Prunnila, M., S. J. Laakso, J. M. Kivioja, and J. Ahopelto, 2008, Appl. Phys. Lett. **93**, 112113.
Pustilnik, M., E. G. Mishchenko, L. I. Glazman, and A. V. Andreev, 2003, Phys. Rev. Lett. **91**, 126805.
Pustilnik, M., E. G. Mishchenko, and O. A. Starykh, 2006, Phys. Rev. Lett. **97**, 246803.
Raichev, O., and P. Vasilopoulos, 2000a, Phys. Rev. B **61**, 7511.
Raichev, O., and P. Vasilopoulos, 2000b, J. Phys. Condens. Matter **12**, 6859.
Raichev, O. E., 1997, J. Appl. Phys. **81**, 1302.

Raichev, O. E., and P. Vasilopoulos, 1999, Phys. Rev. Lett. **83**, 3697.
Raikh, M. E., and F. von Oppen, 2002, Phys. Rev. Lett. **89**, 106601.
Read, N., 1990, Phys. Rev. Lett. **65**, 1502.
Reed, J. P., B. Uchoa, Y. I. Joe, Y. Gan, D. Casa, E. Fradkin, and P. Abbamonte, 2010, Science **330**, 805.
Renn, S. R., 1992, Phys. Rev. Lett. **68**, 658.
Reznikov, M., M. Heiblum, H. Shtrikman, and D. Mahalu, 1995, Phys. Rev. Lett. **75**, 3340.
Rieder, M.-T., T. Micklitz, A. Levchenko, and K. A. Matveev, 2014, Phys. Rev. B **90**, 165405.
Rojo, A. G., 1999, J. Phys. Condens. Matter **11**, R31.
Rojo, A. G., and G. D. Mahan, 1992, Phys. Rev. Lett. **68**, 2074.
Roth, A., C. Brüne, H. Buhmann, L. W. Molenkamp, J. Maciejko, X.-L. Qi, and S.-C. Zhang, 2009, Science **325**, 294.
Rozhkov, A. V., 2008, Phys. Rev. B **77**, 125109; **79**, 249903(E) (2009).
Rubel, H., A. Fischer, W. Dietsche, C. Jörger, K. Klitzing, and K. Eberl, 1997, Physica (Amsterdam) **1E**, 160.
Rubel, H., A. Fischer, W. Dietsche, C. Jörger, K. Klitzing, and K. Eberl, 1998, Physica B (Amsterdam) **249–251**, 859.
Rubel, H., A. Fischer, W. Dietsche, K. von Klitzing, and K. Eberl, 1997, Phys. Rev. Lett. **78**, 1763.
Rubel, H., E. H. Linfield, N. P. R. Hill, J. T. Nicholls, D. A. Ritchie, K. M. Brown, M. Pepper, and G. A. C. Jones, 1995, Semicond. Sci. Technol. **10**, 1229.
Rubel, H., E. H. Linfield, N. P. R. Hill, J. T. Nicholls, D. A. Ritchie, K. M. Brown, M. Pepper, and G. A. C. Jones, 1996, Surf. Sci. **361–362**, 134.
Saberi-Pouya, S., T. Vazifehshenas, M. Farmanbar, and T. Salavati-fard, 2016, arXiv:1602.00338.
Sakhi, S., 1997, Phys. Rev. B **56**, 4098.
Sánchez, R., R. López, D. Sánchez, and M. Büttiker, 2010, Phys. Rev. Lett. **104**, 076801.
Santoro, G. E., and G. F. Giuliani, 1988, Phys. Rev. B **37**, 937.
Scharf, B., and A. Matos-Abiague, 2012, Phys. Rev. B **86**, 115425.
Schliemann, J., S. M. Girvin, and A. H. MacDonald, 2001, Phys. Rev. Lett. **86**, 1849.
Schlottmann, P., 2004a, Phys. Rev. B **69**, 035110.
Schlottmann, P., 2004b, Phys. Rev. B **70**, 115306.
Schmult, S., L. Tiemann, W. Dietsche, and K. von Klitzing, 2010, J. Vac. Sci. Technol. B **28**, C3C1.
Schütt, M., P. M. Ostrovsky, I. V. Gornyi, and A. D. Mirlin, 2011, Phys. Rev. B **83**, 155441.
Schütt, M., P. M. Ostrovsky, M. Titov, I. V. Gornyi, B. N. Narozhny, and A. D. Mirlin, 2013, Phys. Rev. Lett. **110**, 026601.
Seamons, J. A., C. P. Morath, J. L. Reno, and M. P. Lilly, 2009, Phys. Rev. Lett. **102**, 026804.
Seeger, K., 2002, *Semiconductor Physics* (Springer, New York).
Seradjeh, B., J. E. Moore, and M. Franz, 2009, Phys. Rev. Lett. **103**, 066402.
Shahbazyan, T. V., and S. E. Ulloa, 1997a, Phys. Rev. B **55**, 13702.
Shahbazyan, T. V., and S. E. Ulloa, 1997b, Physica (Amsterdam) **1E**, 259.
Shen, S.-Q., 2013, *Topological Insulators: Dirac Equation in Condensed Matters* (Springer, New York).
Shevchenko, S. I., 1976, Fiz. Nizk. Temp. **2**, 505 [Sov. J. Low Temp. Phys. **2**, 251 (1976)].
Shimshoni, E., 1995, Phys. Rev. B **51**, 9415.
Shimshoni, E., and S. L. Sondhi, 1994, Phys. Rev. B **49**, 11484.
Shon, N. H., and T. Ando, 1998, J. Phys. Soc. Jpn. **67**, 2421.
Shylau, A. A., and A.-P. Jauho, 2014, Phys. Rev. B **89**, 165421.
Simon, S. H., E. H. Rezayi, and M. V. Milovanovic, 2003, Phys. Rev. Lett. **91**, 046803.
Singwi, K. S., M. P. Tosi, R. H. Land, and A. Sjölander, 1968, Phys. Rev. **176**, 589.
Sirenko, Y. M., and P. Vasilopoulos, 1992, Phys. Rev. B **46**, 1611.
Sivan, U., P. M. Solomon, and H. Shtrikman, 1992, Phys. Rev. Lett. **68**, 1196.
Smith, H., and H. H. Jensen, 1989, *Transport Phenomena* (Oxford University Press, New York).
Snoke, D. W., 2002, Science **298**, 1368.
Snoke, D. W., 2008, *Solid State Physics. Essential Concepts* (Addison-Wesley, Reading, MA).
Sodemann, I., D. A. Pesin, and A. H. MacDonald, 2012, Phys. Rev. B **85**, 195136.
Söderström, E., A. V. Buyanov, and B. E. Sernelius, 1996, J. Phys. Condens. Matter **8**, 3705.
Solomon, P. M., and B. Laikhtman, 1991, Superlattices Microstruct. **10**, 89.
Solomon, P. M., P. J. Price, D. J. Frank, and D. C. L. Tulipe, 1989, Phys. Rev. Lett. **63**, 2508.
Son, D. T., 2007, Phys. Rev. B **75**, 235423.
Song, J. C. W., D. A. Abanin, and L. S. Levitov, 2013, Nano Lett. **13**, 3631.
Song, J. C. W., and L. S. Levitov, 2012, Phys. Rev. Lett. **109**, 236602.
Song, J. C. W., and L. S. Levitov, 2013, Phys. Rev. Lett. **111**, 126601.
Sothmann, B., R. Sánchez, A. N. Jordan, and M. Büttiker, 2012, Phys. Rev. B **85**, 205301.
Spielman, I. B., J. P. Eisenstein, L. N. Pfeiffer, and K. W. West, 2000, Phys. Rev. Lett. **84**, 5808.
Spielman, I. B., M. Kellogg, J. P. Eisenstein, L. N. Pfeiffer, and K. W. West, 2004, Phys. Rev. B **70**, 081303(R).
Spivak, B., and S. Kivelson, 2005, Phys. Rev. B **72**, 045355.
Spivak, B., S. V. Kravchenko, S. A. Kivelson, and X. P. A. Gao, 2010, Rev. Mod. Phys. **82**, 1743.
Stauber, T., and G. Gómez-Santos, 2012, Phys. Rev. B **85**, 075410.
Stern, A., and B. I. Halperin, 1995, Phys. Rev. B **52**, 5890.
Stern, A., and B. I. Halperin, 2002, Phys. Rev. Lett. **88**, 106801.
Stern, A., S. D. Sarma, M. P. A. Fisher, and S. M. Girvin, 2000, Phys. Rev. Lett. **84**, 139.
Stern, A., and I. Ussishkin, 1997, Physica (Amsterdam) **1E**, 176.
Stern, F., 1967, Phys. Rev. Lett. **18**, 546.
Stormer, H. L., L. N. Pfeiffer, K. W. Baldwin, and K. W. West, 1990, Phys. Rev. B **41**, 1278.
Su, J.-J., and A. H. MacDonald, 2008, Nat. Phys. **4**, 799.
Suen, Y. W., L. W. Engel, M. B. Santos, M. Shayegan, and D. C. Tsui, 1992, Phys. Rev. Lett. **68**, 1379.
Suprunenko, Y. F., V. Cheianov, and V. I. Fal'ko, 2012, Phys. Rev. B **86**, 155405.
Svintsov, D., V. Vyurkov, S. Yurchenko, T. Otsuji, and V. Ryzhii, 2012, J. Appl. Phys. **111**, 083715.
Swierkowski, L., J. Szymanski, and Z. W. Gortel, 1995, Phys. Rev. Lett. **74**, 3245.
Swierkowski, L., J. Szymanski, and Z. W. Gortel, 1996, Surf. Sci. **361–362**, 130.
Swierkowski, L., J. Szymanski, and Z. W. Gortel, 1997, Phys. Rev. B **55**, 2280.
Takashina, K., K. Nishiguchi, Y. Ono, A. Fujiwara, T. Fujisawa, Y. Hirayama, and K. Muraki, 2009, Appl. Phys. Lett. **94**, 142104.
Tan, Y.-W., Y. Zhang, H. L. Stormer, and P. Kim, 2007, Eur. Phys. J. Spec. Top. **148**, 15.
Tanatar, B., 1996, Solid State Commun. **99**, 1.
Tanatar, B., 1998, Phys. Rev. B **58**, 1154.
Tanatar, B., and A. K. Das, 1996, Phys. Rev. B **54**, 13827.

Tiemann, L., W. Dietsche, M. Hauser, and K. von Klitzing, 2008, New J. Phys. **10**, 045018.
Tiemann, L., J. G. S. Lok, W. Dietsche, K. von Klitzing, K. Muraki, D. Schuh, and W. Wegscheider, 2008, Phys. Rev. B **77**, 033306.
Titov, M., B. N. Narozhny, and I. V. Gornyi, 2013 (unpublished).
Titov, M., *et al.*, 2013, Phys. Rev. Lett. **111**, 166601.
Tomonaga, S., 1950, Prog. Theor. Phys. **5**, 544.
Tse, W.-K., and S. Das Sarma, 2007, Phys. Rev. B **75**, 045333.
Tse, W.-K., B. Y.-K. Hu, and S. D. Sarma, 2007, Phys. Rev. B **76**, 081401.
Tso, H. C., D. J. Geldart, and P. Vasilopoulos, 1998, Phys. Rev. B **57**, 6561.
Tso, H. C., and P. Vasilopoulos, 1992, Phys. Rev. B **45**, 1333.
Tso, H. C., P. Vasilopoulos, and F. M. Peeters, 1992, Phys. Rev. Lett. **68**, 2516.
Tso, H. C., P. Vasilopoulos, and F. M. Peeters, 1993, Phys. Rev. Lett. **70**, 2146.
Tso, H. C., P. Vasilopoulos, and F. M. Peeters, 1994, Surf. Sci. **305**, 400.
Tutuc, E., R. Pillarisetty, and M. Shayegan, 2009, Phys. Rev. B **79**, 041303(R).
Tutuc, E., M. Shayegan, and D. A. Huse, 2004, Phys. Rev. Lett. **93**, 036802.
Ussishkin, I., and A. Stern, 1997, Phys. Rev. B **56**, 4013.
Ussishkin, I., and A. Stern, 1998, Phys. Rev. Lett. **81**, 3932.
Varma, C. M., A. I. Larkin, and E. Abrahams, 1994, Phys. Rev. B **49**, 13999.
Vignale, G., 2005, Phys. Rev. B **71**, 125103.
Vignale, G., and A. H. MacDonald, 1996, Phys. Rev. Lett. **76**, 2786.
Vignale, G., and K. S. Singwi, 1985, Phys. Rev. B **31**, 2729.
Vitkalov, S., 1998, Pis'ma Zh. Eksp. Teor. Fiz. **67**, 276 [http://www.jetpletters.ac.ru/ps/998/article_15181.shtml] [JETP Lett. **67**, 295 (1998)].
von Oppen, F., S. H. Simon, and A. Stern, 2001, Phys. Rev. Lett. **87**, 106803.
Walter, A. L., *et al.*, 2011, Phys. Rev. B **84**, 085410.
Wang, D.-W., E. G. Mishchenko, and E. Demler, 2005, Phys. Rev. Lett. **95**, 086802.
Wang, X., and I. C. da Cunha Lima, 2001, Phys. Rev. B **63**, 205312.
Wei, P., W. Bao, Y. Pu, C. N. Lau, and J. Shi, 2009, Phys. Rev. Lett. **102**, 166808.
Wen, X.-G., 1995, Adv. Phys. **44**, 405.
Wen, X.-G., and A. Zee, 1992, Phys. Rev. Lett. **69**, 1811.
Wiersma, R., J. Lok, L. Tiemann, W. Dietsche, K. von Klitzing, D. Schuh, and W. Wegscheider, 2006, Physica (Amsterdam) **35E**, 320.
Wiersma, R. D., J. G. S. Lok, S. Kraus, W. Dietsche, K. von Klitzing, D. Schuh, M. Bichler, H.-P. Tranitz, and W. Wegscheider, 2004, Phys. Rev. Lett. **93**, 266805.
Wiersma, R. D., J. G. S. Lok, L. Tiemann, W. Dietsche, K. von Klitzing, W. Wegscheider, and D. Schuh, 2007, Int. J. Mod. Phys. B **21**, 1256.
Wunsch, B., T. Stauber, F. Sols, and F. Guinea, 2006, New J. Phys. **8**, 318.
Yamamoto, M., M. Stopa, Y. Tokura, Y. Hirayama, and S. Tarucha, 2002, Physica (Amsterdam) **12E**, 726.
Yamamoto, M., M. Stopa, Y. Tokura, Y. Hirayama, and S. Tarucha, 2006, Science **313**, 204.
Yamamoto, M., H. Takagi, M. Stopa, and S. Tarucha, 2012, Phys. Rev. B **85**, 041308(R).
Yan, H., X. Li, B. Chandra, G. Tulevski, Y. Wu, M. Freitag, W. Zhu, P. Avouris, and F. Xia, 2012, Nat. Nanotechnol. **7**, 330.
Yan, H., Z. Li, X. Li, W. Zhu, P. Avouris, and F. Xia, 2012, Nano Lett. **12**, 3766.
Yang, K., 1998, Phys. Rev. B **58**, R4246.
Yang, K., and A. H. MacDonald, 2001, Phys. Rev. B **63**, 073301.
Yang, K., K. Moon, L. Zheng, A. H. MacDonald, S. M. Girvin, D. Yoshioka, and S.-C. Zhang, 1994, Phys. Rev. Lett. **72**, 732.
Yang, L., J. D. Koralek, J. Orenstein, D. R. Tibbetts, J. L. Reno, and M. P. Lilly, 2011, Phys. Rev. Lett. **106**, 246401.
Yoon, Y., L. Tiemann, S. Schmult, W. Dietsche, K. von Klitzing, and W. Wegscheider, 2010, Phys. Rev. Lett. **104**, 116802.
Yoshioka, D., A. H. MacDonald, and S. M. Girvin, 1989, Phys. Rev. B **39**, 1932.
Yurtsever, A., V. Moldoveanu, and B. Tanatar, 2003, Solid State Commun. **125**, 575.
Zala, G., B. Narozhny, and I. Aleiner, 2001, Phys. Rev. B **64**, 214204.
Zelakiewicz, S., H. Noh, T. J. Gramila, L. N. Pfeiffer, and K. W. West, 2000, Phys. Rev. Lett. **85**, 1942.
Zhang, C., and G. Jin, 2013, J. Phys. Condens. Matter **25**, 425604.
Zhang, C., and Y. Takahashi, 1993, J. Phys. Condens. Matter **5**, 5009.
Zhang, C.-H., and Y. N. Joglekar, 2008, Phys. Rev. B **77**, 233405.
Zhang, S. S.-L., and S. Zhang, 2012, Phys. Rev. Lett. **109**, 096603.
Zheng, L., and A. H. MacDonald, 1993, Phys. Rev. B **48**, 8203.
Zhou, F., and Y. B. Kim, 1999, Phys. Rev. B **59**, R7825.
Zhu, J.-J., S. M. Badalyan, and F. M. Peeters, 2013, Phys. Rev. B **87**, 085401.
Ziman, J. M., 1965, *Principles of the Theory of Solids* (Cambridge, Cambridge, England).
Zou, Y., G. Refael, and J. Yoon, 2009, Phys. Rev. B **80**, 180503(R).
Zou, Y., G. Refael, and J. Yoon, 2010, Phys. Rev. B **82**, 104515.
Zuev, Y. M., W. Chang, and P. Kim, 2009, Phys. Rev. Lett. **102**, 096807.
Zyuzin, V. A., and G. A. Fiete, 2010, Phys. Rev. B **82**, 113305.